Title

Stochastic Electronic Structure Methods for Nano- to Microscale Molecular Complexes

Author

Bradbury, Nadine Claire

Publication Date

2024

Peer reviewed|Thesis/dissertation

UNIVERSITY OF CALIFORNIA

Los Angeles

Stochastic Electronic Structure Methods for Nano- to Microscale Molecular Complexes

A dissertation submitted in partial satisfaction

of the requirements for the degree

Doctor of Philosophy in Chemistry

by

Nadine Claire Bradbury

2024

ABSTRACT OF THE DISSERTATION

Stochastic Electronic Structure Methods for Nano- to Microscale Molecular Complexes

by

Nadine Claire Bradbury
Doctor of Philosophy in Chemistry
University of California, Los Angeles, 2024
Professor Daniel Neuhauser, Chair

Molecular excitons in large extended systems are often not well described by local time-dependent density functional theory (TDDFT) due to highly delocalized states with long range electronic coupling. The issue of long-range coupling is made exceptionally more difficult when we consider excitons delocalized over many large molecules in aggregates ranging up to micron scale. In this thesis, we develop a series of electronic structure theory methods leveraging stochastic techniques that enable us to perform higher quality calculations on molecular excitons, and enable us to study extremely large systems in the context of molecular aggregates. We have developed a linear scaling method that can study spectroscopic observables such as the density of states and participation ratio in systems of millions of coupled dye dipoles. For the study of single excitons in large molecular complexes, we have developed a stochastic formalism of the Bethe-Salpeter equation, the linear response formalism that arises from the GW approximation of many-body perturbation theory. Through a series of algorithmic improvements to the method, we have developed new approximations to capture the screened Coulomb interaction at lower computational cost, leading to the study of systems with several thousand electrons.

The dissertation of Nadine Claire Bradbury is approved.

Benjamin J. Schwartz

Anastassia N. Alexandrova

Justin R. Caram

Daniel Neuhauser, Committee Chair

University of California, Los Angeles

2024

To Mum and Dad,

TABLE OF CONTENTS

LIST OF FIGURES

LIST OF TABLES

ACKNOWLEDGMENTS

I would like to thank the guidance and support of both Professors Daniel Neuhauser and Justin Caram. Their support has been essential to my PhD journey throughout. I would like to thank my theoretical collaborators who have taught me plenty about molecular aggregates and exciton-polaritons respectively, Professors Chern Chuang (University of Nevada, Las Vegas) and Raphael Rebeiro (Emory University). I would like to thank the members of both the Neuhauser and Caram research groups for their support and camaraderie regardless of where in the world we are working from. Lastly, I would like to thank the NSF Graduate Research Fellowship for making my PhD the most remote and travel friendly chemistry PhD possible.

Most importantly, I would like to thank my family, new and old, for their continual love, support, guidance and adventure.

Chapter 2 is reprinted with permission from

NC Bradbury, C Chuang, AP Deshmukh, E Rabani, R Bear, JR Caram, and D Neuhauser, Stochastically Realized Observables for Excitonic Molecular Aggregates. *J. Phys. Chem. A*, **124**, 49, 10111-10120 (2020). ©2020 American Chemical Society

Chapter 3 is reprinted with permission from

NC Bradbury, RF Ribeiro, JR Caram, and D Neuhauser, Polaritons in Large Stochastic Simulations of 2D Molecular Aggregates, Phys. Rev B (Accepted) (2024). ©2024 American Physical Society

Chapter 4 is reprinted with permission from

NC Bradbury, M Nguyen , JR Caram, and D Neuhauser, Bethe Salpeter Equation Spectra for Very Large Systems, *J. Chem. Phys.*, **157**, 031104 (2022). ©2022 AIP Publishing

Chapter 5 is reprinted with permission from

NC Bradbury, M Nguyen, K Ibrahim, and D Neuhauser, Optimized Attenuated Interaction: Enabling Stochastic Bethe-Salpeter Spectra for Large Systems, *J. Chem. Phys,* **158**, 154104 (2023).

Chapter 6 is reprinted with permission from

NC Bradbury, T Allen, M Nguyen, and D Neuhauser, Deterministic/Fragmented-Stochastic Exchange for Large Scale Hybrid DFT Calculations, *J. Chem. Theory Comput.*,**19**, 24 (2023).

VITA

2015-2019 B.S. (Chemistry), California Institute of Technology.

2019-2021 M.Sc. (Chemistry), University of California, Los Angeles.

2021-2024 NSF Graduate Research Fellowship

PUBLICATIONS

M Sereda, T Allen, NC Bradbury, KZ Ibrahim, D Neuhauser Sparse-Stochastic Fragmented Exchange for Large-Scale Hybrid TDDFT Calculations, *J. Chem. Theory Comput.*, 20, 10, 4196–4204, (2024).

NC Bradbury, RF Ribeiro, JR Caram, and D Neuhauser, Polaritons in Large Stochastic Simulations of 2D Molecular Aggregates, Phys. Rev. B, (Accepted). Arxiv:2308.04385

NC Bradbury, T Allen, M Nguyen, and D Neuhauser, Deterministic/Fragmented-Stochastic Exchange for Large Scale Hybrid DFT Calculations, *J. Chem. Theory Comput.*, **19**, 24 (2023).

NC Bradbury, M Nguyen, K Ibrahim, and D Neuhauser, Optimized Attenuated Interaction: Enabling Stochastic Bethe-Salpeter Spectra for Large Systems, *J. Chem. Phys,* **158**, 154104 (2023).

A Bailey, AP Deshmukh, NC Bradbury, M Pengshung, T Atallah, J Williams, U Barotov, D Neuhauser, EM Sletten, JR Caram, Exploring the Design of Superradiant J-Aggregates from Amphiphilic Monomer Units, *Nanoscale*, **15**, 3841-3849 (2023).

NC Bradbury, M Nguyen , JR Caram, and D Neuhauser, Bethe Salpeter Equation Spectra for Very Large Systems, *J. Chem. Phys.*, **157**, 031104 (2022).

AP Deshmukh, N Geue, NC Bradbury, C Chuang, M Pengshung, J Cao, EM Sletten, D Neuhauser, and JR Caram Bridging the gap between H- and J-aggregates: Classification and supramolecular tunability for excitonic band structures in two-dimensional molecular aggregates, *Chem. Phys. Rev.,* **3**, 021401 (2022).

NC Bradbury, C Chuang, AP Deshmukh, E Rabani, R Bear, JR Caram, and D Neuhauser, Stochastically Realized Observables for Excitonic Molecular Aggregates. *J. Phys. Chem. A*, **124**, 49, 10111-10120 (2020).

A Baranczak, Y Liu, S Connelly, WG Han Du, ER Greiner, JC Genereux, RL Wiseman, YS Eisele, NC Bradbury, J Dong, L Noodleman, KB Sharpless, IA Wilson, SE Encalada, and JW Kelly, A Fluorogenic Aryl Fluorosulfate for Intraorganellar Transthyretin Imaging in Living Cells and in Caenorhabditis elegans. *JACS*, **137, 23,** 7404-7414 (2015).

CHAPTER 1

Introduction

The central themes of this thesis could be summed up into two ideas, one scientific, one algorithmic: the molecular exciton, and the stochastic resolution of the identity. In each chapter, we focus on a form of Frenkel exciton, and apply a new stochastic methodolgy to better understanding the properties of excitons in molecular and supramolecular systems and accelerate the speed of large-scale computations. In particular, we tackle the problem of modeling micron-large molecular aggregates and polaritons, enabling the prediction of new aggregate properties and geometries. We also tackle the traditional electronic structure problem of optical absorption through the lens of density functional theory (DFT), time-dependent DFT (TDDFT), and the Bethe-Salpeter Equation (BSE). With this we efficiently calculate highly accurate spectra for molecular systems that are unaffordable for conventional electronic structure methods.

An introduction to the exciton: The concept of an exciton was first proposed by Yakov Frenkel in 1931– in which he observed neutral excitations in crystals caused by absorption of light were possible in which an electron is excited but remains bound to a positively charged 'hole' in the lattice.[Pei94] Frenkel was additionally the first to describe the concept postive 'hole' left in the crystal after excitation or ejection of an electron (1926), many years before the notion of the Dirac sea was formalized in quantum mechanics. Today, the exciton quasiparticle is typically divided into two main categories the eponymous Frenkel and the Wannier-Mott exciton, by their binding energies. An exciton binding energy can be defined as the difference in energy in between the fundamental gap (Ionization Energy

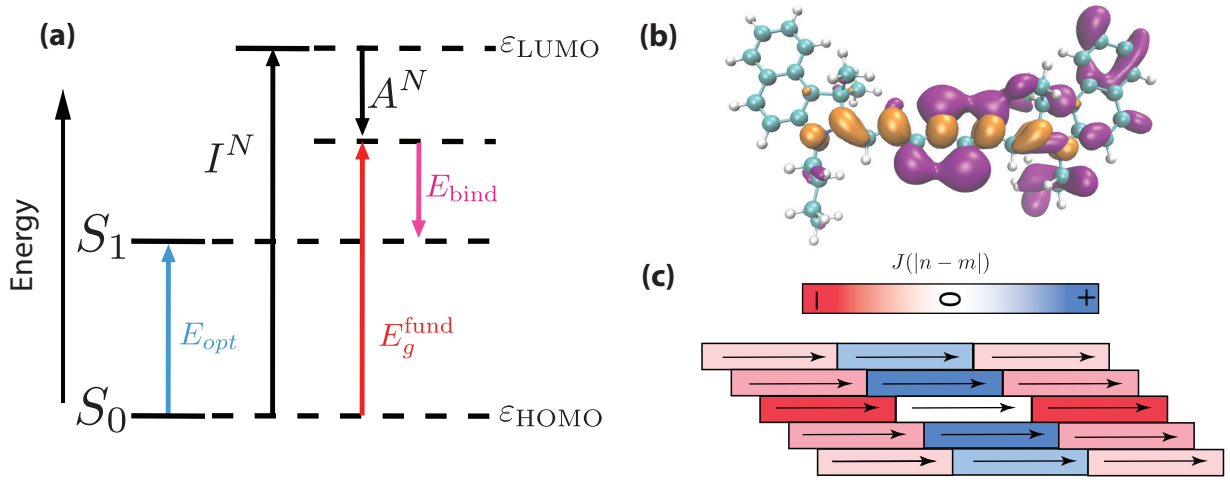

Figure 1.1: (a) Energy diagram showing the various energetic quantities relevant to discussing the study of excitons. (b) Exciton density of indocyanine green dye molecule calculated with the TDHF@v_W method describe in chapter 5. The electron wavefunction density is shown in purple, and the organ hole density is shown in orange. (c) Dipole model of the coupling in a planar molecular Aggregate with coloring by the strength of the transition dipole-dipole coupling.

minus Electron Affinity, E_g^{fund}) and the energy of the absorbed photon (optical gap, E_{opt}), as shown in Figure 1.1 (a).

Wannier-Mott excitons are classified as excitons with small binding energies relative to the optical gap, less than that of a hydrogen atom and often on the order of 0.01 eV.[Wan37] These typically occur in conducting and semiconducting crystalline materials, like CuO_2 and GaAs. Such weak binding energies are correlated with high dielectrics, and thus the electron typically has a wavefunction much larger than the atomic spacings, and typically are well described like hydrogen atoms that can move freely throughout a crystal.[Fox10] At high densities of these excitons (near the Mott density), more complex many-body physics emerges, such as the formation of bound bi-excitons, electron-hole plasmas, or even Bose-Eistein condensation.

While Wannier-Mott excitons are the default description of excitons in a typical solid state

physics textbook, the Frenkel picture is more accurate systems such as molecules and organic semiconductors. Frenkel excitons are classified as excitons with large binding energies relative to the optical gap. In some of the organic systems studied in this work like chlorophylls, the binding energy can be upwards of 2 eV on a system with optical gap near 2 eV! Such large binding energies usually imply a fairly localized excitation, sometimes contained within a single molecule as in the case of fullerenes.[MPP98] This large binding energy and relatively small size, compared to bulk semiconductors, leads to a pictures of these excitons as being bound to one molecule and relatively less mobile in a molecular crystal. While we mention isolated molecular systems and organic crystals as the primary kinds of systems contain Frenkel excitons to be studied in this thesis, they can also occurr in a variety of insulating inorganic materials, famous examples include alkali halide and the crystals of condensed Nobel gases.[Fox10]

If we limit our study of Frenkel excitons to those in large molecular systems, such as the study of fullerenes included in Chapters 4 and 5, a quantum chemist thinks of this as described primarily within the question of calculating an absorption spectrum for a given system. The most widely popular of these methods, like time-dependent Hartree-Fock (TDHF) and TDDFT, belong to a family of methods known as linear response theory. First described by the Kubo formula in 1957,[Kub57] linear response describes the response of a system to a time dependent force, like the description of damped harmonic oscillators.

In the context of TDHF, linear response is provoked within the context of the random phase approximation (RPA), where the perturbing force is an infintessimal perturbation to the density matrix represented by a superposition of electron-hole (exciton) matrix elements.[Neg82] Looking at only the diagonal term of the resulting eigenvalue equation known as the Tamm-Dancoff Approximation (TDA), the resulting exciton Hamiltonian can be written simply as

$$\boldsymbol{A}_{hh'ee'} = (E_e - E_h)\delta_{ee'}\delta_{hh'} - \langle he'|V|eh' - h'e\rangle. \tag{1.1}$$

The terms of this equation clearly demonstrate the concept of the exciton binding energy within a molecular system, in which the absorption energy is reduced from the ground state energy gap (first term) by a binding energy response term (the exchange and Hartree terms). Thus, it is also apparent that the binding energy will be huge in systems carry highly overlaping highest occupied and lowest unnoccupied molecular orbitals (HOMO and LUMO) like organic dyes, shown in Figure 1.1 (b) which shows both a delocalized electron and hole wavefunction in the exciton.

So far we have only discussed the case of Frenkel excitons isolated to only one molecule, but this is not the case in organic semiconducting crystals and even highly disordered systems like molecular aggregates. The absorption energy of organic dyes shifting upon aggregation in solution was first documented by Jelly, concurrently with the discovery of Wannier excitons.[Jel36] Aggregation in these dyes is driven by Van der Waals forces and stabilized by π-stacking of the molecule, yet the spectral shift observed in absorption is a unique phenomena of newly delocalized Frenkel excitons, with electron wavefunction distributed over often dozens of dye molecules. The first theory to understand this shift in absorption was developed by Kasha, describing the dyes as like "stacked cards" in a linear molecular aggregates. Given the strong transition dipole moment in these dyes, classical dipole-dipole coupling with scaling r^{-3} is invoked between dye molecules, shown for a planar molecular aggregate in Figure 1.1 (c). Solving a simplistic exciton Hamiltonian described by Davydov,[Dav71] it is apparent that this coupling induces bands of singlet excitons.

Kasha determined that in the case of tail-to-tail coupling of dipoles, the lowest energy exciton will also be the optically absorbing exciton, with a consistent red-shift from the momeric dye exciton absorption. Lastly, Kasha also deduced that the oscillator strength of this optically absorbing state scales like $N^{1/2}$ for N dyes participating in the excitation. This property is now known as molecular superradiance, with deep similarities to the phenomena observed in cold atoms by Dicke.[Dic54] A deep review of the theory of these systems can be found in Ref. [HS17]. Study of the delocalization and geometry dependent super-radiance of

molecular-aggregates has remained of great importance due to their observation in biological photosynthetic complexes.[CBM12]

Excitons can have interactions with with other objects to form different quasiparticles with known names, such as bound bi-excitons mentioned above. A particularly well known examples, of relevance to chapter 3, is exciton based polaritons, a hybrid photon-molecular particle. Jaynes and Cummings first mathematically described this with a Hamiltonian for independent atoms interacting with an external magnetic field, a quantum mechanical explanation to the phenomena of Rabi oscillations.[JC63] However, organic crystals and molecular aggregates are very popular system choices for the study of these kinds of polaritons, due to their giant oscillator strengths and shorter lifetimes. Polaritons in a Fabry-Perot cavity made of silver mirrors made from a single atom[TRK92] and a crystalline organic material[LBS98] were first realized in the 1990s, with essentially concurrent theoretical description.[ABW97] In these expanded models the coupling between a molecular two-level system (exciton model) and a given wavevector of light is defined by the Rabi splitting, Ω_R, and can be simplified to

$$g_{mp} = \Omega_R e^{ir_m \cdot k_p}, \ \Omega_R = 2\mu_0 \sqrt{N} \sqrt{\frac{\hbar \omega_c}{2\epsilon_0 V}}. \tag{1.2}$$

With the introduction of new light-matter physics, new physical properties emerge, demonstrating the ability of the exciton to be modified by its environment. This has lead to the discovery of ultrafast switching in polaritons,[SHG11] and lasing from room-tempurature polariton Bose-Einstein Condensates.[KF10]

An introduction to stochastic quantum chemistry: To now turn to the history of the methodology used throughout this thesis, the stochastic quantum chemistry paradigm has been developing for at least the last decade,[BNR22] but has deep roots in numerical linear algebra that date back to Lanczos in the 1950's.[Lan50] Such modern use of these ideas are now not at all limited to chemistry applications, but the use of randomizations for better algorithmic scalings in traditional linear algebra calculations have broad effects across all scientific computing.[MDM23] Central to stochastic quantum chemistry is efficient matrix

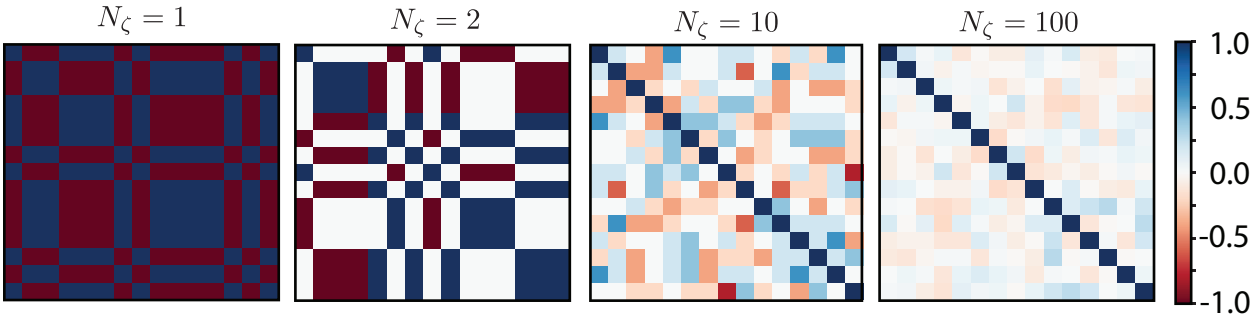

Figure 1.2: Graphical representation of the stochastic resolution of the identity with varying number of stochastic samples.

trace estimation using a set of random vectors pulled from a Randemacher distribution, i.e. a vector ± 1 at every rank with equal probability. Taking the trace, or expectation value, of an observable $\boldsymbol{A}$ with our Rademacher vectors ζ,

$$\mathrm{Tr}[A] \approx \frac{1}{N_\zeta} \sum_{N_\zeta} \langle \zeta | \, \boldsymbol{A} \, | \zeta \rangle \,, \tag{1.3}$$

one gets a estimation of the trace with minimal variance in the answer. The formal error of such a trace is $O(1/N_\zeta^2)$ and was originally shown by Hutchinson.[Hut90] The outer product over our Rademacher vectors ζ is an alternate representation of the stochastic trace central to stochastic chemistry methods: an estimated identity matrix $\frac{1}{N_\zeta} \sum_{N_\zeta} |\zeta\rangle \langle \zeta| \approx \mathbb{1}$. A demonstration of the convergence of the stochastic identity matrix is shown in Figure 1.2.

In in the early 90's the stochastic estimator branched beyond nuclear physics[Gau68, SD71] to electronic structure theory for the calculation of the density of states (DOS).[Wan94, WZ94] The additional key concept that supercharged the stochastic trace estimator was that of a polynomial expansion of the the Dirac delta function, most typically a Chebyshev polynomial expansion,

$$\delta(\boldsymbol{A} - E) \approx \sum_{N_{\mathrm{Cheby}}} c_n(E) T_n(\boldsymbol{A}'). \tag{1.4}$$

Chebyshev polynomials are preferred due to their optimal error distribution and a clean recursive formula for ease of calculations. These two methods combined, polynomial expansions

of opperators and stochastic trace, has sometimes gone by the name of the 'kernel-polynomial method' or filter-diagonalization more generally.[WWA06, Neu90a]

Summary of the contents of the subsequent chapters: In the remainder of this introduction, we do not endeavour to teach the cornucopia of electronic structure methodologies studied in this thesis, but to instead show these basic stochastic sampling techniques have been applied and updated in their application to the methodologies included in this thesis.

In Chapter 2 we apply a stochastic DOS method to the case of large micron-scale molecular aggregates. Using such an efficient method allows us to screen tens of thousands of geometrical parameters to find system conditions that most closely match experimental absorption measurements. We have applied this mass screening work in several collaborations.[DGB22, BDB23]

From the perspective of the stochastic quantum chemist, the most unique aspect of Chapter 2 is the development of a stochastic estimator for a *property of the eigenstates of the system*, rather than an estimator of the spectrum such as the trace. In Chapter 2 Eq. 2.18, we state a stochastic vector formalism for calculating the (inverse) participation ratio of the system. Defined by Thouless in the 1970's, the inverse of the participation ratio is proportional to the the fourth power of a normalized wavefunction $\psi(r)$, [Tho74]

$$\mathcal{P}^{-1} = \int dV |\psi(r)|^4. \tag{1.5}$$

For a system that is maximally delocalized, i.e. $\psi(r_i) = \frac{1}{\sqrt{dV}}$, $\mathcal{P} = V$ will be maximal for a given wavefunction. Alternatively for a Dirac delta wavefunction, $\mathcal{P} = 1$ is minimized. In molecular crystal and aggregate systems, this measure of the static disorder averaged Hamiltonian forms an excellent measure of predicted transport properties. We employ a novel stochastic formulation to extract this quantity at a given energy, summing over all eigenstates.

In Chapter 3 we extend the efficient stochastic density of states to systems of aggregate

exciton-polaritons. Central to an efficient stochastic trace estimator of this system is development of a linear scaling algorithm for applying the Hamiltonian, for generation of the recursive polynomial expansion. By noticing that light-matter coupling will always take the form of a plane wave, $H_{pm} \approx e^{ikr}$, this coupling can be applied using a Fourier transform, enabling the calculation of properties for systems of tens of millions of molecules in a multi-mode optical cavity. Additionally, we apply a stochastic trace differently in this work, using the statistical average to enable extracting the density of the systems at all angles in one shot, the so called angle-resolved transmission spectrum.

Polynomial projections of a random wavefunction is also the central concept of stochastic electronic structure methodologies, starting with stochastic DFT. A random wavefunction is projected to the occupied subspace using a polynomial filter of a smoothed Heavyside step function. Once in the occupied subspace, these wave-functions can be used to construct the density of the full system, so the Kohn-Sham Hamiltonian can be constructed for diagonalization.[NBR14a]

In stochastic GW, a many-body perturbation theory method for calculating corrected energies of a system, these stochastically filtered orbitals come to great use. Since the quantity desired, the screened Coulomb interaction W, is a property of the polarization response of the whole system, averaged TD-Hartree (TDH) propagations of a few stochastic occupied vectors can represent the polarization response of the whole density.[VRN18, VLB18a, VBR18b] In Chapter 4,we use these same stochastic TDH propogations to capture the action of the W, i.e. it's effect on a pair density

$$W_{ij}(r) = \int dr' W(r, r')\phi_i(r')\phi_j(r'). \tag{1.6}$$

In this example, $W_{ij}(r)$ is propagated with a source potential shaped by $\phi_i(r)\phi_j(r)$ rather than the whole density. Paired with an iterative Chebyshev expansion method to extract the absorption spectrum, we reduce the total cost of evaluating the spectrum of the BSE to cubic scaling.

Within this method, only the generation of the action of W is generated stochastically. Extraction of the spectrum through iteration is deterministic. Finding ways to improve the total number of W actions that are needed and faster application of the exciton Hamiltonian on a vector required more particular techniques to contain stochastic error. In Chapter 5, we introduce the optimized attenuated interaction, a translationally invariant exchange kernel $v_W(|r-r'|)$ that contains as much as possible the effect of the full $W(r,r')$ kernel. We validate this approach various multi-dimensional hydrocarbons and show how realistically, most of the effect of the screened Coulomb interaction W is a smooth function in wavevector space. Then, we enhance this method by stochastically sampling the small remainder $\{W(r,r') - v_W(|r-r'|)\}$, which allows us to capture the total BSE with a finite number of samples that does not scale with the system size.

Pleased with the performance of the optimized attenuated interaction on its own for a modified TDHF like calculation, to achieve spectra for even larger molecular systems we also needed to address the cost of explicit Fock exchange in real-space and plane wave DFT and TDDFT codes.

In Chapter 6, we draw on two stochastic tools to enable fast and memory-light full Fock exchange in ground state self-consistent field (SCF) calculations for DFT: mixed stochastic-deterministic evaluation of the action of the exchange in wavevector space [DTC19] and sparse compression of the stochastic vectors.[VLB18b] Additionally, we pull on a basis used in many time-dependent and multi-wavefunction based methodologies: "cheap" local DFT wavfunctions as a basis for "more expensive" wavefunctions. Together, this means that all possible exchange integrals are written as $(\phi_p\phi_q|v(|r-r'|)|\phi_r\phi_s)$. Under our mixed deterministic/sparse-compression, this integral is fractured by the stochastic resolution of the identity as $\sum_{N_\xi}(\phi_p\phi_q|\xi)(\xi|\phi_r\phi_s)$, where the elements of ξ originate from either a deterministic long wavelength of the grid, or a sparse snippet of high-k vectors. With such a general methodology, this can be implemented either in the ground state as in Chapter 6 or in the linear response regime as BSE or TDDFT, as is later done in collaboration.[SAB24]

In each work, we hope to demonstrate the power and versatility of the stochastic vector based estimators in quantum chemistry. Such techniques are so successful not only due to the underlying statistics, but due to careful algorithmic design that minimizes the impact of statistical error and reduces the computational cost of large calculations.

CHAPTER 2

Stochastic Simulations of Molecular Aggregates

2.1 Introduction to Simulations of Molecular Aggregates

Excitonic molecular aggregates are ubiquitous in molecular electronics and photosynthetic light harvesting systems.[BHK17] In these systems, coupling among transition dipole moments enables collective interactions with the electromagnetic field. Long-range dipole-dipole interactions induce complex and tunable photophysical properties, such as superradiance,[DSK18, SM89] exchange narrowing,[MD99] strong polarization dependent behavior,[SKO02] and long-range transport properties.[FKW93, CDE16, PCG19] Particular applications of these materials are as photo-emitters and antennas, and they are highly desired for numerous technological, medical, and biological imaging applications.[CCC19, HM08, BWB07, WWH20] Given the interest in the optical properties of these dye aggregates, approaches to rationalize and control excitonic properties aggregation are a subject of recent research.[BKS15, HS17, DKC19] Thoroughly testing design principles new aggregate complexes is difficult, as the traditional Frenkel exciton matrix diagonalization approach becomes prohibitively expensive for large systems.

Experimental and theoretical exploration of the optical properties of molecular aggregates is nearly a century old.[Jel36, Dav64, Kas63] In recent years, advances in chromophore design and self assembly has allowed for the creation of tubular and 2D aggregates which have potential as excitonic antennae.[BJK20, DKC19, CBC19] However, the slow convergence of the r^{-3} dipolar coupling necessitates calculating band structures for extremely

large systems.[CLM16] This is exacerbated in 2-D and quasi-2D tubular systems for which the number of sites grows non-linearly with system size. Without methods which treat large systems, computational studies are limited to diagonalizing Hamiltonians representing a few thousand dye monomers, and observed localization effects of disorder depend on the size of the calculation.[BJK20, DPH04] Larger systems are approached analytically with highly limiting assumptions, such as nearest-neighbor interactions or zero disorder. Probing 2-D aggregates at the length scales observed experimentally (microns),[ECB12] stochastic methods provide an appealing alternative to insurmountable diagonalization tasks.

The idea of calculating the density of states through stochastic expectation values of a polynomial approximation for the delta density operator is well established. Its foundations go back to Lanczos in 1950,[Lan88] but the essential algorithm has been significantly refined in the 1970s and 1990s in the fields of nuclear physics and quantum chemistry.[Gau68, Gau70, SD71, WB72, BW73, DS93, SR94, Wan94] Based off its numerical accuracy and ease of implementation, it has become a staple method for computation of large quantum systems, and is now often known as the kernel polynomial method.[WWA06] To date, similar stochastic methods have been applied to complex excitonic systems with similar computational requirements as molecular aggregates, like quantum dots.[Wan94, BR12]

The stochastic approach for calculating the density of states is highly suitable for our specific case of dipole-coupled dyes in ordered 2D planar or tubular systems. This is because the effective exciton Hamiltonian that needs to be diagonalized has a special form, i.e., the coupling between sites depends only on the distance between them. This makes it very efficient to calculate, in a quasi-linear scaling, the required kernel moments using convolution. An additional advantage is that the method is automatically suitable for including many kinds of energy disorder, without additional cost, as the averaging over the different disorder is included as part of the stochastic averaging of the moments.

Following earlier work on the stochastic resolution of the identity (SIR),[BN12, NRB12, NRB13, BNR13a] we show that, in addition to the calculation of the density of states,

the stochastic approach enables the calculation of a further quantity that measures exciton delocalization. This quantity, the participation ratio,[Tho74] is obtained here with the same overall scaling as the density of states.

The overall approach presented here enables extremely fast screening of aggregate geometries and disorder, unlocking rapid computation of experimentally relevant parameters optical parameters.

2.2 Stochastic Methodology Methods

2.2.1 Hamiltonian, spectra and participation ratio

We study here the Frenkel-Exciton Hamiltonian for interacting molecular chromophores,[Dav64]

$$H = \sum_n \epsilon_n |n\rangle \langle n| + \sum_{nm} J(\boldsymbol{n} - \boldsymbol{m}) |n\rangle \langle m| , \tag{2.1}$$

where n represents the site basis of an exciton localized on a single monomer. ϵ_n are the on site excitation energies. We set the average monomer excitation energy to 0 artificially to study specifically the effects of aggregation.

The primary tool by which optical properties of excitonic molecular aggregates are usually studied is through explicit construction and diagonalization of the Frenkel Hamiltonian matrix. A variety of different off-diagonal coupling functions may be used to capture the transition dipole coupling or charge transfer effects .[HS17, May11, Mer61, HKW16] The important optical properties are then assessed through several quantities defined below: optical absorption, density of states, and participation ratios.

The optical absorption coefficient (abbreviated here as optical absorption) is

$$A(\omega) = \sum_i (\boldsymbol{E} \cdot \boldsymbol{\mu})^2 \delta(\omega - \epsilon_i) \tag{2.2}$$

$$= \sum_i |\langle \psi | \phi_i \rangle|^2 \delta(\omega - \epsilon_i). \tag{2.3}$$

Here, ε_i and $|\phi_i\rangle$ are the eigenvalues and eigenvectors of H. $\boldsymbol{\mu}$ is the dipole moment operator, and $\boldsymbol{E}$ is the electric field polarization. For a system small relative to the wavelength of the absorbed radiation, the so called optically bright state $|\psi\rangle$ would be the $\boldsymbol{k} = 0$ state, with elements

$$\langle n|\psi\rangle = \boldsymbol{\mu_n} \cdot \boldsymbol{E} \tag{2.4}$$

where $\boldsymbol{\mu_n}$ is now refers to the dipole vector of an individual monomer. The $\boldsymbol{k} = 0$ state is the most studied, so it is what we restrict to in this paper, though the systems are large enough that full consideration beyond the dipole limit may be appropriate for future work.

The density of states is,

$$\rho(\omega) = \mathrm{Tr}[\delta(H - \omega)] = \sum_i \delta(\varepsilon_i - \omega), \tag{2.5}$$

and the participation ratio is defined as,

$$\mathcal{P}(\omega) = \frac{\rho(\omega)}{K(\omega)}, \tag{2.6}$$

where

$$K(\omega) \equiv \sum_i \delta(\varepsilon_i - \omega) \sum_n |\langle n|\phi_i\rangle|^4. \tag{2.7}$$

Average aggregate properties should be estimated by many realizations of the Hamiltonian with different disorder. This additional cost further reduces the maximum practical aggregate size that can be studied using direct diagonalization.

2.2.2 The Chebyshev expansion

As mentioned, in this paper we use a stochastic trace of the delta density operator to retrieve the density of states. Before we can take the trace, the delta function is first numerically implemented with Gaussian regularization.[WWA06] One can realize the gaussian regularization as a gaussian linebroadening on the tradition time correlation function, from which the density of states is directly related by a transform.

$$\rho(\omega) = \sum_i \langle\phi_i| \int dt\, e^{-iHt} e^{i\omega t} e^{\gamma^2 t^2/2} |\phi_i\rangle = \sum_i \frac{1}{\gamma\sqrt{\pi}} \langle\phi_i| e^{-(H-\omega)^2/\gamma^2} |\phi_i\rangle \tag{2.8}$$

For practical calculation, the regularized density operator is defined through the Chebyshev polynomial expansion [Kos88]

$$F(\omega) = \frac{1}{\gamma\sqrt{\pi}} e^{-(H-\omega)^2/\gamma^2} = \sum_{\ell=0}^{N_{Chebyshev}} c_\ell(\omega) T_\ell(H') \tag{2.9}$$

and of course in the small γ limit, $F(\omega) \to \delta(H-\omega)$. Here, $T_\ell(H')$ is the ℓ'th Chebyshev polynomial of a linearly scaled Hamiltonian $H' = (H - \bar{h})/\Delta H$ constructed so that its eigenvalues are within the interval $[-1, 1]$; $\bar{h}$ is an estimate for the center of the spectrum of H, and $2\Delta H$ is an upper bound for its spectral width. $N_{Chebyshev}$ is the required number of Chebyshev polynomials, which is proportional to $\Delta H/\gamma$.

As discussed later, the coupling in the Hamiltonian only depends on the difference of position between sites, so if there is no disorder ΔH can easily be shown to be given from a 2D Fourier transform of the elements in the Hamiltonian. Accounting for the effect of the disorder, we enlarge the spectral width by a factor to ensure the stability of the Chebyshev expansion.

The scalar Chebyshev coefficients are calculated using the transform $\theta = \cos^{-1}(x)$.

$$c_\ell(\omega) = \frac{1}{\sqrt{\pi}\gamma} \int_{-\infty}^{\infty} dx \frac{e^{-(\Delta H x - \bar{h} - \omega)^2/\gamma^2} T_\ell(x)}{\sqrt{1-|x|^2}} \tag{2.10}$$

$$= \frac{2-\delta_{\ell,0}}{\sqrt{\pi}\gamma} \int_0^{2\pi} d\theta e^{-(\Delta H \cos\theta - \bar{h} - \omega)^2/\gamma^2} e^{i\ell\theta}. \tag{2.11}$$

The coefficients are then calculated via Eq. (2.11) using a fast Fourier Transform (FFT).

2.2.3 Absorption Spectrum

From Eq. (2.2), the absorption spectra is calculated with the Chebyshev expansion using only the optically absorbing bright state

$$A(\omega) = \langle\psi| F(\omega) |\psi\rangle . \tag{2.12}$$

This expectation value can be calculated for each coordinate of the electric field, $\boldsymbol{E}$, and therefore a bright state along each coordinate can be defined via (Eq. (2.4)). This gives

the dichroism response. An important thing to note as, since we know the $\boldsymbol{k} = 0$ wavefunction, $|\psi\rangle$, we only need our propagator to find the absorption correlation function, and no additional stochastic methods are required besides averaging over instances of the diagonal disorder. Note that if we were to consider $\boldsymbol{k} > 0$ the full absorption could still be obtained through a trace formula with the addition of a spatial filter (See SI).

2.2.4 Stochastic Density of States

To take the trace of the moments operator, a stochastic state is introduced, which Monte-Carlo samples a complete basis for H (see Ref.[Wan94]). The stochastic excitation has a random ± 1 amplitude at each site, $\zeta(n) \equiv \langle n|\zeta\rangle = \pm 1$. Thus, the DOS is calculated directly as

$$\rho(\omega) = \Big\{ \langle\zeta|\, F(\omega)\, |\zeta\rangle \Big\} = \sum_{\ell} c_\ell(\omega) R_\ell, \tag{2.13}$$

where curly brackets are introduced to represent a classical expectation value over the random excitations, and the kernels are

$$R_\ell \equiv \Big\{ \big\langle \zeta \big| \zeta^\ell \big\rangle \Big\}, \tag{2.14}$$

where we defined the Chebyshev vectors,

$$\big|\zeta^\ell\big\rangle \equiv T_\ell(H')\, |\zeta\rangle \tag{2.15}$$

obtained recursively by the usual Chebyshev recursion relation, $\big|\zeta^\ell\big\rangle = 2H' \big|\zeta^{\ell-1}\big\rangle - \big|\zeta^{\ell-2}\big\rangle$.

The proof of Eq. (2.13) follows once we expand the random vector in terms of the site basis set $|\zeta\rangle = \sum_n \zeta(n)\, |n\rangle$, and use $\{\zeta(n)\zeta(m)\} = \delta_{nm}$. This approach to the density of states converges rapidly with the line broadening parameter γ, and is memory friendly, as one stores only the kernels and coefficients.

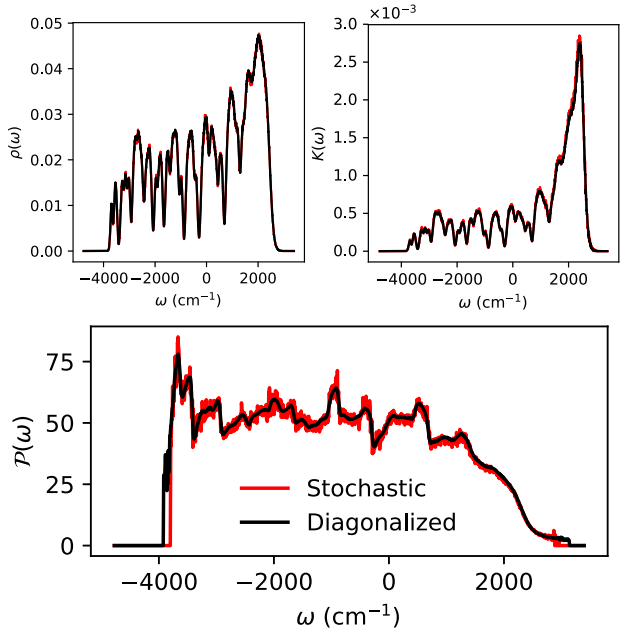

Figure 2.1: Demonstration of the accuracy of the stochastic resolution of the participation ratio. Top left is the density of states, top right the denominator of the participation ratio $K(\omega)$, and the participation ratio is shown at the bottom. A small system of $N = 15\times9 = 135$ monomers is simulated here with $N_{stochastic} = 5 \times 10^5$ samplings (of ζ and the noisy diagonal energies, with disorder $\sigma = 400\,\mathrm{cm}^{-1}$ and no site-to-site correlation of the diagonal energies). In accordance with the small γ limit necessary for the accuracy of the ratio, we used $\gamma = 2\,\mathrm{cm}^{-1}$ and $N_{Chebyshev} = 16384$. The very high-wavelength fluctuations are due to stochastic error, and can be flattened either by more samplings or by explicit smoothing.

2.2.5 Stochastic Participation Ratio

To have a fully stochastic expression for the participation ratio, we need a stochastic formalism that samples the fourth power of the eigenvectors accurately, i.e., the denominator of Eq. (2.6). This is done here analogously to the stochastic estimation of the exchange and MP2 energies.[BN12, NRB12, GGB13, NRC15a]

For a given broadening parameter, γ, we first pick two independent random vectors, $|\zeta\rangle$ and $|\xi\rangle$, each defined similarly to the random vector in the previous section with ± 1 at each grid site. We then define filtered-vectors:

$$\left|\bar{\zeta}(\omega)\right\rangle \equiv F^{1/4}(\omega)\,|\zeta\rangle\,, \quad \left|\bar{\xi}(\omega)\right\rangle \equiv F^{1/4}(\omega)\,|\xi\rangle\,, \tag{2.16}$$

where $F^{1/4}(\omega) = \frac{1}{\gamma^{1/4}\pi^{1/8}} e^{-(H-\omega)^2/4\gamma^2}$. These vectors are calculated using Eq. (2.9), i.e.,

$$\left|\bar{\zeta}(\omega)\right\rangle = \sum_{\ell} \bar{c}_{\ell}(\omega)\left|\zeta^{\ell}\right\rangle. \tag{2.17}$$

Here, $\bar{c}_{\ell}(\omega)$ are the Chebyshev coefficients associated with $F^{1/4}(\omega)$. Given the filtered vectors, the stochastic expression for the denominator in Eq. (2.6) is $K(\omega) = \lim_{\gamma\to 0} K_{\gamma}(\omega)$ where

$$K_{\gamma}(\omega) = \Big\{\sum_{n} \left|\left\langle n\middle|\bar{\zeta}(\omega)\right\rangle \left\langle n\middle|\bar{\xi}(\omega)\right\rangle\right|^2\Big\}. \tag{2.18}$$

To prove this expression, we first formally expand each vector in terms of the complete basis of eigenstates of H,

$$|\zeta\rangle = \sum_{i} a_i\,|\phi_i\rangle\,,\ |\xi\rangle = \sum_{j} b_j\,|\phi_j\rangle\,, \tag{2.19}$$

where $a_i \equiv \langle\phi_i|\zeta\rangle$, etc. While the coeficients a_i do not have a closed form like the elements of $|\zeta\rangle$, they remain uncorrelated ($\{a_i a_j\} = \delta_{ij}$) due to their construction from $|\zeta\rangle$. We also define

$$f_i(n) = \langle n|\,F^{1/4}(\omega)\,|\phi_i\rangle = \delta^{1/4}(\epsilon_i - \omega)\phi_i(n)$$

without explicitly denoting the ω dependence of $f_i(n)$.

Plugging to the expression for $K_\gamma(\omega)$, we get

$$K_\gamma(\omega) = \sum_n \sum_{ijkl} \left\{ a_i a_j b_k b_l \right\} f_i(n) f_j(n) f_k(n) f_l(n) \tag{2.20}$$

and using

$$\{a_i a_j b_k b_l\} = \{a_i a_j\} \cdot \{b_k b_l\} = \delta_{ij}\delta_{kl}, \tag{2.21}$$

leads to

$$\begin{aligned} K_\gamma(\omega) &= \sum_n \left(\sum_i \left(f_i^{1/4}(n) \right)^2 \right)^2 \\ &= \frac{1}{\gamma\sqrt{\pi}} \sum_n \sum_{ij} e^{-(\varepsilon_i-\omega)^2/2\gamma^2} e^{-(\varepsilon_j-\omega)^2/2\gamma^2} \left\langle n|\phi_i \right\rangle^2 \left\langle n|\phi_j \right\rangle^2 \end{aligned} \tag{2.22}$$

and taking the limit $\gamma \to 0$ and in the limit of any disorder to break eigenstate degeneracies,

$$\begin{aligned} K(\omega) &= \lim_{\gamma\to 0} \frac{1}{\gamma\sqrt{\pi}} e^{-(\varepsilon_i-\omega)^2/2\gamma^2} e^{-(\varepsilon_j-\omega)^2/2\gamma^2} \left\langle n|\phi_i \right\rangle^2 \left\langle n|\phi_j \right\rangle^2 \\ &= \delta_{ij}\delta(\varepsilon_i - \omega). \left\langle n|\phi_i \right\rangle^4, \end{aligned} \tag{2.23}$$

finally leading to Eq. (2.7), as stipulated.

The estimate for the denominator in the participation ratio, Eq. (2.18), converges well statistically, since it is an average of positive definite quantities, but its γ dependence relates to the system size and disorder strength:

- For small N the accuracy of the overall participation ratio depends much more strongly on reaching the small gamma limit than for the density of states alone, as shown in Fig. 2.1.

- In contrast, for large N (beyond 10^4) the participation ratio converges rapidly with the number of stochastic samples and with gamma, due to self-averaging and the fact that different states have little spatial overlap. Put differently, the $i \neq j$ terms in Eq. (2.23) become minuscule due to the reduced overlap of eigenvectors for large systems, not just due to being a sum over spatially destinct Gaussians at small γ. For further details, see Figure S2.

A complication in the participation ratio calculation is that memory-constraints rather than CPU time usually limit the fesible system size, N. This is due to the need to store the set of $\left|\bar{\zeta}(\omega)\right\rangle$ vectors, of size $N_\omega \cdot N$, which for a large system quickly reaches gigabytes of CPU memory per core if significant resolution across the band is desired.

2.2.6 Choice of Coupling Function

An underlying key element of the iterative stochastic approach is the use of a Hamiltonian with off diagonal components that depend only on the distance between sites, or difference of indices, and the use of a perfect lattice. This makes it feasible to apply the Hamiltonian on a vector with quasi-linear cost. Specifically, here we use the point dipole approximation,

$$J(\boldsymbol{n}-\boldsymbol{m}) = \frac{\boldsymbol{\mu_n}\cdot\boldsymbol{\mu_m}}{|\boldsymbol{r_{nm}}|^3} - 3\frac{(\boldsymbol{\mu_n}\cdot\boldsymbol{r_{nm}})(\boldsymbol{\mu_m}\cdot\boldsymbol{r_{nm}})}{|\boldsymbol{r_{nm}}|^5} \tag{2.24}$$

with $\boldsymbol{r_{nm}} = \boldsymbol{r_n} - \boldsymbol{r_m}$. Eq. (2.24) is applied to aggregates with both planar and tubular geometry.[CBC19, DKK02, DPH04] Fig. 2.2 contains a diagram showing how the coupling is constructed from the aggregate geometry. System geometry is further discussed in the SI.

For perfect toroidal boundary conditions, the Frenkel Exciton Hamiltonian, Eq. (2.1), forms a block circulant matrix, with block sizes N_x and N_y, and is thus diagonalized by a 2D Fourier Transform.[1] At sufficiently large block sizes, perfect periodic boundaries (toroidal) do not impose an issue with self coupling. Multiplication by a block circulant matrix is done by the two dimensional convolution theorem,

$$b_j = (Ha)_j = \sum_i H_{ji}a_i = \epsilon_j a_j + \sum_i J(\boldsymbol{i}-\boldsymbol{j})a_i \tag{2.25}$$

$$= \epsilon_j a_j + \mathcal{F}^{-1}[\tilde{J}(\boldsymbol{k})\mathcal{F}[a]] \tag{2.26}$$

[1]This is formally true if N_x and N_y are odd, due to the even nature of the coupling functions. For sufficiently large N_x and N_y the phase introduced by an even number of samples is suppressed below machine error. Thus for small systems, products of small odd primes are suggested, but divisors of 2 are acceptable for macroscopic systems.

where $\mathcal{F}$ represents the Fourier transform. Open boundary conditions, such as in the most recent computational work on tubular aggregates,[BJK20] can be achieved via zero-padding of the coupling matrix.

Stochastic fluctuations in the direction of the dipoles will easily be extended by treating ζ as a $3N$ vector, where each site is weighted by the 3 elements of $\boldsymbol{\mu^i}$, and the coupling is the $3N * 3N$ dipole tensor. Short-range fluctuations in the J_{ij} elements are easily included explicitly, i.e., $J_{ij} = J_0(i-j) + \delta J_{ij}$, where J_0 labels now the perfect coupling from above, and the action of δJ_{ij} on a vector is taken explicitly.

Large-range fluctuations are more challenging and potentially more interesting, since they interfere with the long-range dipole which is a dominant mechanism in 2D sheets. They would be taken care of by our resolution-of-the-identity approach; essentially $\delta J_{ij} = \{\xi(i)\xi(j)\}$ where ξ is constructed to yield the required statistics, and would be guided by ab-initio. In practice, we will access such fluctuations by calculating the correlation function with a split operator approach, so that at every time step the action of $e^{-idt\cdot\delta\hat{J}}$ on a vector amounts to essentially $(1 - i\delta t|\xi\rangle\langle\xi|)$, and ξ is chosen stochastically at every time step.

2.2.7 Overall Algorithm Scaling

The main numerical CPU cost is due to the repeated application of the Hamiltonian ($N_{Chebyshev}$ times) and specifically the convolutions parts, costing in FFT about $10N\log_2(N)$ each time. In addition, when we calculate the participation ratio we need to accumulate frequency-resolved Chebyshev vectors. Thus the total cost is approximately

$$N_{opperations} = N_{Stochastic}N_{Chebyshev}N\Big(10\log_2(N) + N_\omega\Big) \tag{2.27}$$

The Monte-Carlo sampling is done in parallel on each node (using MPI) with every node starting from a different random excitation.

The scaling is exemplified in Fig. 2.3. Both $N_{Chebyshev}$ and $N_{Stochastic}$ do not scale up with N, so the algorithm scales quasi-linearly with N. Specifically:

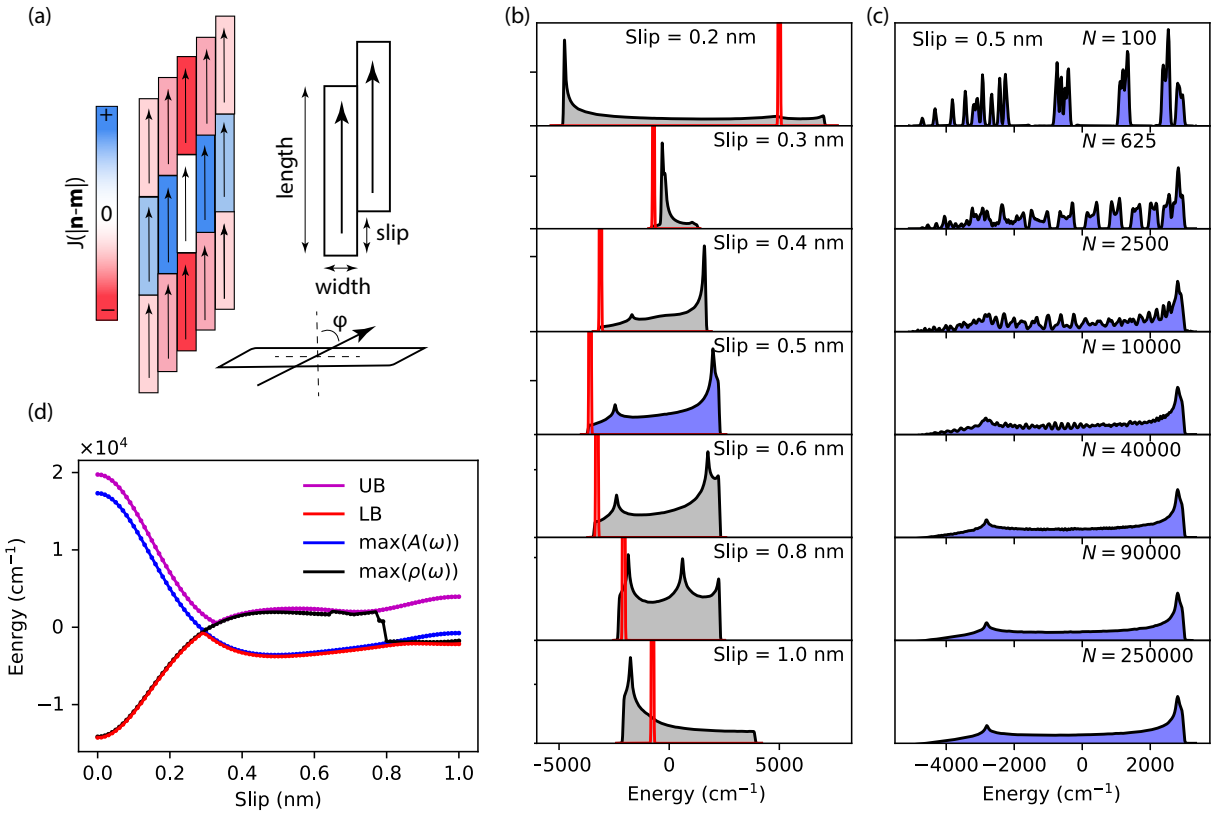

Figure 2.2: (a) Diagram of section of 2D planar aggregate. The relative coupling strengths for near neighbors of a given site are shown by different colors. (b) DOS (grey) and Absorption spectra (red) for various slip values. Standard geometry parameters of length and width of 2nm and 0.4nm respectively are used for all aggregates (see SI).[CBC19] (c) Examples of the Slip=0.5 planar DOS for different system sizes. As with all calculations, we have done perfect toriodal lattice boundary conditions. Fluctuations in the center of the DOS still appear at system sizes of about 10,000. Further driving the need to simulate big systems, or use artificial boundary conditions. Mild disorder of 50 cm^{-1} is additionally used to help smooth out the DOS. (d) Scan across 100 slip values, showing the upper (UB) and lower (LB) band edges as well as the position of the absorption peak and position of the tallest Van Hove peak.

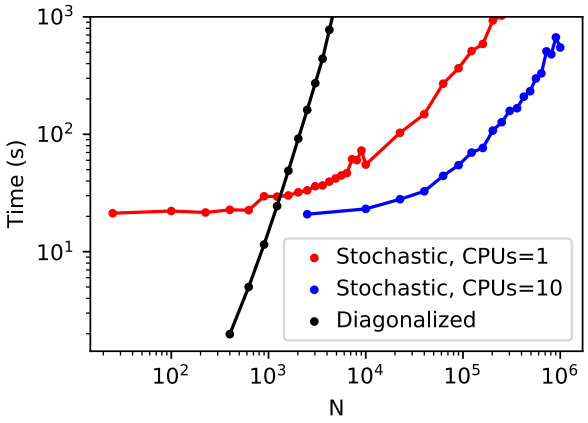

Figure 2.3: Timing test on the program that calculates absorption and density of states, comparing a single core (red) and ten cores (blue). For very small systems, the time is approximately constant, and then scales like $\propto N \log(N)$ for larger systems. For all calculations $N_{stochastic} = 10$ and $N_{Chebyshev} = 4096$, which is enough to converge the integral density of states to the exact value of N. Small wiggles in the timing are due to the different relative efficiency of the FFT package used, FFTW3,[FJ05] at different array sizes. For the diagonalization method, the full dimension $N \times N$ hermitian Hamiltonian matrix is constructed, diagonalized, and the density of states is calculated from the eigenvalues. Only a single instant of diagonalization (no disorder) is considered here. All times were recorded with the Linux 'time' command on an AMD EPYC 7452 32-Core Processor at 3 GHz.

- N_ω is fixed for constant resolution, since ΔH does not really scale with system size.

- $N_{Chebyshev}$ is about $5\frac{\Delta H}{\gamma} \sim 2000 - 8000$. For most of these aggregate systems without extreme disorder, the spectral width is on the order of about $10^5\,\mathrm{cm}^{-1}$, while the spectral line width, γ, need only be about as good as one could achieve experimentally, i.e., $\approx 1\,\mathrm{cm}^{-1}$ or larger. Note that our choice of using the most studied point dipole coupling function is known to overestimate nearest-neighbor couplings, and thus the spectral width.[DKC19] One would expect a decrease in the number of coefficients with more sophisticated or system specific coupling functions.

- In the regime of disorder studied, $N_{Stochastic}$ does not scale with system size. In fact, due to self averaging in large systems the error goes like $\propto 1/\sqrt{NN_{Stochastic}}$,[Wan94, WWA06], so $N_{Stochastic}$ is reduced commensurately with the system size.

2.2.8 Disorder

A key feature of a Monte-Carlo based approach is the ability to vary multiple input parameters at once and still sample the general spectrum. As such, disorder poses no new additional cost to the algorithm, in which we sample a new realization of the diagonal disorder and a new random eigenstate, ζ, simultaneously and compute one classical average over both disorder and random eigenstates at the end of the calculation. We study the most common kind of disorder, diagonal site disorder ϵ_i. Latter papers will study the effects of disorder in the dipole direction and of deviations from the ideal lattice positions.

The simplest model of diagonal-site disorder is non-correlated noise, usually via a normal distribution of standard deviation σ. More sophisticated models introduce correlations into the site disorder. Specifically, the study of the effects of exponentially correlated site disorder is known as Knapp's model in molecular aggregates.[HS18] Knapp suggested that correlation in disorder may be important in organic molecular aggregates, modeling lattice defects and mixtures with glasses, and strong low-frequency exciton-phonon coupling where there is no

resolvable vibronic structure.[Kna84] Such a strongly coupled low energy phonon mode was indeed recently observed in light-harvesting nanotube aggregates, prompting new interest in correlation in two dimensional and tubular aggregates.[PCC18]

Computational work on correlated disorder has a rich literature in one-dimensional systems,[IKM12, Kno93, Spa05, SCS09] and recent work on two-dimensional nearest-neighbor lattices.[Mou10] Correlation has yet to be studied in large non-biological aggregate systems, or in two dimensional systems with full coupling. Studies of correlated disorder in 1D and higher dimensions have long suggested that localized states may exist at all levels of disorder.[DKP89, FKW91]

In photosynthetic systems, there are common claims that small-scale correlated fluctuations may effect their emissive properties. The most heavily studied model is the Fenna–Matthews–Olson (FMO) complex, in which long lived quantum coherences between chromophores suggest relevant spatial correlations between chromophores.[LCF07, FCH12, PHF10] Similarly long lived quantum coherences due to spatial correlation in multi-exciton dynamics have been observed in quantum dots.[CZD13, CPM15, PNF17] These experiments all suggest relevant correlation length scales of sub-nm scale or smaller.

There have been studies using mixed quantum and classical photosynthetic systems showing the effects of intersite correlation .[OSS11] Few-state quantum mechanical models, similar to the calculations done here (but for much smaller scales), show large influence of even small correlations between chromophores, and agree qualitatively with the experimentally observed lifetimes and coherences.[AM11, HC12, RMA09] Without an experimentally solved system structure and the difficulty in treating these large aggregate systems quantum mechanically, the full significance of intersite correlation has not been yet known.

In this work, we apply correlation through convolution.[AM11] Any correlation functions that strictly decreases with distance can be studied with this method. A strictly decreasing correlation function implies that its Fourier transform is positive, and the existence of the square root of the covariance matrix. In either case, we assume that the disorder covariance

matrix is block circulant (as is the Hamiltonian)

$$C_{ij} = \langle \varepsilon_i \varepsilon_j \rangle / \langle \varepsilon_i^2 \rangle = e^{-r_{ij}/R} \tag{2.28}$$

so that it is diagonalized by a 2D plane-wave Fourier-transform matrix, with eigenvalues denoted by g.

$$C = \mathcal{F}^{-1} g \mathcal{F}. \tag{2.29}$$

Correlated noise is then generated with convolution with $\sqrt{C}$.

$$\boldsymbol{\varepsilon} = \boldsymbol{\varepsilon_0} * \sqrt{C} = \mathcal{F}^{-1}[\sqrt{g} \cdot \mathcal{F}[\boldsymbol{\varepsilon_0}]] \tag{2.30}$$

and $\boldsymbol{\varepsilon_0}$ is the initial uncorrelated normal disorder with standard deviation σ.

In the infinite space limit, $\sqrt{g}$ is the square root of the Hankel transform of the exponential decay $\approx \sqrt{\frac{2\pi}{Rlw}}(R^{-2} + |\boldsymbol{k}|^2)^{-3/4}$. For small correlation lengths it is better to numerically FFT the desired convolution matrix, rather than simply use the infinite lattice functional form of $\sqrt{g}$, to avoid edge effects in the correlation.

2.3 Results and Discussion

Through a series of simple applications we show the power of a stochastic approach in describing molecular aggregates. Our studies include a scan of the point dipole coupling function parameter space in Fig. 2.2, efficiently reproducing the earlier deterministic results of Chuang et al.[CBC19]

Fig. 2.3 demonstrates the speed of the method for very large systems. The stochastic method has a roughly constant cost for small systems (where the time is dominated by the cost of extracting the Chebyshev coefficients), and the cost only rises mildly once N is beyond a thousand side. While Fig. 2.3 shows the same calculation for a fixed number of stochastic samples, the true scaling is better than linear due to self-averaging, i.e., fewer stochastic orbitals are needed for larger systems to achieve the same level of stochastic error in $\rho(\omega)$ and $\mathcal{P}(\omega)$.

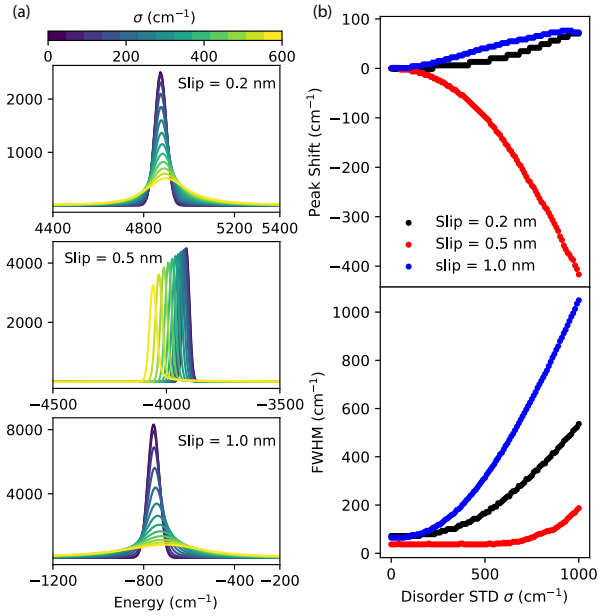

Figure 2.4: (a) Absorption lineshapes at varying degrees of disorder, with the same system setup as in Fig.2.2. (b) The maximum absorption peak shift and FWHM of a H, J, and I planar aggregates of Slip = 0.2, 0.5 and 1.0 nm respectively. For the Slip = 0.5 nm band-edge J aggregate, a scaling power law of FWHM $\propto \sigma^{2.1}$ was observed.

Simulating a single "sampling" of a typical 2D aggregate with half a million monomers, as in Fig. 2.2, takes a mere five wall minutes on a single node. Ten such stochastic samplings (each on its own core) are sufficient for converging the DOS and absorption cross section with the full effect of disorder to within a percent at each frequency. Each of these samplings uses a different stochastic vector ζ and a different diagonal energies. Such a system is about two order of magnitudes larger than systems that could be studied with numerical diagonalization on any current computing system. Whether it be geometry, or disorder (Fig. 2.4), a key point of the demonstrated application of this method is the ease of screening through parameter space.

In Fig. 2.4 we track the width and position of the absorption spectra at varying magnitudes of on-site disorder (without correlation). When beyond the exhange narrowing small-

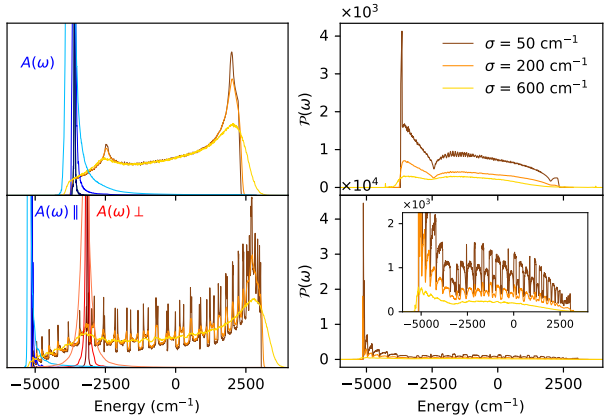

Figure 2.5: Density of states (left) and participation ratios (right) for macroscopic systems at three different levels of disorder for a band edge planar aggregate (top) and the equivalent tubular aggregate (bottom). Incresing color lightness is signifies increasing system disorder. $N \approx 5 \times 10^4$. For the tubular aggregate, a low disorder value, 50 cm^{-1}, is not strong enough to destroy a fully delocalized bright state, while the planar aggregate is not able to support such a delocalized state. These calculations were performed with $\gamma = 2\,\mathrm{cm}^{-1}$, and have not been interpolated to the $\gamma \to 0$ limit.

N regime (as demonstrated in Figure S2), our method produces non-linearities in the peak width that are similar to previous 2D tubular simulations[DSK18, BJK20] and well established scalings for 1D Kasha aggregates.[MM01] Since the power law exponent scaling of the width is sensitive to the underlying geometry (slip), this method may be used as a tool for designing aggregates for particular optical properties.[TSB17, BKS15].

Moving beyond the kernel approach for absorption spectra and density of states, we show in Fig. 2.5 the participation ratio for large aggregates with both tubular and planar geometry. This is the first simulation that can access an eigenvector-based observable like the participation ratio for very large systems, and also the largest participation ratio calculations for molecular aggregate systems. The figure shows that the tubular geometry is able to support a largely delocalized bright state at the higher levels of disorder of 50-200 cm^{-1},

while such a state is not observed in a planar aggregate for those parameters. Controlling the system localization is important for potential applications of these aggregates as photo-emitters,[HM08] and this work is merely a beginning for full exploration of the model space with the stochastic approach.

In Fig. 2.6, we apply correlated disorder to a 2D planar aggregate and track the properties of the absorption spectra, fully mapping out the disorder strength and correlation space. This figure demonstrates that even small correlation lengths extending over just a few monomers can have a drastic effect of the observed width on the absorption spectrum. Previous studies on the effect of local inter-site correlation in 1D molecular aggregates has discussed the change to absorption width in terms of the small-N phenomena of motional narrowing.[Kno93, Kna84] Given how different the landscape and coupling of the 2D aggregate systems is compared with 1D and the change to the large N limit,[DKC19] a new mechanism is needed to explain the effect of short length correlation.

2.4 Conclusion

This work shows that a stochastic approach rapidly yields the DOS, absorption, and participation ratio for large and disordered molecular aggregate systems over the full range of frequencies. We demonstrated the ability to efficiently screen the large modeling parameter space for these systems, and accurately model realistic micron-scale systems of up to a million monomers with the ability to extend to even larger systems if needed. A new stochastic approach was introduced to model delocalization via the participation ratio, going beyond previous work with the DOS.

This work adds to the current knowledge of 2D and tubular molecular aggregates. We map out the entirety of the parameter space due to varying the lattice angle (Slip), and the effects of disorder and correlated disorder on the optical spectrum. We find that the effect of correlation on the absorption is strong even at short length scales, and is not separable

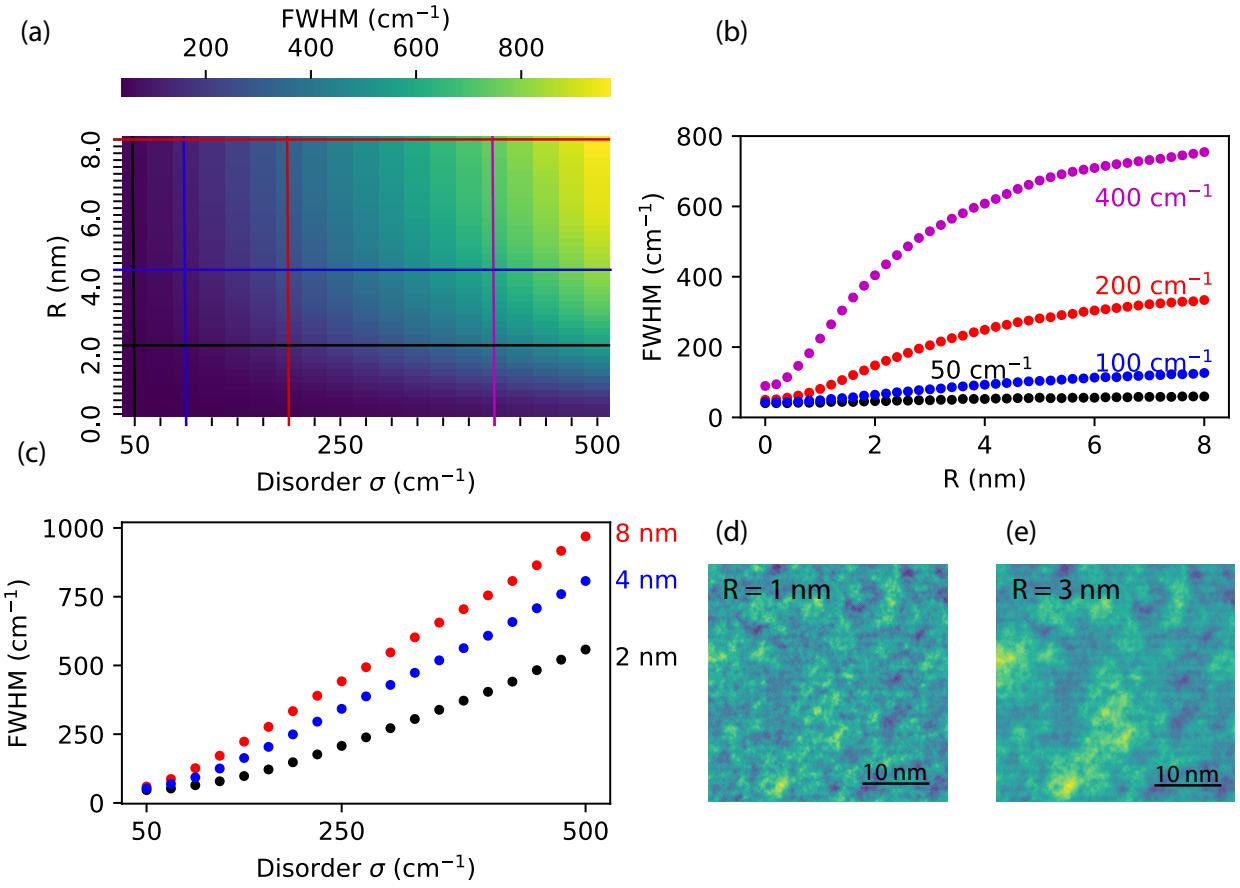

Figure 2.6: The width (FWHM) of the absorption spectra at varying disorder strengths and exponential correlation lengths. The full parameter space is mapped out in (a), while curves of constant disorder are shown in (b), and constant correlation (c). (d) and (e) show an instance of exponentially correlated disorder at two different correlation lengths, as generated by the same random seed. We observe that σ is not a separable variable from R, and a more complicated re-normalization is occurring. Calculations were done on a square planar aggregate of $N = 243 * 1215 \approx 2 \times 10^5$ corresponding to a real space side length of $48.6nm$.

from the strength of the disorder.

Future extensions of the stochastic method presented here would tackle more challenging dynamic optical properties that are not be feasible for large systems with a deterministic approach. Sample applications include time-dependent treatment of exciton lifetime, coherences, and diffusion,[CLM16] system environment and vibronic bath effects,[PCC18], or a multi-excitonic basis looking at transport and recombination properties.[TJK17]

2.5 Appendix

2.5.1 Stochastic Absorption beyond the Dipole Approximation

Calculating the absorption beyond the dipole approximation requires filtering of the collective dipoles of each exciton to obtain the eigenstate at a particular wavevector $\mathbf{k}$. Stochastically, we will extract the k-dependent information by starting with spatially random state and filtering them, spatially, after the frequency filtering, i.e.,

$$A_{\boldsymbol{k}}(\omega) \propto \Big\{ \langle\zeta|\ \boldsymbol{\mu}\cdot\boldsymbol{\epsilon}\, P_{\boldsymbol{k}}\, \delta(H-\omega)\, \boldsymbol{\mu}\cdot\boldsymbol{\epsilon}\, |\zeta\rangle \Big\}, \tag{2.31}$$

where $P_{\boldsymbol{k}} = |\boldsymbol{k}\rangle\langle\boldsymbol{k}|$ is a spatial filter at the wavevector $\boldsymbol{k}$. Thus, we will apply a delta Chebyshev filter to select for frequency-selected eigenstates followed by a spatial filter that selects for overlap with the applied wavevector of the radiation. Dichroism can similarly be extracted as we do under the dipole approximation in the main section.

CHAPTER 3

Exciton-Polaritons with Large Molecular Aggregates

3.1 Introduction to Exciton Polaritons

Experiments have shown that photophysical and even chemical properties can be modulated by optical cavities, leading to promising potential applications across chemical and materials science domains. [CSM14, RMG18, DKP21, ZCW16, ZCZ17, MDR18] Thus far, many different types of substrates have been demonstrated with strong electronic coupling to cavities, including semiconductor crystals, molecular aggregates, and organic polymers. Despite this breadth, treatments of experimental data typically rely on the simple Tavis-Cummings Hamiltonian,[TC68] which neglects direct intermolecular interactions between emitters. Any complete description of light-matter interactions should account for the often complex DOS availed by extended matter.

Furthermore, even when multiple molecules are considered, most theoretical studies of molecular polaritons only represent the electromagnetic field with a single boson mode. For system sizes up to a few dozen molecules, high level theoretical methods accurately reproduce simple optical observables. [TMS22, CY22, CLH22]. However, with the inclusion of long-range coupling, 'giant' systems are needed to predict accurate delocalization and transport properties.

Intermolecular interactions and multiple photonic modes are especially important for molecular aggregates and related biological light harvesting systems– all of which have strongly internal-structure-dependent collective superradiant properties. This is especially

true in J-aggregates, one of the first studied systems that can form molecular optical polaritons.[Kas63, LBS98] The energy transfer properties in J-aggregates relate to internal geometry and the corresponding electronic band structure. [CDE16] Interestingly, tight-binding models suggest strong light-matter coupling can be employed to manipulate spectral and transport properties of dark exciton states (i.e. states with low photonic content). [BHS20, Sch20, Rib22, AW22, EC22, ZCS22, AKR23]

The importance of using a full multi-mode cavity is highlighted in recent works. [ALL03, MR05, AG07, TFG21, Rib22, EC22, MXM23, EC23, AKR23] For example, it was shown in red detuned devices the anticrossing between optical and exciton modes is shifted to higher wavevectors, protecting a greater fraction of lower polariton states from localization induced by static molecular disorder. [MR05, LR06, Rib22, SR23] Thus, a many-mode cavity representation is essential for a rigorous investigation of disorder-resistant transport in polaritonic materials.

Here we apply an extremely efficient linearly-scaling stochastic approach to study polaritons in large micron-sized multi-mode cavities containing two-dimensional (2D) molecular aggregates/crystals with tens of millions of molecules. Stochastic trace techniques[BCD20] are used to visualize the density of states (DOS), participation ratio, and angle dependent transmission. Our main finding is that the aggregate structure drastically affects the disorder-dependent properties of the resulting cavity-induced polaritons and weakly coupled states, including lineshapes and delocalization measures. These results reinforce that inaccurate characterization of the intermolecular interactions will yield poor results in describing photophysical and transport properties of molecular agreggates in the strong coupling regime.

To show the importance of the intermolecular coupling and its effects on the observables of the traditional Tavis-Cummings Hamiltonian, we employ the J-aggregate transition dipolar coupling as a minimal model that both shows this effect and has direct experimental parallels. The band-like delocalized density of states in J-aggregates leads to fundamentally different light-matter density of states in the strong coupling regime as shown in the cartoon of Fig.

3.1 A. In the SI, we analyze another case, I-aggregation [DGB22], where there are dark molecular exciton states lower in energy than the collective aggregate peak at $k = 0$, leading again to distinct exciton delocalization properties relative to J-aggregates. The methods presented here are also applicable to any material where the intermolecular interactions are translationally invariant, such as most semi-empirical semiconductor Hamiltonians.

3.2 The Exciton-Polariton Hamiltonian

Our starting point is a dielectric cavity of thickness L_C, encompassed by two ideal mirrors. We only consider the lowest band of photon modes with $q_z = \pi/L_c$, and the s and p polarizations have the same dispersion, $\omega(q_\parallel) = \frac{\hbar c}{\sqrt{\varepsilon_c}}\sqrt{q_\parallel^2 + \frac{\pi^2}{L_C^2}}$, where the zero-wavevector energy, $\omega_0 = \omega(q_\parallel = 0) = \frac{\hbar c}{L_C\sqrt{\varepsilon_0}}$, is almost matched to E_0, the transition energy of the molecular (dye) exciton, with a detuning $\Delta \equiv \omega_0 - E_0$. The empty cavity Hamiltonian is ($\hbar = 1$)

$$H_C = \sum_q \sum_{\lambda=s,p} \omega(q) a_\lambda^\dagger(q) a_\lambda(q). \tag{3.1}$$

A dielectric slab, either an ordered molecular aggregate or a crystal, with small thickness relative to L_C (Fig. 3.1), is then placed inside the cavity, along its center plane to enhance the light-matter coupling [KRE65, HS18]. The dyes are placed on a 2D lattice, with crystal vectors defined as $a_1 = (0, l)$, $a_2 = (w, s)$, and the lengths of the molecular aggregate are $L_x = wN_x$, $L_y = lN_y$; the cavity volume is $V_C = L_x L_y L_C$. On each 2D site j a dye is placed, with a transition dipole μ_j and an excitation energy E_j, shown in Fig. 3.1 B. The dipoles are presumed planar, all pointing in the same direction, here taken to be the y axis, so $\mu_j = \mu_0 \equiv \hat{y}$. We assume that the photons and molecule systems share the same Brillouin zone, and share periodic boundary conditions in the plane of the molecule.

We assume energetic site-disorder, $E_j = E_0 + \delta_j$, where δ_j is an uncorrelated Gaussian noise with variance σ^2. Only energetic disorder is considered, rather than positional or orientational, as previous works show that energetic disorder is dominant in molecular aggregates

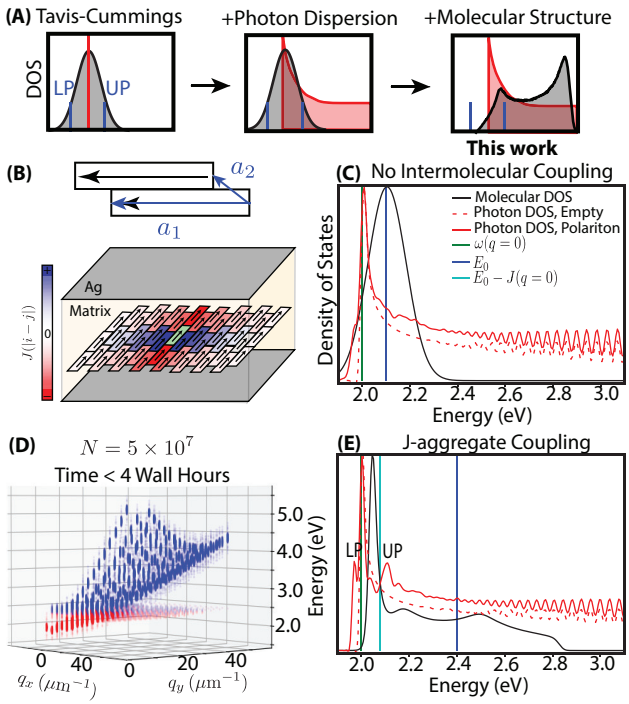

Figure 3.1: (A) Cartoon diagrams displaying the increase in Hamiltonian complexity in the DOS in this work. Black is used for the molecular DOS, red for photon DOS, and blue to label the $q = 0$ polariton states. (B) System geometry diagram shows the Coulomb coupling function, J, displayed as the coupling to the center green dipole. (C) and (E) DOS diagrams for a J-aggregate and a crystal without Coulombic intermolecular coupling. A macroscopic number of molecules is used, $N_x = 84375$, $N_y = 25$, with a total of 65-75 photons mode along the long crystal axis below a cutoff of 5.5 eV. The Rabi splitting is around ~ 0.07 eV, the energetic disorder (Gaussian) standard deviation is of 0.1 eV and the Chebyshev resolution is of 0.01 eV. (D) 3D plot of the angle resolved absorption spectrum of a molecular aggregate measuring 11 x 13 μm, including 196 photon wavevectors; modes with energy less than $E_0 - J(q = 0)$ are colored in red while those above are in blue.

and polaritons. [AKR23, Rib22, DSK18, LR06] The fixed-direction dyes interact via a transitionally invariant dipole-dipole interaction, labeled J_{i-j}, which to fit experiment is based on finite closely-spaced point-charge interactions (see SI). [DKC19, DGB22]

The molecular Hamiltonian is then

$$H_M = \sum_j E_j b_j^\dagger b_j + \sum_{ij} J_{ij} b_i^\dagger b_j. \tag{3.2}$$

With the rotating wave approximation and the Coulomb gauge, the molecule-photon interaction is [LR06]

$$H_{MC} = \sum_{j,q} \sum_{\lambda=s,p} [g_{j\lambda}(q) a_\lambda^\dagger(q) b_j + g_{j\lambda}^*(q) b_j^\dagger a_\lambda(q)], \tag{3.3}$$

with a coupling strength

$$g_{j\lambda}(q) = i\Omega_R \frac{E_j}{E_0} \sqrt{\frac{\omega_0}{N\omega(q)}} p_\lambda e^{ir_j \cdot q}, \tag{3.4}$$

where the projections along and perpendicular to the field mode are $p_s = (\hat{\mu}_j \cdot \hat{n}_q)$, and $p_p = (\hat{\mu}_j \cdot \hat{q})$, and $\hat{n}_q = [\hat{q} \times \hat{z}]$. The projections are j-independent as here all dipoles are parallel. The Rabi splitting strength is $\Omega_R = \mu_0 \sqrt{\frac{\pi E_0^2 N}{\varepsilon_0 \omega_0 V_C}}$.[LR06]

3.2.1 Expanding the Analytical solution to include Aggregate Coupling

The full Hamiltonian is then the sum of the cavity, molecular and coupling terms, $H = H_C + H_M + H_{MC}$. Without molecular disorder ($E_j = E_0$) and dye-dye interaction ($J_{ij} = 0$), one obtains the analytically solvable multi-mode Tavis-Cummings Hamiltonian. [ALL03] Similarly, in the absence of disorder, we can also exactly resolve the effects of the aggregate internal structure due to the translational invariance of the Coulomb interaction, which implies the in-plane wave vector q is a good quantum number for both molecular and cavity subspaces. In the latter exactly-solvable scenario, using a Fourier-transformed exciton basis, $b^\dagger(q) = \sum_j b_j^\dagger e^{iq \cdot r_j}/\sqrt{N}$, the Hamiltonian separates into a sum over mode-specific terms,

$$\begin{aligned} H_{TOT} = \sum_q \Big[& E'(q) b^\dagger(q) b(q) + \sum_\lambda \big(\omega(q) a_\lambda^\dagger(q) a_\lambda(q) \\ & + g_\lambda(q) a_\lambda^\dagger(q) b(q) + g_\lambda^*(q) a_\lambda(q) b^\dagger(q) \big) \Big], \end{aligned} \tag{3.5}$$

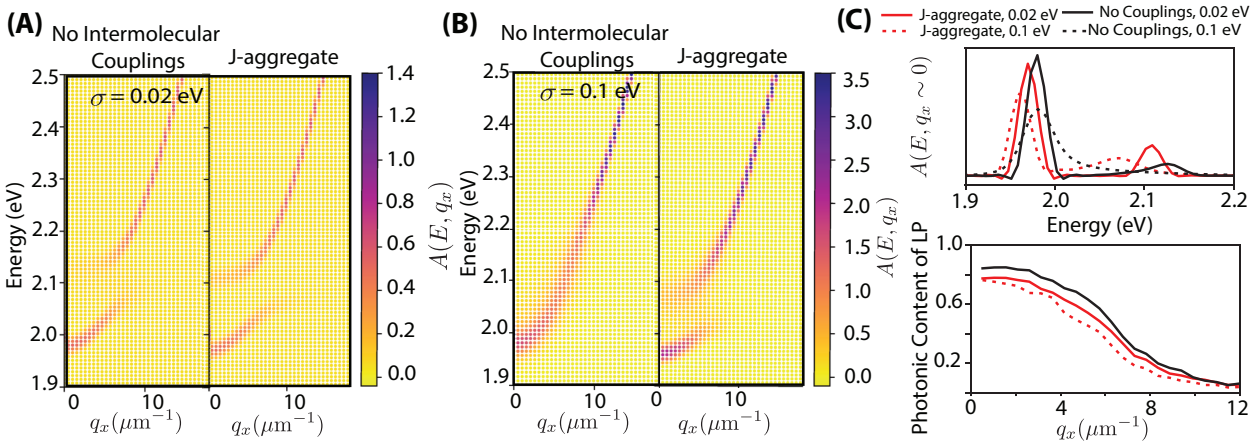

Figure 3.2: (A) Angle resolved absorption spectrum of a J-aggregate, and an equivalent (with the same number of monomers) material with no intermolecular interactions in the weak disorder regime $\sigma/\Omega_R \ll 1$ and (B) strong disorder regime $\sigma/\Omega_R \geq 1$. The photonic content of the LP in (C) was obtained by piecewise integration of the angle resolved photon (transmission spectra) and molecular density of states. Here, the same quasi-1D ribbon was used as in Figure 3.1, but $N_\zeta = 120$ stochastic samples were sufficient to resolve the presented spectra

where the modified exciton energies are $E'(q) = E + J(q)$, with $J(q) = \sum_j J(j)e^{iq\cdot r_j}$, $E(q) = E_0$ is the (constant) exciton energy, while the delocalized exciton-photon coupling term is $g_\lambda(q) = 2i\Omega_R p_\lambda \sqrt{\frac{\omega_0}{\omega(q)}}$. The mode specific exciton-photon Hamiltonian is trivially diagonalized, yielding polariton states $\xi(q) = \beta(q)b(q) + \sum_\lambda \alpha_\lambda(q)a_\lambda(q)$, with coeficients constrained by

$$\alpha_\lambda(q)[E - \omega(q)] = g_\lambda(q)\beta(q) \tag{3.6}$$

$$\beta(q)[E - J'(q)] = g^*_\lambda(q)\alpha_\lambda(q) \tag{3.7}$$

$$\sum_{\lambda=s,p} |\alpha_\lambda(q)|^2 + |\beta(q)|^2 = 1. \tag{3.8}$$

Solving this system leads to a simple modification to the usual expressions for the upper and lower polariton (UP/LP) energies

$$E_{UP/LP}(q) = \frac{\omega(q) + E'(q)}{2} \pm \sqrt{\Omega_R^2 + \frac{(\omega(q) - E'(q))^2}{4}}. \tag{3.9}$$

The obtained spectra is exactly the same as that given by the multimode Tavis-Cummings, except that here the momentum-specific interaction replaces the usual non-interacting $E(q)$ molecular energies. For strong interactions as in molecular crystals, with $J(q)$ that may reach up to 0.3eV or more, the Hamiltonian spectrum is substantially modified due to the inter-molecular couplings. Note also that as usual, for each polariton the wavefunction amplitudes satisfy:

$$|\alpha(q)|^2[E] = \frac{(E - J'(q))^2}{(E - J'(q))^2 + \Omega_R^2} \tag{3.10}$$

$$|\beta(q)|^2[E] = \frac{\omega_0}{N\omega(q)} \frac{4\Omega_R^2}{(E - J'(q))^2 + \Omega_R^2} \tag{3.11}$$

where $E \equiv E_{UP/LP}$, while the photon amplitude $\beta(q)$ is determined from the polariton normalization, $|\beta(q)^2| + \sum_\lambda |\alpha_\lambda(q)^2| = 1$.

3.2.2 Efficient Application of the Hamiltonian on a Vector

We now turn to the nontrivial case of both strong molecular energetic-disorder and intermolecular coupling, $J \sim \sigma \sim \Omega_R$. To model this realistically, we must return to the complete light-matter Hamiltonian. The key to efficient very large-scale calculations is the use of stochastic methods, which require that the action of the Hamiltonian on a given vector be efficient. As the bilinear Hamiltonian conserves the number of polaritons, a single-polariton wavefunction ψ will be a direct sum of a molecular and cavity (photonic) parts, $\psi = \psi^M \oplus \psi^C$, so computationally it is a vector of length $N + 2C$, where N and C are the numbers of dye molecules and included cavity modes (the factor of 2 is due to the s and p photon polarizations). Since the vast majority of photon wavevectors are not in resonance with the excitonic system, an energy cutoff is imposed so $C \ll N$. The photon index is denoted by $\ell = (\ell_x, \ell_y)$, associated with a photon mode $q(\ell)$.

When applying the Hamiltonian on such a function, $H|\psi\rangle$, the H_M action involves an efficient convolution of the dye-dye interaction, $\sum_{j \le N} J_{\ell j} \psi^M_j$. [BCD20] For the cavity-molecule part H_{MC}, one can use a similar transform, but it is even faster to apply consecutively fractional 1D Fourier transforms. Define $\mathcal{F}_x(\ell_x, j_x) = e^{2\pi i \, j_x \, \ell_x / N_x}$, for elements $j_x = 1 \cdots N_x$, $\ell_x = 1 \cdots C_x$ with $\mathcal{F}_y$ analogous. Then, for example,

$$\langle \ell\lambda | H_{MC} | \psi^M \rangle = 2i\Omega_R p_\lambda \sqrt{\frac{\omega_0}{\omega\left(q(\ell)\right) N}} \mathcal{F}_y \left[\mathcal{F}_x \left[\frac{E_j}{E_0} \psi^M(j) \right] \right]. \tag{3.12}$$

The scaling of this step is $\mathrm{O}(N\sqrt{C})$, and since practical cavities involve at most a few thousand relevant-energy photons, the action of H_{MC} is very efficient.

3.3 Molecular Observables for Polaritons

Given the efficient representation of the action of the Hamiltonian, we use a stochastic resolution of the density of states operator, a common technique in condensed matter

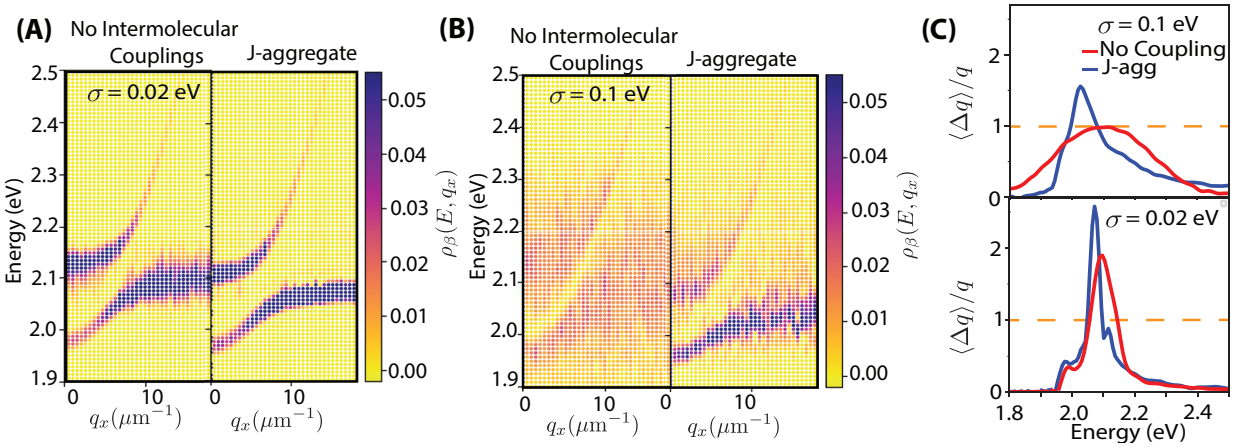

Figure 3.3: (A) Angle resolved molecular density of states for a J-aggregate and an equivalent system with no intermolecular interactions in the weak and (B) strong disorder regimes. (C) Relative wavevector uncertainty $\langle \Delta q \rangle / q$ of the molecular wavefunctions derived from $\rho_\beta(E, q)$ (Eq. 11) in the case of strong disorder at 0.1 eV (top) and weak disorder 0.02 eV (bottom).

systems[WZ94, WWA06, BCD20]

$$\rho(E) = \mathrm{Tr}[\delta(H - E)] = \{\langle\zeta|\delta(H - E)|\zeta\rangle\}_\zeta \,, \tag{3.13}$$

where ζ is here a vector of length $N + 2C$ with random $e^{i\theta}$ elements at each site, and the curly-brackets indicate a statistical average over the random ζ elements, and simultaneously over the site disorder. The error in the stochastic trace scales as $\mathrm{O}(1/\sqrt{NN_\zeta})$,[WWA06] and is thus negligible, for sufficiently large crystals, even for very few (here $N_\zeta \approx 10-200$) random samples. For the action of the DOS operator on a vector, $\delta(H-E)|\zeta\rangle$, the efficient Chebyshev approach is used, [Kos88] with a number of Hamiltonian-vector operations, determined by the desired energetic resolution relative to the spectral width, that is typically less than 2000. [BCD20]

The overall scaling of the method is then limited by the operations needed to incorporate the intermolecular interactions. In our case the application of the dipolar coupling via convolution is effectively linear in time. In Figure 3.1 (D) we show a large calculation possible with this algorithm, requiring only modest computational time that can be paral-

lelized on a standard 128-core AMD Milan cluster. Given the size of the total basis of 10^7 elements, memory costs associated with wavefunction storage quickly become the limiting computational factor for this method.

To examine the local properties of the molecular and photonic subsystems, we similarly stochastically compute the projected matter and light local DOS, $\rho_M(E) \equiv \mathrm{Tr}\,(P_M \delta(H-E))$ and $\rho_C(E) \equiv \mathrm{Tr}\,(P_C \delta(H-E))$, respectively, introducing the projection operators onto the molecular and cavity(photon) spaces, P_M and P_C respectively. As there are so many more molecules than photon mode involved in strong light-matter coupling, their local density of states are shown separately in Figure 3.1.

The angle resolved photonic density of states (directly proportional to the measurable microcavity angle resolved transmission spectrum), is similarly defined as $A(E,q) \equiv \sum_\lambda \langle q,\lambda|\delta(H-E)|q,\lambda\rangle$, where $|q,\lambda\rangle \equiv a^\dagger_\lambda(q)|0\rangle$. To efficiently sample it, we introduce a stochastic resolution of the identity, $\mathbb{1} = \{|\zeta\rangle\langle\zeta|\}_\zeta$, which when plugged in yields

$$A(E,q) = \sum_\lambda \{\langle q_\lambda|\delta(H-E)|\zeta\rangle\langle\zeta|q_\lambda\rangle\}_\zeta\,, \tag{3.14}$$

so it is evaluated in the same stochastic process as the total DOS (Eq. 9), as both use the $\delta(H-E)|\zeta\rangle$ vector.

Without static disorder, the angle resolved transmission is simply proportional to $A^0(E,q) = \sum_{\eta=LP,UP}\sum_\lambda |\alpha_\lambda(q)|^2\delta[E-E_\eta(q)]$. Static disorder broadens $A(E,q)$. Its linewidth in q-space at fixed E reveals information about the delocalized character of polariton modes at this energy, and whether q is a good quantum number in the presence of disorder.[IR60, ALL03, LR06, Rib22]

Complementary information is given by the molecular angle resolved DOS obtained from the vectors $|\beta(q)\rangle \equiv \frac{1}{\sqrt{N}}\sum_j e^{iq\cdot r_j} b^\dagger_j|0\rangle$. This quantity provides information on the matter component of optically bright upper/lower polariton states at a given wavevector:

$$\rho_\beta(E,q) \equiv \langle\beta(q)|\delta(H-E)|\beta(q)\rangle, \tag{3.15}$$

which is evaluated stochastically analogously to Eq. (3.14). While in the presence of disorder q is no longer a good quantum number, we clearly visualize (Fig. 3.3) the trade-off between molecular and photon contributions, and the energy broadening of the bright states in each subspace.

Figure 3.1 shows the photonic density of states, for a J-aggregate, and an identical lattice with no Coulombic intermolecular terms in the strong disorder regime $\sigma \sim J \sim \Omega_R$. As the number of photon modes is tiny compared to the number of molecular dipoles, there is essentially no change in the total DOS when the cavity is turned on. However, the $q \approx 0$ UP/LP states can be identified in the photon DOS when the J-aggregate is placed inside the microcavity.

For all observables that include some form of internal aggregate structure there is exchange narrowing, i.e., interaction-induced narrowing of peaks and increase in the participation ratios. [HS18] Figure 3.2 shows that, in J-aggregates, microcavity coupling induces substantially greater splitting between the LP/UP bands in the face of strong disorder, substantial exchange narrowing, and largely asymmetric line shapes skewing higher in energy. The additional narrowing (i.e., resistance to disorder), relates to the fact that the J-aggregate molecular DOS (Figure 3.1(E)) extends higher in energy than an uncoupled system DOS, thus allowing higher energy photons to remain in resonance with the molecular system. The significant differences in line shape observed between the analyzed aggregates are entirely due to the delocalization of their respective dark exciton states as demonstrated in Figure 3.3.

Figure 3.3 shows the angle resolved molecular density of states and relative wavepacket uncertainty for a J-aggregate and noninteracting (uncoupled) emitters. We observe much greater wave character in the (weakly coupled) J-aggregate dark exciton modes at higher q, despite the influence of strong disorder. The enhanced wave character of the high q weakly coupled modes is a byproduct of the strong intermolecular interactions in J-aggregates which also lead to the reduced photonic content in the J-aggregate LP band shown in Fig.

3.2(C) bottom. Additionally, as reported in the SI, the average participation ratio of J-aggregate molecular states is of order 10^4, while an uncoupled polariton Hamiltonian leads to a maximum participation of 300. Lastly, the well-studied phenomena of exchange narrowing in molecular aggregates,[HS18, AW53, Sum77] is also clearly visible in the $q \sim 0$ polariton transmission spectrum at the top of Fig. 3.2(C).

Overall, our results show that the long-range intermolecular interactions of organic aggregates lead to substantial effects in their (multimode) cavity-polariton spectra and dark state delocalization measures. This demonstrates the need to include accurate internal models for the electronic coupling in polaritonic systems made from crystals, polymers or aggregates. For example, the large Rabi splitting (0.06 eV) obtained in the present 2D studies was the result of realistic $5-10$ D dipole and realistic molecular geometries. To attempt to produce such a Rabi splitting in a 1D lattice would require unrealistic dipoles on length scales where transition dipole coupling effects are no longer meaningful, leading to especially inadequate description of the dark modes. We expect this substantial delocalization of the molecular states to have important effects on photophysical properties and transport phenomena in these systems, leaving the door open for further studies that consider this effect.

The stochastically-evaluated observables are obtained here through an efficient molecular-coupling scheme that will apply to other, more sophisticated model Hamiltonians, enabling future work to consider even more realistic system geometries and internal structure when studying energy and charge transfer in many-molecules polariton systems.

CHAPTER 4

Stochastic Iterative Bethe-Salpeter Equation

4.1 Introduction to the Bethe-Salpeter Equation

Accurate calculation of optical spectra for large systems is essential for future novel optical and electronic devices. High level theoretical calculations have been applied in a variety of fields ranging from the basics of photovoltaics,[KB09] photocatalysis,[ISB16] organic semiconductors,[CWB02, TMK02] and even for understanding the mechanisms of UV damage on DNA.[WCT19] The Bethe-Salpeter Equation (BSE) formalism has become a ubiquitous method for calculating electronic spectra.[BDJ20] The success of the BSE is due to the proper inclusion of an effective long range exchange kernel, which solves the failures of TD-DFT in accurately describe excitations and avoiding crossings.[DH04, BSV04]

Current conventional methods for solving the BSE are substantially more computationally demanding than most implementations of TD-DFT due the explicit calculation of a large number of occupied and virtual electronic states and the evaluation of a large number of screened exchange integrals between valence and conduction states, yielding a typical scaling of $\mathcal{O}(n_o^6)$, for n_o valence orbitals.[DSS12, SFM19, GPA20] Previous work in TD-DFT has reduced its conventional scaling, $\mathcal{O}(n_o^4)$, using a technique that only requires the occupied orbitals which implicitly interact with all conduction states.[BGC01, BN04, NB05, WSG06, WGG08, GBR14, ZL15, RPG12]

To go beyond TD-DFT to BSE requires constructing the effective Coulombic interaction, W, a computationally expensive step. Here we therefore adopt our previous stable itera-

tive methods[BN04, NB05], and pull from our previous works in both TD-DFT/BSE[BN04, NB05, NBR14a, RBN15, GNB15] and stochastic GW[NGA14a, VRN18, VLB18a, VBR18b, VLR18] to present an efficient stochastic generation of W within an iterative BSE technique. Our combined approach uses stochastic time-dependent propagation to obtain the action of W on each required term in linear scaling,[NGA14a] and this results in an efficient method that overall scales at most cubically with system size. The method and its application to a large organic semiconductor are detailed below.

4.2 New Methodology

Overall, every method for solving the BSE has two numerical parts. Construction of the "kernels", i.e., the action of the effective interaction W on a given transition, and then diagonalizing or iterating the resulting Bethe-Salpeter Hamiltonian-like operator for the excitons. The full algorithm is covered here for completeness.

The starting point is a closed shell molecular system with charge $2N_{occ}$. We are interested in excitons composed of a mixture of n_o occupied (valence) orbitals, $\phi_i, \phi_j, ...$, times n_c conduction (virtual) ones written as $\phi_a, \phi_b, ...$ Typically $n_o \ll N_{occ}$ states are considered. The orbitals are eigenstates of a zero-order Hamiltonian H_0, with occupied-state eigenvalues $\varepsilon_i, \varepsilon_j, ...$ and $\varepsilon_a, \varepsilon_b, ...$ Formally the zero-order Hamiltonian should come from a very accurate method, specifically self-consistent GW, but in practice, especially for large systems, it is sufficient to use the DFT eigenstates and just correct the eigenvalues by GW, as explained later. Further, for simplicity we will use the well established Tamm-Dancoff approximation, although the derivations are easily extended to the full Bethe-Salpeter equation.

For singlet excitations, the excitation energies of the system are the eigenvalues of the $(n_o n_c \times n_o n_c)$ Tamm-Dancoff matrix A that couples excitons, i.e., occupied-virtual pairs:

$$\begin{aligned} A(i,a;j,b) = &(\varepsilon_a^{GW} - \varepsilon_j^{GW})\delta_{a,b}\delta_{i,j} \\ &+ 2(ia|jb) - (\phi_a\phi_b|W|\phi_i\phi_j) \end{aligned} \tag{4.1}$$

with exchange elements

$$(ia|jb) = \int \phi_i(r)\phi_a(r)|r-r'|^{-1}\phi_j(r')\phi_b(r')drdr'$$

while $W \equiv W(\omega = 0)$ refers to the static effective Columbic interaction approximation, and its matrix elements are

$$(\phi_a\phi_b|W|\phi_i\phi_j) \equiv \int \phi_a(r)\phi_b(r)W(r,r')\phi_i(r')\phi_j(r')drdr'.$$

The superscript in ε^{GW} denotes, as mentioned, that high quality GW single particle energies should be used. In practice, we calculate the HOMO and LUMO GW energies by the linear-scaling stochastic-GW (sGW) method [NGA14a, VRN18, VLB18a, VBR18b, VLR18] and use the scissors approximation, which is reasonable for large systems: $\varepsilon_i^{GW} \simeq \varepsilon_i + \delta_o$, $\varepsilon_a^{GW} \simeq \varepsilon_a + \delta_c$, where $\delta_o \equiv \varepsilon_{HOMO}^{GW} - \varepsilon_{HOMO}$ and analogously for δ_c. Further, for higher accuracy we use the self-consistent ΔGW_0 approach where the sGW HOMO and LUMO corrections are *a posteriori* shifted self-consistently; for large systems this approach was found to be an excellent approximating to eigenvalue-only self-consistent GW_0 and to experiment.[VBR18b]

4.2.1 Mixed Representation Iterative Solution

The simplest derivation of an iterative method for the BSE spectrum starts with the linear-response time-dependent Hartree-Fock (TD-HF) equation.[Neg82, Str88, NB05] For an initially real occupied state perturbed along the x axis, $\psi_j(r, t = 0) = e^{-i\alpha x}\phi_j$, one performs a linear response expansion in α, $\psi_j(r,t) \simeq e^{-i\varepsilon_j t}(\phi_j(r) - i\alpha f_j(r,t))$, where $f_j(r, t = 0) = x\phi_j(r)$. The formally non-linear TD-HF equation for ψ_j then converts, for small α, to a linear equation for f_j. In the Tamm-Dancoff approximation, (where f_j is not coupled to f_j^*) this evolution equation reads

$$i|\dot{f}_j\rangle = A|f_j\rangle \tag{4.2}$$

where

$$A \equiv Q\bar{A} \tag{4.3}$$

and

$$\bar{A}|f_j\rangle = (H_0 + \Delta - \varepsilon_j)|f_j\rangle + (\delta v - \delta X)|\phi_j\rangle. \tag{4.4}$$

Here we introduced several terms. $\Delta \equiv \delta_c - \delta_o$ is the ΔGW_0 scissors shift. The exciton Coulomb potential ia $\delta v(r,t) = \int |r-r'|^{-1}\delta n(r',t)dr'$, where the exciton density is $\delta n(r,t) = 2\sum_i \phi_i(r)f_i(r,t)$ and the sum extends over the occupied states. The exciton exchange δX is defined analogously, again under the Tamm Dancoff approximation,

$$\langle r|\delta X(t)|\phi_j\rangle = \sum_i f_i(r,t)\int |r-r'|^{-1}\phi_i(r')\phi_j(r')dr'. \tag{4.5}$$

Finally, Q is a projection operator that ensures that the excited functions f_j have no overlap with the occupied space, i.e., $Q = I - P$, with $P \equiv \sum_{s\leq N_{occ}} |\phi_s\rangle\langle\phi_s|$.

The BSE equation results then when the static effective interaction W replaces the Coulombic interaction in the exchange operator, yielding eventually (hiding the time-dependence of f):

$$\begin{aligned}\langle r|\bar{A}|f_j\rangle \equiv (H_0 + \Delta - \varepsilon_j)f_j(r) \\ + \delta v(r)\phi_j(r) - \sum_i f_i(r)W_{ij}(r),\end{aligned} \tag{4.6}$$

where the action of W on the occupied-occupied term is $W_{ij}(r) \equiv \int W(r,r';\omega=0)\phi_i(r')\phi_j(r')dr'$.

The linear form of the time-dependent equation readily implies that the frequency-dependent spectrum can be obtained from the dipole-dipole correlation function, where up to a constant

$$\sigma(\omega) = \omega\left\langle f^0\right|\delta(A-\omega)\left|f^0\right\rangle \equiv \omega\langle f^0|f(\omega)\rangle \tag{4.7}$$

where $f_j^0(r) = \langle r|Q|f_j(t=0)\rangle = \langle r|Qx|\phi_j\rangle$, and the (smoothed) delta function is readily expressed using a Chebyshev (or alternately a Lancsoz) expansion in A,

$$|f(\omega)\rangle \equiv \delta(A-\omega)\left|f^0\right\rangle \simeq \sum_n g_n(\omega)\left|f^n\right\rangle \tag{4.8}$$

where $|f^n\rangle$ are obtained by iteratively applying a scaled A, starting from $|f^0\rangle$, while $g_n(\omega)$ are numerical coefficients.[Kos88, Wan94, WWA06] The spectrum evaluation therefore reduces to calculation of the residues, $R_n \equiv \langle f^0|f^n|f^0|f^n\rangle$. Numerically, one just requires the application of A on an arbitrary exciton vector $f_j(r)$, i.e., $f \to Af$.

A side note: while here we use Eq. (4.6), based on the mixed hole-grid representation $f_j(r)$, we note that in many cases one would want to use an explicit electron-hole basis. For example, for systems such as large quantum dots, where N_{occ} is very large and we are interested in a smaller number of conduction states relative to the total number of occupied electron states, $n_c < N_{occ}$, it is numerically better to replace Q by a projection to the n_c conduction states, $Q = \sum_{c \le n_c} |\phi_c\rangle\langle\phi_c|$. Then, the fundamental iterated object is the electron-hole basis coefficients, $f_{ia} \equiv \langle\phi_a|f_i\rangle$. In the electron-hole basis, the initial state is simply the x-dipoles elements, $f^0_{ia} \equiv f_{ia}(t=0) = \langle\phi_a|\, x\, |\phi_i\rangle$. Further, is easy to see that the iterative application of A on f, as given in Eqs. (4.3),(4.6), becomes in the electron-hole basis: $(Af)_{ia} = \sum_{j,b} A(i,a;j,b) f_{jb}$ and A is here exactly the BSE matrix from Eq. (4.1). Practically the action by A would be done then as:

$$(Af)_{ia} = (\varepsilon_a - \varepsilon_i + \Delta) f_{ia} + \langle\phi_a|\, \delta v - \delta X\, |\phi_j\rangle\,. \tag{4.9}$$

i.e., given the set of coefficients f_{jb}, one would calculate the mixed representation vectors $f_j(r)$, from which δv and δX follows, and then dot product per the equation above. Note that using the electron-hole basis coefficients reduces the spectral range of A, which will be controlled now by highest conduction state included, instead of the (much larger) highest eigenvalue of H_0, thereby reducing the number of required Chebyshev terms. Also, the same formalism carries over trivially to localized orthogonal basis sets, where ε_a and ε_i would be replaced by the Hamiltonian matrices within the electron and hole spaces, respectively. The expressions for non-orthogonal basis sets can be similarly derived.

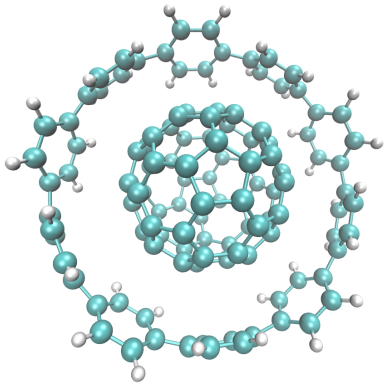

Figure 4.1: Structure of [10]-CPP+C_{60}, where atomic coordinate information can be found in [MXF20].

4.2.2 Stochastic evaluation of the action of W

The main numerical task in our formalism is the preparation of all $n_o(n_o+1)/2$ functions $W_{ij}(r)$. W is made from a static Coulomb part and a polarization component, $W = v + v\chi v \equiv v + W^{\rm pol}$ (where $v(r,r') = |r-r'|^{-1}$), so $W_{ij}(r) = q_{ij} + W^{\rm pol}_{ij}$, where $q_{ij} \equiv \int |r-r'|^{-1}\phi_i(r')\phi_j(r')dr'$.

As is well-known, the action of $W^{\rm pol}$ is doable by time-dependent Hartree (TD-H) calculations.[HL85, TC06] Specifically, for each pair of occupied functions $1 \le i,j \le n_o$ one calculates the source "potential" $q_{ij}(r)$ due to the $\phi_i\phi_j$ density-like source term. Then the full set of all occupied states is perturbed, $\psi_s(r,t=0) = e^{-i\alpha q_{ij}(r)}\phi_s(r), s = 1,...,N_{occ}$, where $\alpha \approx 10^{-6} - 10^{-4}$ is a small perturbation strength, just as in the linear-response TD-HF derivation above. Note that to avoid a plethora of indices we do not denote the dependence of ψ_s on i,j.

The perturbed states are then numerically propagated with a TD-H Hamiltonian,

$$i\dot{\psi}_s(r,t) = (H_0 + u_{ij}(r,t))\psi_s(r,t), \tag{4.10}$$

where $u_{ij}(r,t)$ is the potential due to the time-dependent density perturbation,

$$u_{ij}(r,t) \equiv \int |r-r'|^{-1}(n^{\alpha}(r',t) - n^{\alpha=0}(r',t=0))dr', \tag{4.11}$$

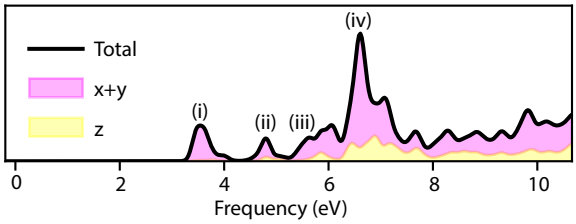

Figure 4.2: Absorption spectrum of [10]-CPP+C_{60} calculated from an iterative solution of the BSE with a stochastic W.

where $n^{\alpha}(r,t) = 2\sum_s |\psi_s(r,t)|^2$ is the density due to the propagated perturbed orbitals. This potential, used to propagate the time-dependent Hamiltonian, is then scaled to give the result of acting with the time-dependent effective potential, $W(t)$, i.e.,

$$\langle r| W^{\rm pol}(t) |\phi_i\phi_j\rangle = \alpha^{-1} u_{ij}(r,t). \tag{4.12}$$

Finally, the desired action of the static polarization is obtained by damped integration of the action of the time-dependent polarization, $W^{pol}(\omega=0) = \int_0^\infty e^{-\gamma^2 t^2/2} W^{pol}(t) dt$, i.e.,

$$\begin{aligned} W_{ij}^{\rm pol}(r) &= \langle r| W^{\rm pol}(\omega=0) |\phi_i\phi_j\rangle \\ &= \alpha^{-1} \int_0^\infty e^{-\gamma^2 t^2/2} u_{ij}(r,t) dt, \end{aligned} \tag{4.13}$$

where we introduced a Gaussian damping function where the width γ is a numerical convergence parameter.

The one caveat in this overall approach is that the propagation of the full set of occupied orbitals is very expensive for large systems, and is in fact the most expensive portion of other large system BSE codes.[DSS12, SFM19] We therefore use here our stochastic-TD-H approach [NGA14a, GNB15] which leads to a stochastic W, outlined below. (Note that this is exactly the same approach we use in our stochastic GW method,[NGA14a] with a small improvement detailed later). Briefly, in stochastic-TD-H (or stochastic-TD-DFT in the general case) we replace the full set of occupied orbitals by a few random-sign combinations of all occupied states,

$$\eta_\ell(r) = L^{-\frac{1}{2}} \sum_{s \le N_{occ}} (\pm 1)\phi_s(r), \tag{4.14}$$

where $\ell = 1, .., , L$ and for large systems a very small number of states is sufficient, $L \ll N_{occ}$. The L stochastic occupied states are then treated in the TD-H procedure as if they were the full set of $N_{\rm occ}$ molecular orbitals, i.e., they are perturbed ($\eta_\ell(r, t = 0^+) = e^{-i\alpha q_{ij}(r)}\eta_\ell(r)$) and propagated with $H_0 + u_{ij}(r, t)$, where the time-dependent density used in constructing u is now obtained from $n(r, t) = 2\sum_{\ell \le L} |\eta_\ell(r, t)|^2$, etc. Note that two sets need to be propagated, the perturbed $|\eta^\alpha_\ell(t)\rangle$ and unperturbed $|\eta^{\alpha=0}(t)\rangle$ stochastic orbitals.

At long times, this simple stochastic TD-H approach would eventually become unstable, due to "contamination" by occupied states. This means that the excited component, $\eta^\alpha_\ell(r, t) - \eta^{\alpha=0}_\ell(r, t)$, has in it an occupied-states' amplitudes. For regular TD-H propagation of all states this is not a problem since in the overall density the "contamination" of a propagated state $\psi_j(r, t)$ by an occupied $\phi_i(r)$ is exactly cancelled by the "contamination" of the opposite pair.[ZL15] However, in our stochastic occupied orbitals there is no such cancellation. Luckily the instability gets tamed as the system size gets bigger, but we did find that it affects the results here if untreated for medium system sizes.

To prevent the instability we simply "clean" the stochastic orbitals periodically, so after every M'th time step we write:

$$|\eta^\alpha_\ell(t)\rangle \to \left|\eta^{\alpha=0}_\ell(t)\right\rangle + Q\left|\eta^\alpha_\ell(t) - \eta^{\alpha=0}_\ell(t)\right\rangle, \tag{4.15}$$

with $t = 0, Mdt, 2Mdt, ...$ This does not increase the scaling of the method since the required cleaning frequency decreases (i.e., a larger M is possible) with increasing system size. Also note that after each cleaning step we renormalize each $|\eta^\alpha_\ell(t)\rangle$ orbital so it keeps its initial norm.

Finally, a well-known technical aspect is that due to the use of a finite grid box size, the scissors parameter needs to be shifted down by the $W(k \to 0)$ term. We use a variation of the existing procedures to find this term.[ORG95, RVM06] We repeat the iterative calculation for a medium size (i.e., a lesser n_o than the one eventually used) at several different box sizes, and for each run find the average Kohn-Sham potential on the box boundary, $v^{\rm bndry}$.

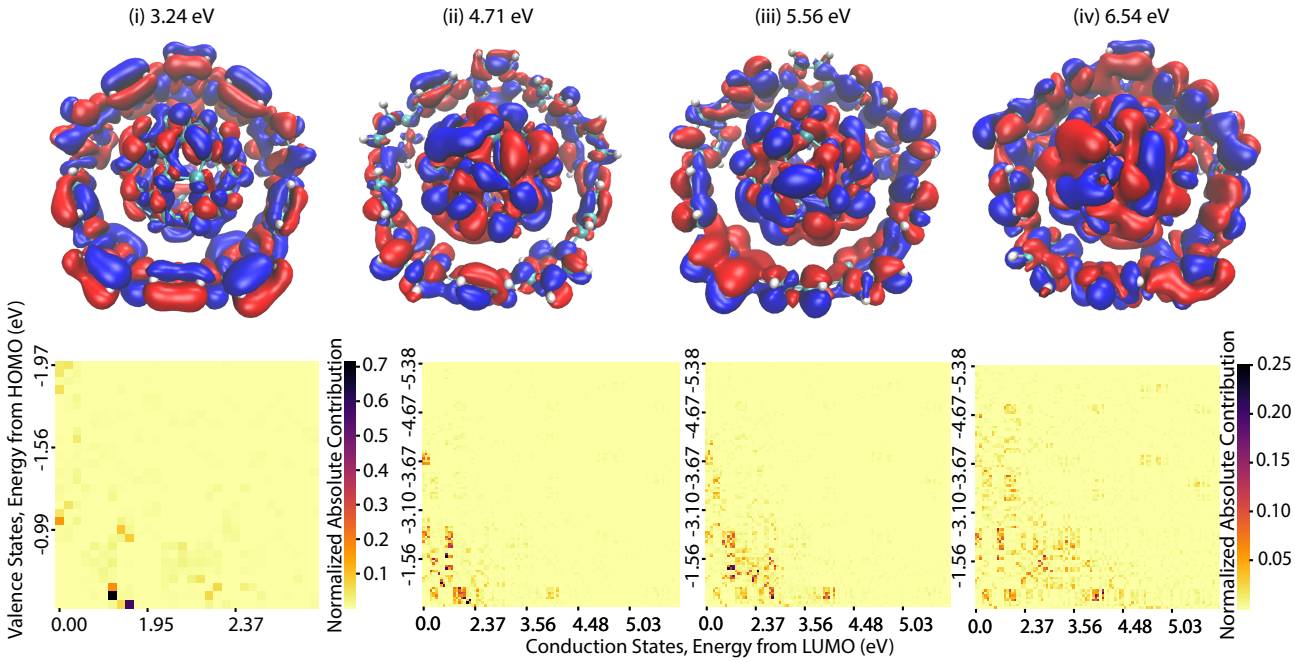

Figure 4.3: (Top) Exciton densities for the four lowest prominent exciton peaks, as labeled in Figure 4.2. (Bottom) Matrix of the corresponding (valence, conduction) transition $|f_{ia}(\omega)|$ to the exciton density above for each of these frequencies. A small window $(n_o, n_c) = (30, 30)$ is shown for the lowest exciton which includes prominent contributions from only a few electron-hole states, while a (100,100) window is used to show the higher energy excitons. The axis are labeled by the corresponding valence/conduction energies. The square pixels are for a given valence to conduction transition, and due to degeneracy and rising density of states, the energy labels are not linear. Also note that while the many weaker-intensity higher n_o and/or n_c transitions are not visible in this colored matrix, they are important for the quantitative spectrum.

Then we approximate $W(k \to 0) = \epsilon_{eff}^{-1} v^{bndry}$, and the parameter ϵ_{eff}^{-1}, playing the role of an inverse dielectric constant, is fit so that the spectra from the different box-sizes runs overlap.

Summarizing the resulting algorithm: we use stochastic TD-H to prepare $W_{ij}(r)$ for $n_o(n_o+1)/2$ occupied-state pairs. Separately we use sGW to calculate the self-consistent GW scissors shift Δ and subtract from it the $W(k \to 0)$ term. Then for each polarization we start with the dipole exciton state. The Tamm-Dancoff operator, Eq. (4.6), is successively applied and the Chebyshev residues R_n are used to calculate the absorption frequencies. As usual, if one wants to characterize the different peaks then the Chebyshev expansion of the frequency-resolved exciton state, Eq. (4.8), can be used (potentially with filter-diagonalization[Neu90b, MRT93] for resolving different sub-peaks).

The two parts of the method, preparing W_{ij} and applying the A operator, both scale as $O(n_o^2 n_g)$ for n_g grid points, more gentle than current methods. Formally, this is cubic scaling with system size but in practice the scaling is better since n_o often rises only gently with N_{occ}. In addition, the number of grid points would be reduced in future studies as we have shown that very sparse grids suffice when using orthogonal projected augmented waves (OPAW) instead of pseudo-potentials.[LN20]

4.3 Results

We demonstrate the algorithm on a characteristic large organic semiconducting system, a carbon nanohoop-fullerene complex. In the last decade, cycloparaphenylenes (CPPs), also known as carbon nanohoops, have emerged as highly structurally tunable emitters, with rich size-dependent opto-electronic properties and host-guest chemistry.[LJ19] While substantial DFT modeling has been completed on CPP+fullerene complexes,[Won09, YZZ15, MXF20, SSS21] extraction of optical properties at this level of theory is difficult due to the characteristic charge transfer states in CPPs. Further, it has already been established that the BSE formalism is very accurate in predicting the properties of other fullerene-polymer complexes.[NDQ14] Here we present detailed results for the smallest such CPP+fullerene

"pea-pod,"[IWS11, XBJ12] [10]-CPP+C_{60}.

To simulate [10]-CPP+C_{60}, we use a generous box of $(N_x, N_y, Nz) = (100, 100, 84)$ with a grid spacing of 0.5Bohr, using norm-conserving pseudo-potentials (NCPP).[RPM03, WKG13] The effective inverse dielectric constant was found to be 0.30, which gives, at this grid size, a shift of $-W(k \to 0) = -0.29eV$.

The DFT gap is 1.02eV. This gap is corrected with stochastic GW by an amount of 1.24eV, and after applying the self-consistent self-consistent ΔGW_0 this gap correction rises to 1.33 eV (i.e., a fundamental ΔGW_0 gap of 2.35eV). Combined with $-W(k \to 0)$, the overall scissors shift used is $\Delta = 1.04$.

The calculations of the action of W, Eqs. (4.10)-(4.13), were done with a broadening of $\gamma = 0.1$ Hartree. A time-step $dt = 0.1$ a.u. was used for a split-operator propagation of $L = 10$ stochastic states, and the cleaning was done every $M = 10$ steps. The runs were done for $n_0 = 100$ valence states, requiring $n_0(n_0 + 1)/2 = 5005$ actions of W.

The BSE iterative Chebyshev procedure was then done using the $n_o = 100$ valence states. The Chebyshev expansion of $\delta(A - \omega)$ is evaluated with a Gaussian broadening of 0.08 eV; this does not effect the spectrum significantly as it is naturally broadened due to the large number of excitons. The runs took a total of 4000 core hours, i.e., 40 wall hours on a 100-core AMD Milan cluster.

In Figure 4.2, we show the calculated absorption spectrum, both total and separated to in-plane (x and y), and perpendicular (z) polarizations. While there are no gas phase spectra of [10]-CPP+C_{60} due to the fullerene slipping out of its "pea-pod", for the lowest exciton energy, we get reasonable agreement with just [10]-CPP,[ANC14, FCI12] and a stabilizing [10]-CPP+C_{60}-[2]-Rotaxane complex.[XKW18] For just 10-[CPP] in the gas phase the lowest strong transition sits 0.4 eV higher than shown in Figure 4.2. Qualitatively, with the addition of the fullerene in the middle in our simulations, the overall dielectric constant would increase, thereby lowering the energy of the first exciton state. This shift is consistent with the shift

to lower energies seen in the stabilized [10]-CPP+C_{60}-[2]-Rotaxane complex in solution.

In Figure 4.3, we show the exciton density of four prominent excitons as labeled in Figure 4.2, and, for the sake of analysis we also extract the exciton density in the electron-hole state basis. Specifically, we calculate $|f_j(\omega)\rangle$ at the four exciton peak frequencies and then calculate the overlap onto to a set of unoccupied wave functions, giving us f_{ia} for as many a as we desire. For the lowest peak most of the exciton density is concentrated at near-gap i, a states. However, for the largest spectrum peak at 6.83 eV, labeled (iv) in Figure 4.2, one ought to go beyond the figure and use (100,250) states to capture the same amount of density, a basis size that's very substantial. This demonstrates the strengths of the stochastic resolution of the action of W in our present approach, as the full unoccupied space is sampled rather than just a subset of conduction states.

4.4 Forward perspective

Our results show that even larger systems are feasible. This is evident by the fact that the runs were not optimised. For example, while we used $n_0 = 100$, a smaller number $n_0 = 70$ would have sufficed, reducing the cost by a factor of two. Similarly, the box size was very large, and a grid with almost half the points (or even less with OPAW) would have sufficed. With optimized parameters, one can therefore easily reach systems with 1000-2000 electrons.

An interesting feature of the method is that for larger systems it becomes less and less sensitive to stochastic errors. Those errors appear primarily in the sGW calculation of the scissors shift, but this calculation scales sub-linearly with system size. Already here the sGW calculation took less than 20% of the total calculation and had an error of 0.05eV, so for larger systems an even higher accuracy would be obtained with a small fraction of the total cost.

An interesting question is how to go to huge systems, with many thousands of electrons. For this we note that that while this implementation of the BSE scales formally cubically,

it holds promise to give eventually quadratic scaling. To achieve this, one would need to implement localized occupied basis sets sets (see references [BLH16, PPG22]) for reducing the number of i, j pairs for which $W_{ij}(r)$ needs to be calculated, and perhaps even stochastically sample these $\phi_i(r)\phi_j(r)$ pairs. Work along this lines would be reported in future publications.

CHAPTER 5

Optimized Attenuated Interaction for Enabling Large Stochastic Bethe-Salpeter Equation Spectra

5.1 Introduction to Optimized Atenuated Interaction

The Bethe-Salpeter Equation (BSE), a many-body perturbation theory method, is becoming increasingly popular for predicting optical spectra of chemical systems. [BDJ20] Physically, BSE goes beyond time-dependent density functional theory (TDDFT) by the inclusion of the correct long range exchange kernel in the effective interaction W. Numerically, however, the BSE is quite expensive, mostly due to the cost of generating the two-electron integrals of the effective interaction W, which scales formally as $\mathrm{O}(N^4)$, or in specially optimized cases these integrals can be made at an $\mathrm{O}(N^2) - \mathrm{O}(N^3)$ cost,[LKF15, DB19], where N is the number of electrons. Due to the steep scaling, the BSE is typically applied for systems with up to about 100 valence and conduction states. However, thanks to many advancements in the algorithms used,[RPG12, DSS12, SFM19, FV21] the method was recently applied to a system of nearly 2000 total electrons. [FV22a]

Recently we developed a numerically efficient approach to the BSE that relies on a stochastic evaluation of W. [BNC22a] In the BSE in general, W is applied on many pair densities of states (see later for details). Since its evaluation is linear in system size, systems with hundreds of active electrons become feasible.

In this work we go a step beyond, and show that not only is the action of W obtained efficiently with a stochastic approach, but, equally important, the explicit matrix elements

can be replaced by a stochastic sampling of the sea of pair-densities. This, in principle, limits the major cost of the BSE to quadratic scaling, thereby opening the possibility of calculating spectra for very large systems.

A key in our proposed approach is the numerically exact rewriting of the action of W by subtracting and adding a simple Coulomb-like interaction v_W. Thus, the stochastic sampling only needs to be applied on this small difference $W - v_W$, with the bulk of the action of W done by v_W. This stabilizes the stochastic approach ensuring that for larger systems we do not need more stochastic samples to represent W.

Choosing an analytical Coulombic-like interaction to substitute for W has been done before in some efficient implementations of the BSE,[FRS08, RBN15] but here we choose an optimized v_W which is fitted to the actual W of each system. The use of v_W is also reminiscent of TDDFT based approaches with long range exchange and a polarizable medium that mimics the dielectric function. [BBM20] In our work, since v_W is built from W, the ab initio nature of the BSE is retained, while still reducing the complexity of the exchange to be similar to traditional Fock exchange.

Using v_W by itself also gives fairly reasonable spectral results. Thus, our work is not only a numerically more efficient way to calculate the BSE spectra, but gives an alternative, fairly cheap algorithm, at the same cost as time-dependent Hartree-Fock (TDHF), which itself can be done cheaply with a stochastic approach,[NRC15b, GNB15, RBN15] that has an improving accuracy for increasingly large systems.

The paper is organized as follows. The methodology is reviewed in Section 5.2. Section 5.3 shows results for a variety of medium to large carbon based systems. Conclusions follow in Section 5.4.

5.2 Methods

5.2.1 Iterative BSE formulation

We first overview the methodology for obtaining spectra from the BSE for a given W using an iterative method. The full derivation for this method from the time-dependent Hartree-Fock (TDHF) formalism was given in previous work on the BSE[BNC22a], and good reviews of this kind of derivation can be found in Refs. [Neg82, NB05].

The starting point is a closed shell system with $2N_{occ}$ electrons. The exciton (electron-hole) basis is a set of n_o occupied (valence) states $\phi_i, \phi_j, ...$, times a set of n_c conduction states, $\phi_a, \phi_b, ...$, which are eigenstates of a zero order (typically DFT) Hamiltonian. Further, we use the TDA, although the approach is generalizable to the full BSE.

The starting optically excited vector f^0 corresponds to the infintessimal change to a ground state orbital perturbed along a coordinate in the direction of the laser polarization, which takes the form of:

$$f^0_{ja} = \langle \phi_a | x | \phi_j \rangle. \tag{5.1}$$

The spectrum is then obtained from a matrix element of $\delta(w - A)$, where A is Liouvilian operator of the BSE matrix which governs the motion of the excitons:

$$\sigma(\omega) \propto \omega \langle f^0 | \delta(A - \omega) | f^0 \rangle, \tag{5.2}$$

where the broadened delta function is obtained by a Chebyshev series,

$$\delta(A - \omega)|f^0\rangle = \sum_n c_n(\omega)|f^n\rangle, \tag{5.3}$$

where c_n are numerical coefficients and f^n are Chebyshev vectors, obtained by iteratively applying A on f^0. In practice we find that the best results are obtained by simple smoothly-decaying weights, in the spirit of those used in Ref. [WWA06]

$$c_n(\omega) = \left| \frac{d\theta_\omega}{\omega} \right| \cos^2 \left(\frac{\pi n}{2N_{\text{cheby}}} \right) \cos(n\theta_\omega), \tag{5.4}$$

where N_{cheby} is the number of Chebyshev terms used, which determines the frequency resolution. Here we introduced the Chebyshev angle $\theta_\omega \equiv \cos^{-1}(\omega/\delta A)$, while δA is an upper bound on the half-width of the spectrum of A. Note that without the $|d\theta_\omega/\omega|$ term, these weights would yield a delta function in θ_ω, and this term converts the overall function to a delta function over ω.

Formally A is made from three terms: diagonal, Hartree and the so-called direct term (in a somewhat confusing notation, since it resembles Fock exchange):

$$A_{ia,jb} = (\varepsilon_a - \varepsilon_i + \Delta)\delta_{ij}\delta_{jb} + \kappa(ia|jb) - (\phi_a\phi_b|W|\phi_i\phi_j), \tag{5.5}$$

where we introduced the electron and hole energies associated with the respective zero order eigenstates as ε_a and ε_i respectively, while the round brackets refer to an $(r, r|...|r', r')$ notation, and $\kappa = 2$ is used for singlet excitations and $\kappa = 0$ for triplet excitations. Δ is a scissors shift that corrects the gap to match accurate GW calculations, and could, if wished, depend on the exciton (i, a) indices – as is especially important for small systems. [GHK18, MHB22] In practice we use the cheap sGW, i.e., stochastic GW (see below) to calculate the scissors term,[NGA14a, VRN18] and for further accuracy we implement the scissor-shift self-consistent GW_0 approach, labeled ΔGW_0,[VBR18b] which post-processes the results of sGW and generally raises the gap by a few tenths of eV.

The Hartree integral is (assuming real orbitals):

$$(ia|jb) = \int \phi_i(r)\phi_a(r)v(r - r')\phi_j(r')\phi_b(r')drdr', \tag{5.6}$$

where $v(r - r') = 1/|r - r'|$ is the Coulomb interaction. Finally, the most numerically costly part involves the effective interaction

$$(\phi_a\phi_b|W|\phi_i\phi_j) = \int \phi_a(r)\phi_b(r)W(r, r')\phi_i(r')\phi_j(r')drdr'. \tag{5.7}$$

Note that W refers to the static part of the effective interaction, and we ignore here the effects of the dynamic part.

Numerically, one acts with A on an arbitrary vector f as follows:

$$\begin{aligned} g_{ia} \equiv (Af)_{ia} = \\ (\varepsilon_a - \varepsilon_i + \Delta) f_{ia} + \frac{\kappa}{2} \langle \phi_a | \delta v_H | f_i \rangle - \langle \phi_a | y_i \rangle, \end{aligned} \tag{5.8}$$

where the grid-representation of the exciton is

$$f_i(r) = \sum_b f_{ib} \phi_b(r) \tag{5.9}$$

while the exciton Coulomb density, $\delta n(r) = 4 \sum_j f_j(r) \phi_j(r)$, is used to generate the Hartree potential,

$$\delta v_H(r) = \int \frac{\delta n(r')}{r - r'} dr'. \tag{5.10}$$

The numerically expensive part in Eq. (5.8) comes from the direct term, involving the action of the effective interaction,

$$y_i(r) \equiv \sum_j W_{ij}(r) f_j(r), \tag{5.11}$$

where

$$W_{ij}(r) \equiv \int W(r, r') \phi_i(r') \phi_j(r') dr'. \tag{5.12}$$

In our recent work,[BNC22a] we used the stochastic time-dependent Hartree (i.e., stochastic W) approach,[GNB15] developed originally for sGW,[NGA14a, VRN18] to evaluate each specific W_{ij} function in linear scaling; see Ref. ([BNC22a]) for full details on this step of the method. The application of stochastic W makes is feasible to study systems with up to several hundred valence states. Nevertheless, as there are $\simeq N_v^2/2$ such terms for N_v valence states, the overall cost is cubic in system size with a large pre-factor, so that including more than ≈ 300 valence states will be numerically challenging.

Lastly, we note that this method directly obtains the BSE spectrum without capturing all excitonic eigenstates of the system. As demonstrated in our previous work on the subject,[BNC22a] specific excitonic states (for instance but not limited to the lowest energy exciton), can be purified out from this formalism using the filter diagonalization approach.[Neu90b, MRT93]

5.2.2 Stochastic evaluation of matrix elements

To overcome the scaling problem, we use a stochastic representation of the sum. Specifically, we define a stochastic process, made from "instances". For each such instance, we define two independent stochastic vectors,

$$\begin{aligned} \bar{\beta}(r) &= \sum_l \bar{\beta}_l \phi_l(r), \\ \bar{\bar{\beta}}(r) &= \sum_l \bar{\bar{\beta}}_l \phi_l(r), \end{aligned} \tag{5.13}$$

where $\bar{\beta}_l = \pm 1$, $\bar{\bar{\beta}}_l = \pm 1$.

Using

$$\left\{ \bar{\beta}_i \bar{\beta}_j \right\} = \left\{ \bar{\bar{\beta}}_i \bar{\bar{\beta}}_j \right\} = \delta_{ij}, \tag{5.14}$$

where curly brackets denote an average over many stochastic instances, it follows that

$$\left\{ \bar{\beta}_i \bar{\bar{\beta}}_j \beta(r) \right\} = \phi_i(r) \phi_j(r), \tag{5.15}$$

where

$$\beta(r) \equiv \bar{\beta}(r) \bar{\bar{\beta}}(r). \tag{5.16}$$

Inserting the relations above to the numerically expensive effective potential term in Eq. (5.8), the latter becomes

$$y_i(r) = \left\{ \bar{\beta}_i \langle r|W|\beta\rangle f_{\bar{\bar{\beta}}}(r) \right\}, \tag{5.17}$$

where we defined

$$f_{\bar{\bar{\beta}}}(r) = \sum_j \bar{\bar{\beta}}_j f_j(r), \tag{5.18}$$

while $\langle r|W|\bar{\beta}\bar{\bar{\beta}}\rangle \equiv \int W(r,r')\bar{\beta}(r)\bar{\bar{\beta}}(r)dr'$.

The resulting algorithm is thus quite simple. A large but finite number of stochastic instances, N_β, is defined. Then, one applies W (calculated itself stochastically) on the stochastic representation of the valence density $\bar{\beta}(r)\bar{\bar{\beta}}(r)$, to yield a set of N_β vectors, $\langle r|W|\bar{\beta}\bar{\bar{\beta}}\rangle$, which is stored and used in the Chebyshev iterative step, $f \to Af$. The formulae are further detailed in the next section.

5.2.3 Optimized attenuated interaction

5.2.3.1 Sampling a small difference

The formalism above is clearly a member of our stochastic approaches to quantum chemistry. [BNR22, NBR14a, NGA14a, NRC15b, RBN15] The key in these approaches is the replacement of individual molecular orbitals by random orbitals, that are stochastic combination of individual orbitals. For example, a valence orbital is replaced by a stochastic combination of valence orbitals, etc.

A key practical point in this paradigm is that it is best to stochastically sample numerically small quantities. This is best achieved by sampling just the difference between the desired quantity and a simpler one, i.e., writing

$$W = \{W - v_W\} + v_W \tag{5.19}$$

where curly brackets indicate again a statistical average and $v_W(r, r')$ is an interaction which is "cheap" to act with. Here we use the simplest such form, a translationally invariant two-body interaction,

$$v_W(r, r') = v_W(r - r') \tag{5.20}$$

The specifics of v_W are delineated later.

Using this decomposition, the action of W, Eq. (5.17), is modified to

$$\begin{aligned} y_i(r) &= \left\{ \bar{\beta}_i \langle r|W - v_W|\beta\rangle f_{\bar{\beta}}(r) \right\} + \sum_j f_j(r) \langle r|v_W|\phi_i\phi_j\rangle \\ &= \left\{ \bar{\beta}_i \langle r|W - v_W|\beta\rangle f_{\bar{\beta}}(r) \right\} + \sum_j f_j(r) v_{W,ij}(r), \end{aligned} \tag{5.21}$$

where $v_{W,ij}(r) = \int v_W(r, r')\phi_i(r')\phi_j(r')dr'$.

5.2.3.2 Optimizing the effective interaction potential

The equation above is exact no matter what v_W is – a better choice of v_W would simply lead to faster convergence of the sampling of $\{W - v_W\}$. Further, to avoid the singularities of

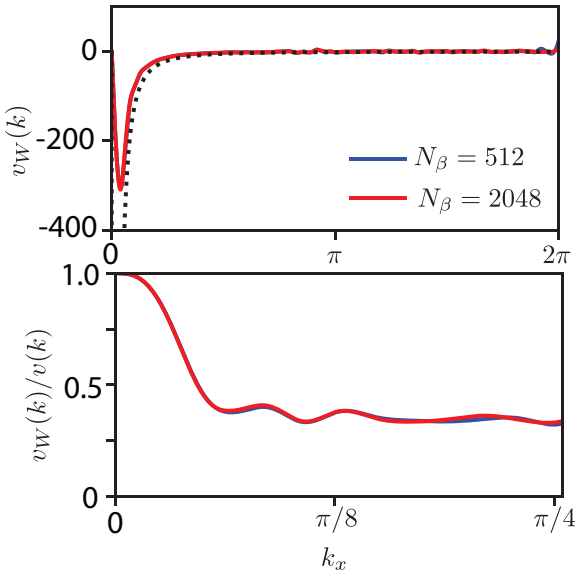

Figure 5.1: (Top) The fitted $v_{W\,\mathrm{pol}}(k)$ potentials (red) and the bare Coulomb interaction $v(k)$ (black dots) for $C_{96}H_{24}$, shown for a range of k_x, for $k_y = k_z = 0$. (Bottom) The ratio $v_W(k)/v(k)$ for this system, calculated for the same k-values range as in the top panel. The results converge quickly with the number of stochastic sampling functions, N_β.

the Coulomb potential we fit only the polarization part, i.e., $W - v_W = W_{\mathrm{pol}} - v_{W\,\mathrm{pol}}$, where $W_{\mathrm{pol}} = W - v(k)$, and similarly for $v_{W\,\mathrm{pol}}$. Here $v(k)$ is the Coulomb potential for finite systems, which is obtained with the Martyna-Tuckerman approach;[MT99b] this potential is the usual $4\pi/k^2$ at high momenta but levels off to a finite large value at $k = 0$.

Given an arbitrary large system, we can ask what will be the optimized $v_W(r - r')$. Interestingly, the stochastic paradigm answers that question easily. Specifically, optimize the functional

$$J = \sum_{ij} (\phi_i\phi_j|(W - v_W)^2|\phi_i\phi_j) \tag{5.22}$$

where again i, j are occupied states. Calculate the sum then stochastically

$$J = \Big\{\langle\beta|(W - v_W)^2|\beta\rangle\Big\} = \Big\{\int |\langle k|W - v_W|\beta\rangle|^2 dk\Big\}, \tag{5.23}$$

where, as before, β is a stochastic combination of the occupied two-electron product terms

from Eq. (5.16).

Since our choice of v_W is diagonal in momentum space, $\langle k|v_W|\beta\rangle = v_W(k)\beta(k)$, it is easy to show that the optimised J, giving $\delta J/\delta v_W^*(k) = 0$, is obtained with

$$v_W(k) = \frac{\left\{\beta^*(k)\langle k|W|\beta\rangle\right\}}{\left\{\left|\langle k|\beta\rangle\right|^2\right\}}. \tag{5.24}$$

In practice a very small numbers of terms, typically $N_\beta \approx 500$, is sufficient to converge the values of $v_W(k)$. This convergence is demonstrated in Fig. 5.1.

5.2.3.3 Replacing W by the optimized attenuated interaction

If v_W is a good enough approximation to W, so the objective J is sufficiently small, we may even, as mentioned, throw out the stochastic $\{W - v_W\}$ term in Eq. (5.21), i.e., approximate

$$y_i(r) \simeq \sum_j f_j(r) v_{W,ij}(r). \tag{5.25}$$

More generally, we can approximate the full BSE by replacing W by v_W, converting thereby the equation to TDHF-like with a modified Fock kernel, where $|r-r'|^{-1}$ is replaced by v_W. Note that simplified forms have been used to approximate W, see e.g.,[FRS08], but here the optimized attenuated interaction is based on the true system-dependent $W(r, r')$, yielding a fully ab-initio approach. We label the resulting method as Time-Dependent Optimized-Attenuated-Interaction (TDOAI).

5.2.4 Overall Algorithm

The overall algorithm is then:

- First, a set of stochastic-GW calculations on the HOMO and LUMO is performed to find the necessary scissors shift.
- Second, a set of N_β random representations β of the occupied-states product is calculated and stored per Eqs. (5.13) and (5.16).

- Each of these β's is then used as input for a stochastic-GW calculation, yielding the action of the static effective interaction $\langle r|W|\beta\rangle$.

- The Fourier-components of the optimized attenuated interaction, $v_W(k)$, are then calculated from Eq. (5.24).

At that point one has the optimized attenuated interaction, but there are still several possibilities for the dynamics, i.e., how to propagate and solve the BSE and with which terms included. We summarize four such possibilities, and the Results section below exemplifies the first two, which use the Chebyshev approach (based on Eqs. (5.2), (5.3) and (5.8))

1. The BSE kernel, in the Tamm-Dancoff approximation, can be calculated by stochastically sampling the $\{W - v_W\}$ difference, Eq. (5.21).

2. Another direction is to ignore the $W - v_W$ term and act only with the optimized effective interactionv_W, i.e., use Eq. (5.25) instead of Eq. (5.21).

3. One could use the first option, but go past the Tamm-Dancoff approximation, i.e., include off-diagonal terms. The simplest option, without increasing the numerical effort substantially, would be to use the optimized attenuated interaction in the off-diagonal portion of the BSE. Since the off-diagonal BSE term (i.e., the term that goes beyond the Tamm-Dancoff approximation) is quite small, it should be accurate to replace in it W entirely by v_W. This would reduce the numerical cost substantially compared to the full cost of applying $\{W - v_W\}$ stochastically in the off-diagonal term, which would have required a different samplings of the action of W, this time acting on an occupied-unoccupied pair density.

4. Finally, just like the second option above, we could use only the attenuated interaction while avoiding the Tamm-Dancoff approximation. This could be done by either extending the exciton vector space to go beyond the TDA, or by replacing the Chebyshev method altogether by a full-fledged TDHF-like study that uses stochastic-exchange

[RBN15] but would employ here the optimized TDOAI exchange-interaction v_W; this direction would be pursued in a latter publication.

5.3 Results

We demonstrate the new method on a sample set of hydrocarbons, including linear acenes, polycyclic-aromatic hydrocarbons (PCH), and fullerene based systems; see Table 5.1 and Fig. 5.2. The structures for these molecules were taken from Refs. [YDY16, MXF20] and the open source library associated with Ref. [al21]. For all systems, we use a generous box size extended at least 6 Bohr beyond the edge of the molecule, with a grid spacing of 0.5 Bohr. For the planar molecules, we use a grid size of 15 Bohr in the out-of-plane direction, such that no size effects are seen on the DFT band gap. All DFT calculations were performed with norm-conserving pseudo-potentials and used the PW-MT LDA exchange-correlation functional. [GNB15, RPM03, WKG13]

To determine the correct scissor shift, Δ in Eq. (5.8), we first correct the DFT band gap through a stochastic GW calculation,[NGA14a, VRN18, VLB18a] done self-consistently. [VBR18b] Further, the dielectric correction $W(k \to 0)$, was determined by a linear fit of the BSE spectra at different grid sizes. [BNC22a, ORG95, RVM06] The final scissor shift is then the sum of the dielectric correction and the GW band-gap correction.

The calculations of the action of W on either deterministic or stochastic DFT orbital pairs, $\langle r|W|\phi_i\phi_j\rangle$ and $\langle r|W|\beta\rangle$ respectively, were done with only 10 stochastic time-dependent orbitals. Refer to Ref. [BNC22a] for explicit details of this step. The sGW calculations were done with a broadening of 0.1 Hartree. A time-step $dt = 0.1$ a.u. was used for a split-operator propagation, and "cleaning" (i.e., projection of the excited component of the orbitals to be orthogonal to the occupied space – see [BNC22a]) was done every 10 steps.

The number of samples needed for a deterministic calculation is $N_v(N_v + 1)/2$ for N_v valence orbitals. In calculations where W is acting on stochastic orbitals, N_β=2000 was

Table 5.1: The grid size, number of occupied orbitals, and the chosen number of valence and conduction subset sizes for each system. The final column shows the remaining fraction of the polarization $W_{\rm pol}$ interaction not captured by the optimally fitted $v_{W\,\rm pol}$ interaction.

System	N_g	N_o	N_v	N_c	$\frac{\langle (W_{\rm pol}-v_{W\,\rm pol})^2\rangle}{\langle W_{\rm pol}^2\rangle}$
Nap	50,688	24	16	40	0.18
Tet	76,800	42	24	64	0.13
Hex	113,520	60	36	80	0.11
Oct	132,000	78	45	100	0.10
Cor	69,984	45	27	70	0.18
C_{60}	195,112	120	64	120	0.25
Kek	147,000	108	54	110	0.09
$C_{96}H_{24}$	324,480	204	100	500	0.09
10-CPP+C_{60}	381,024	260	100	500	0.13

generally used.

We first discuss the convergence of the fitted v_W and how does it compare with W.

Figure 5.1 shows the convergence of the fitting of the polarization portion of v_W. The top sub figure shows $v_{W\,\rm pol}$ in comparison to (minus) the bare Coulomb potential $v(k)$ for this finite system. Note that $v_{W\,\rm pol}$ is automatically zero at $k = 0$ as $W_{\rm pol}$ emanates from a polarization $\chi_{\rm pol}$ which vanishes at $k = 0$ due to the orthogonality of the particle-hole pairs which make it. (For periodic systems this effect is counteracted by the singularity of the Coulomb potential at $k = 0$, unlike finite systems, where $v(k = 0)$ is large but does not diverge so $W_{\rm pol}(k = 0)$ vanishes.)

In the bottom panel of Figure 5.1 we compare the ratio of $v_W(k)$ and $v(k)$. The ratio is 1 for low k due to the finite size of the systems, but levels down at higher k values.

Table 5.1 shows the fraction of $W_{\rm pol}$ left for stochastic sampling after removal of $v_{W\,\rm pol}$. This fraction is quite small and is clearly independent of system size. Additionally, it does

not appear to change with the approximate dimensionality of the system– linear, planar or spherical. Similarly, Figure 5.3 shows, for a slice along the x-axis, the action of both W and v_W on two pair densities. The results are very similar, but the total magnitude is often decreased when applying v_W.

We now turn to the spectra. We used an iterative BSE Chebyshev procedure, and for all systems the upper bound on the half-width of the Liouvillian was taken as $\delta A = 16.5$ eV. We used $N_{\text{cheby}} = 500$ terms (Eq. 5.4), which is approximately equivalent to a Gaussian energy broadening with half width of 0.08 eV. The effect of the broadening is negligible for the larger systems where the spectrum is naturally quite broadened.

In Figure 5.4 we show the spectra of all nine systems using a deterministic BSE,[BNC22a] the v_W only TD-OAI, and the stochastic $v_W + \{W - v_w\}$ approach of this paper. Using v_W by itself is only qualitatively accurate, but stochastic sampling of $\{W - v_W\}$ quickly restores the accuracy of the deterministic calculation.

As is clear from Figure 5.5, at least $N_\beta = 300-400$ stochastic samples are needed to get a 0.1 eV accuracy on the optical gap. Generally, the low-energies spectral peaks in Figure 5.4 are converged to 0.02 eV at low energies by 2000 stochastic samples. (The one exception is fullerene, where the lowest-energy spectral peak converges to only 0.08 eV at $N_\beta = 5000$; this is in line with the lower quality of the v_W fit to W for fullerene, see Table 5.1.) Depending on Depending on the quality of v_W, we find on average that the $W - v_W$ formalism converges at least 20 times faster than using a stochastic W by itself, i.e., without using v_W.

The rapid convergence with N_β implies that the stochastically sampled $\{W - v_W\}$ is generally numerically superior to the deterministic approach for systems with more than ≈ 70 calculated valence orbitals. This is because of the $N_v^2/2$ scaling of the number of pairs W_{ij} when using directly the deterministic approach, Eq. (5.11).

In Table 5.2 we summarize the evolution of the gap for each system. The results are in fair agreement with the experimental values, considering the Tamm-Dancoff approximation

Table 5.2: Gaps (eV) from stochastic DFT at the LDA level, stochastic G_0W_0, self consistent ΔGW_0,[VBR18b] the stochastic BSE optical gap (this work), and a reference experimental optical gap.

	DFT	G_0W_0	ΔGW_0	BSE	Experimental Optical Gap	
Nap	3.4	7.6	8.0	4.3	4.1	[CTL16, MDM19]
Tet	1.6	5.1	5.4	2.7	2.6	[CTL16, MDM19]
Hex	0.8	3.7	3.9	1.8	1.9	[TB10, KEA17, TB20]
Oct	0.4	2.9	3.1	1.3	1.5	[TB20, KEA17, MTK09]
Cor	3.2	6.7	7.1	4.3	3.7	[RJS08]
C_{60}	1.7	4.4	4.7	2.3	1.8	[RSK93, LVJ95]
Kek	2.1	4.8	5.1	3.2		
$C_{96}H_{24}$	1.2	3.0	3.1	1.9	2.0	[LTZ22]
10-CPP+C_{60}	0.7	3.3	3.5	3.5	3.4 †	[XKW18]

† Stabilized system complex.

and the lack of dynamic corrections.

5.4 Conclusions

We introduced here an optimized effective potential v_W to reduce the magnitude of the W term in BSE, enabling an efficient stochastic evaluation. With the introduction of v_W, the required number of stochastic orbitals is small relative to system size, thereby reducing the scaling of the method so that large system sizes are now feasible. The new algorithm was checked successfully on nine molecules of varying dimension and size.

The present work overcomes the cost of the most expensive part in the BSE algorithm, preparing the action of W on the product states, by dividing W to an exchange-type potential v_W, and a stochastically sampled remainder $\{W - v_W\}$. There is, however, a lot of room for further scaling improvements. Currently, we do not implement the exchange in a particularly efficient way, so that the scaling is still cubic, but a fully stochastic exchange could further reduce the scaling. [NRC15b, XKW18, RV22] Similarly, for both the exchange and the Coulombic part, i.e., the matrix elements in Eq. (5.8), a localized basis set would have reduced the scaling as many exchange matrix elements would then vanish the grid extent for the exchange integrals would be reduced. Once these improvements are made the overall scaling of the method would reach quadratic. [FV21, FV22a]

Further work on this method will include fitting W to give a v_W interaction that goes beyond a translationally invariant interaction but preserves the quasi-linear scaling of $\int v_W(r, r')\beta(r')dr'$. An improved fit would make it possible to use very few stochastic samplings of the difference operator $\{W - v_W\}$ or just forego this term completely, keeping only v_W.

Further improvements include the anti-resonant to resonant transition couplings to go beyond the Tamm-Dancoff approximation. As mentioned in Section 5.2.4, since the contribution of this 'off-diagonal' coupling in the BSE is substantially smaller than that of the resonant W, they could be represented by v_W alone rather than the full W, so no addtional

W samplings would be needed.

In addition, dynamical corrections are needed in many systems with dominant $n \to \pi^*$ and $\pi \to \pi^*$ excitations. [MRM09, BAM12] While recent work has shown best results with a matrix perturbation theory method,[LB20] TDDFT-type approaches have been successful at capturing double excitations with a dynamical exchange kernel. [RSB09, HIR11, RT16]

While the formalism we present is naturally suitable to systems with fairly extended active (occupied and unoccupied) states, its extension to systems where the optically active states are very localized, e.g., defects in otherwise homogeneous solids, should be straightforward. In such cases, as far as action of W, the occupied (as well as the active unoccupied) state space should be divided to a few isolated states, while the rest of the states would be treated stochastically, as done here. This will be developed in a future publication.

Finally, the grid-based approach presented here should be extendable to basis-set techniques, since in the BSE stage it just uses the eigenstates and eigenvalues, and those come from an underlying DFT calculation, which could be grid-based (as done here) or use basis-sets. Similarly, the action of stochastic W via time-dependent Hartree propagation can also be done with basis-sets. The only fine points are that some of the intermediate calculations are most easily done on a grid, such as the calculation of the stochastic pair functions $\beta(r)$, and the resulting convolutions; but as these are mostly dependent on low wavelengths, rather rough grids could be employed, as done in several basis-set techniques that use intermediate grids.

To summarize, our main point in this paper is that the optimized attenuated potential reduces the magnitude of the effective interaction W. This reduces the required number of stochastic sampling of $\{W - v_W\}$ to a manageable number, in the few thousands, enabling efficient BSE simulations. Further, when fitting W to a translationally-invariant interaction (which is applied by convolution), the resulting TDHF spectra with v_W as the exchange interaction are in quite good agreement with the exact W-based BSE results.

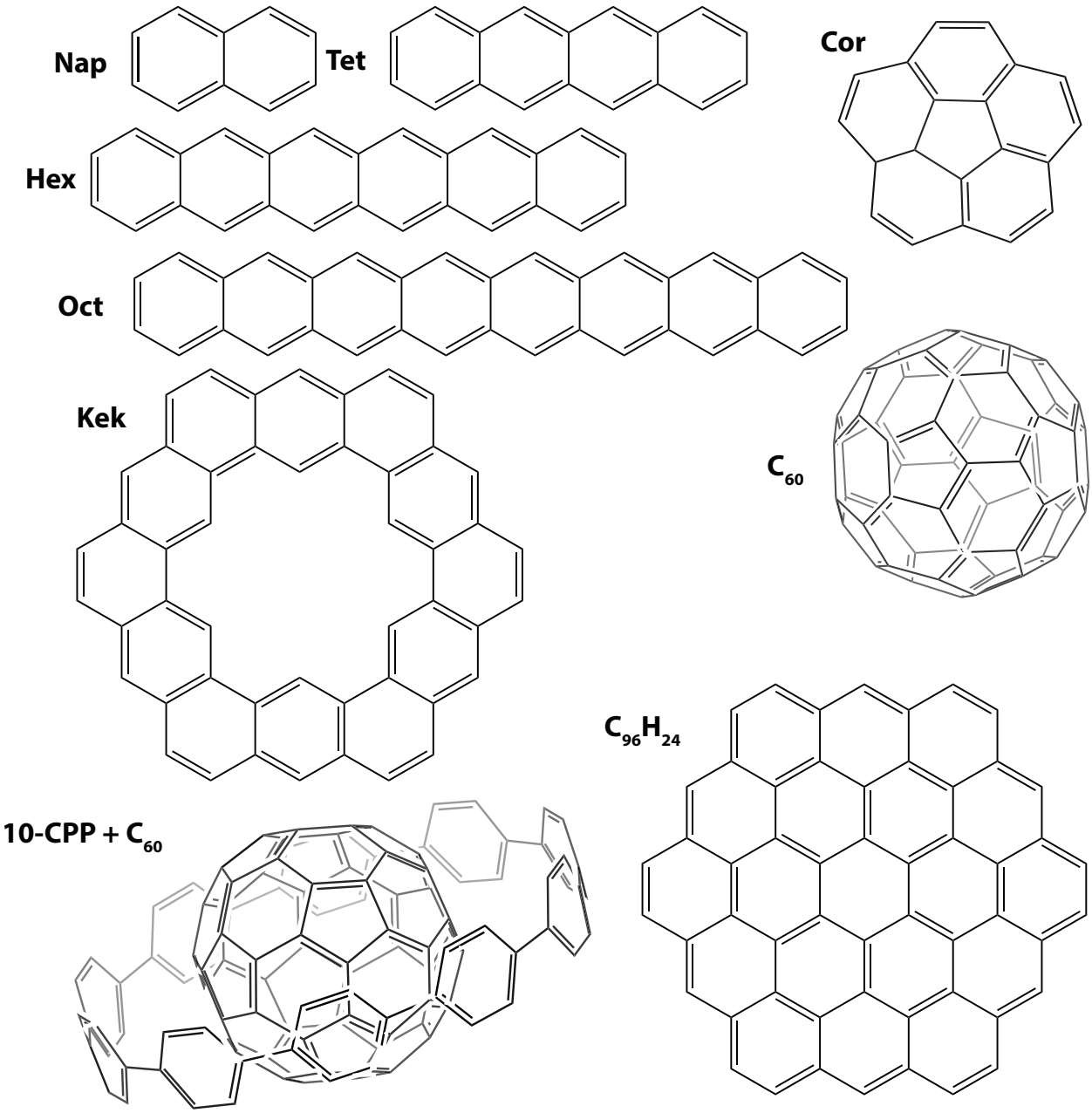

Figure 5.2: Structures and abbreviations for all the systems used in this paper.

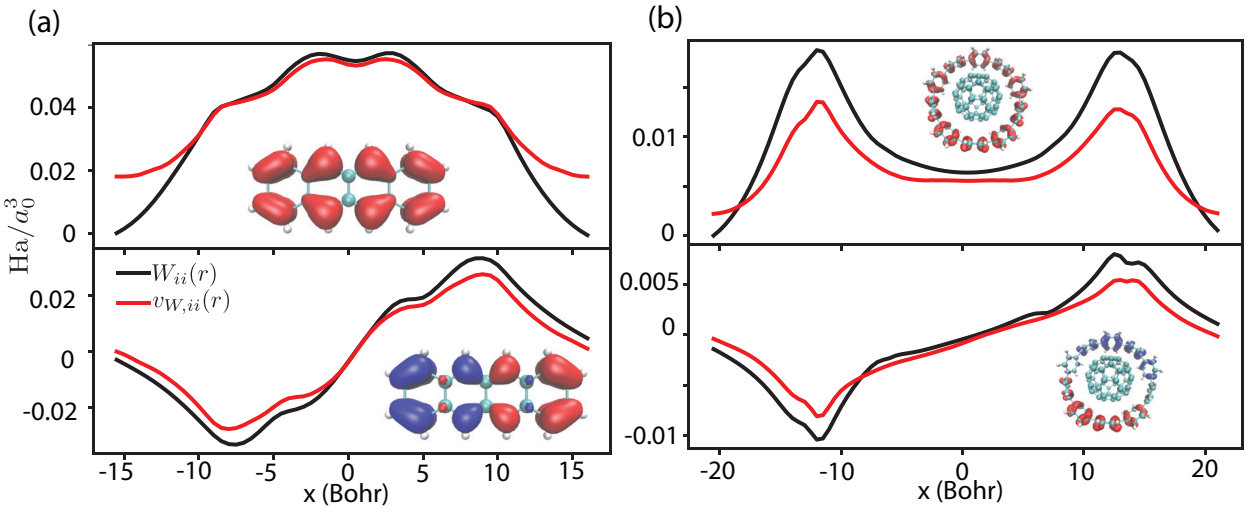

Figure 5.3: X-axis slice of $\langle r|W|\phi_i\phi_j\rangle$ and $\langle r|v_W|\phi_i\phi_j\rangle$, i.e., the action of the true W (black) and the optimized v_W (red) on a two-orbital pair density. In the top row W and v_W act on the HOMO density ($i = j =$ HOMO). In the bottom row they act on the pair density of the HOMO $\times$ HOMO $-$ 1 orbitals. The left part, Column (a), is for tetracene, while Column (b) shows the same plots for the much larger 10-CPP+C_{60}.

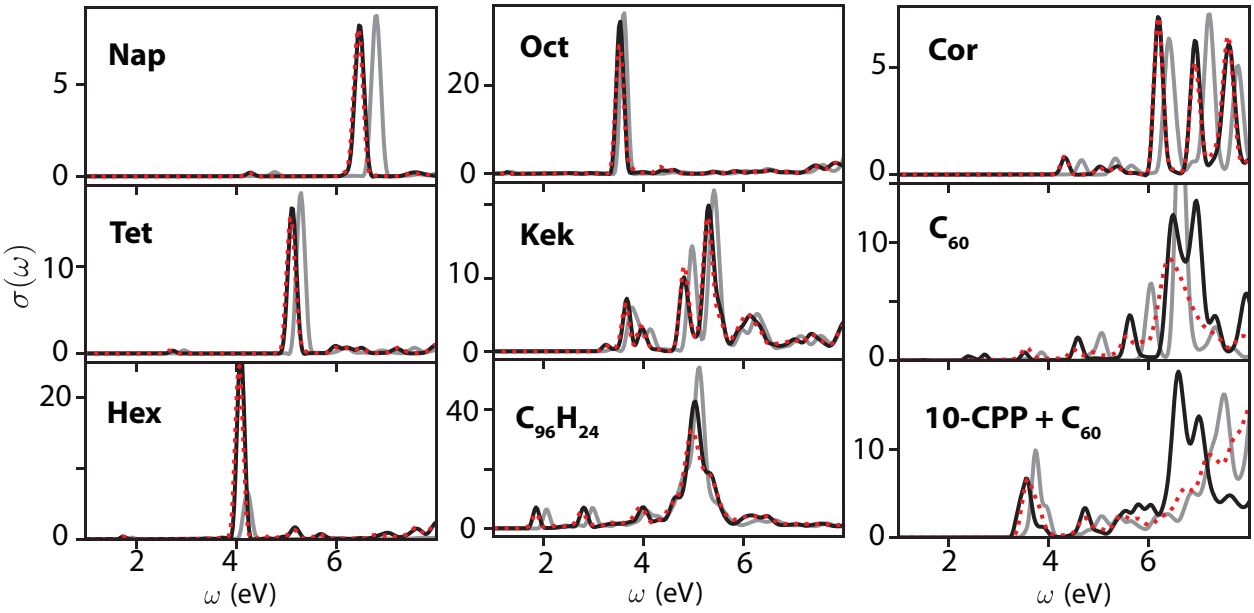

Figure 5.4: Spectra of singlet excitations for all systems using a BSE with deterministic orbitals (black) and full stochastic $v_W + \{W - v_W\}$ approach using $N_\beta = 2000$ (red dots). The TD-OAI calculation, where v_W is used for exchange alone, is shown in grey. For almost all cases, the stochastic approach matches the deterministic optical gap to within 0.02 eV or better; the one exception was fullerene, where $N_\beta = 5000$ was needed for convergence to 0.08 eV, in line with the lower quality of the v_W fit (Table 5.1).

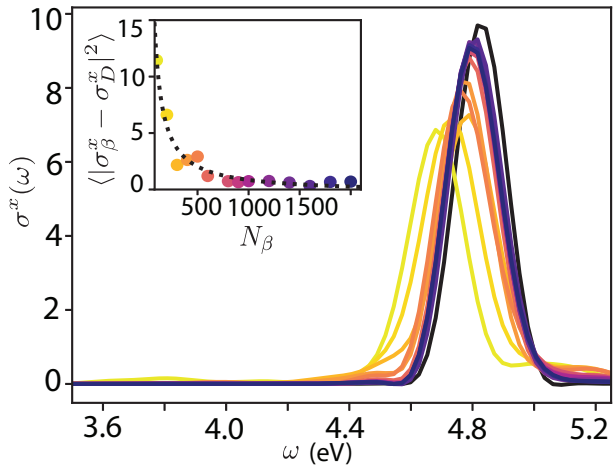

Figure 5.5: X-polarization spectra for tetracene (zooming in on the dominant spectral peak at 4.75 eV) at varying levels of stochastic approximation (colors), converging to the deterministic BSE (black dashes). The inlay shows the average variance over the 0-6 eV spectral region from the deterministic spectra for each level of approximation, N_β, with corresponding colors. The dotted curve is a fit to $1/N_\beta$.

CHAPTER 6

Neargap DFT: Sparse Compressed Stochastic Exchange for hybrid-functional DFT

6.1 Introduction to the Resolution of the Identity

The introduction of hybrid exchange and long-range hybrid functionals into density functional theory (DFT) dramatically improved their accuracy.[Bec93b, Bec93a, SDC94, HSE03, KSP08, BN05, LSW97] These improvements, now thirty years old, enabled the rapid growth of DFT as a standard tool in the chemistry lab, with the establishment of many popular commercial and open-source software. Unfortunately, it is this key improvement in functional design, exact exchange, that limits the size of computation feasible for most researchers with a set budget of computing power and time. Traditional Hartree-Fock type exchange requires the generation of all 2-electron integrals in a given basis, scaling naively as $\mathrm{O}(N_o^4)$ for N_o spatially occupied orbitals.

The most substantial advancement in improving the computational cost of exact exchange in ab-initio DFT has come in the form of the so-called "resolution of the identity" (RI) methods.[RRB12] Now widely adopted, these methods reduce exact exchange to cubic in scaling. For the entire set of 2e-integrals, $\langle pq|rs\rangle$, one expands the identity in another auxiliary basis, β, reducing a 4-center integral tensor to a product of two 3-center integral tensors, $\langle pq|rs\rangle = \sum_\beta \langle pq|\beta\rangle\langle\beta|rs\rangle$. Such auxiliary basis sets are optimized with density fitting.[MD82, VAF93] With this intelligent design, one can cap the number of β to be comparable to the number of atomic orbitals needed for the calculation,[JSG05] but without

fundamental improvements, this auxiliary basis still scales with system size.

Other efforts involve the power of parallel computing, such as fragmented systems, localized auxiliary orbitals, and sparse matrix algorithms.[DLY15, GK22] In extended systems, the sparsity of overlap integrals allows for highly optimized localized auxiliary orbitals and near linear scaling.[PAW20, GBS18] Multi-level fragmented approaches have also recently improved scaling, especially in spatially localized cases.[GK22] Modern graphical-processing units (GPUs) also contribute to unlocking larger and larger calculations with RI methods.[UM08, KLO21]

Separately, we introduced a stochastic formalism for Hartree-Fock or long-range exchange for grid based DFT codes.[NRC16] In this formalism the exchange becomes a projection to a stochastic occupied orbital, which is a random linear combination of all occupied orbitals represented on a grid basis, times a random amplitude due to the Coulomb potential. A statistical average over multiple random vectors converges to the matrix elements of the exchange operator. In this case, each random orbital covers the entire eigenbasis of the molecule, and the number of such operators typically does not grow with system size, and occasionally shrinks due to self averaging.[NRC16]

In this work we employ a different strategy whereby the individual molecular states are treated deterministically. However, the usual cost of making all the matrix elements of the Coulomb interaction is reduced by orders of magnitude (and its scaling made constant) by the fragmented-stochastic compression approach we developed in a different context, stochastic GW. [VLB18b] Basically, we have shown that data over a large grid can be efficiently represented by a stochastic basis made of many small "fragments". Beyond a small threshold, the error does not depend on the fragment size, only on the number of fragments, so a large number of short fragments can be used to represent efficiently data on a giant grid.

In this work, we combine the best of sparse stochastic basis compression with the resolution of the identity technique. In short, we split the Coulomb kernel for the exchange

calculation to two sets (see also Ref. [DCT20]). The first is the large interaction at few low-wavevectors (small k) which is treated deterministically. The remainder, the interaction at the very many (often millions) of high k's, is represented here cheaply and accurately by fragmented stochastic compression, i.e., by representing the interaction through a small number (few thousands here) of short stochastic vectors, and this number does not increase with system size.

The second ingredient to the present deterministic/fragmented-stochastic approach is to represent the hybrid-DFT Hamiltonian in the basis of molecular orbital states (MOs) near the Fermi energy (near-gap) from local-DFT. Specifically, we first perform a local- (or semi-local) functional DFT calculation, by any efficient basis-set or plane-wave method. We then divide the resulting local-DFT MOs to core, valence and conduction, as well as high virtual orbitals which are ignored.

The core orbitals of this preliminary calculation are assumed to be a good representation of the core orbitals in the eventual hybrid calculation. We therefore assume that the valence and conduction orbitals of the hybrid case can be expanded from the valence and conduction MOs of the local-DFT calculation. This restriction to top valence and bottom conduction orbitals is of course routinely done in beyond-DFT methods, such as RPA, TD-DFT and the Bethe-Salpeter Equation.

With the introduction of sparse stochastic compression to the plane wave auxiliary basis, the scaling of the resulting approach is very gentle with system size, so that in practice the hybrid exchange correction costs less than the underlying local-DFT calculation. Further, the approach is easily parallelizable. We label it as near-gap Hybrid DFT (ngH-DFT).

In the sections below, we develop the ngH-DFT formalism, benchmark its convergence for naphthalene and fullerene, and then show the method's power by solving for a hexamer dye complex, a large system of biological significance. The proper inclusion of exact exchange here in such a large biomolecule is promising for future use of general post-DFT methods in giant systems.

6.2 Neargap DFT: Methodology

6.2.1 Hybrid DFT in the Valence-Conduction Subspace

We begin with the Kohn-Sham (KS) orbitals $\{\phi_s\}$ and associated eigenvalues $\{\varepsilon_s\}$ of a ground-state DFT calculation approximately satisfying $h_0\phi_s \approx \varepsilon_s\phi_s$. It is not necessary that the starting calculation be fully converged, and it can originate from LDA, PBE, or whichever DFT flavor of choice, but for simplicity it will be denoted here as LDA-DFT.

The molecular orbitals from the LDA-DFT calculation, denoted by ϕ, are then divided into four set of states: N_{core} core, $N_v(= N_o - N_{core})$ valence, N_c conduction, and the remainder are high conduction states which are neglected.

We then assume that the core states from the LDA calculation are unchanged in the GKS-DFT, i.e.,

$$\psi_f = \phi_f,\ f \in core \tag{6.1}$$

where ψ refers to a GKS molecular orbital. Therefore, the $M \equiv N_v + N_c$ GKS near-gap (i.e., valence+conduction) states are assumed to be described by the valence-conduction LDA states, i.e.,

$$\psi_s(r) = \sum_p \phi_p(r) C_{ps}, \tag{6.2}$$

where s, p, q are indices over the M near-gap states.

The converged LDA-DFT Hamiltonian is expressed as (using atomic units throughout)

$$h_0 = -\frac{1}{2}\nabla^2 + v_{eN}^{NL} + v^0[n_0](r), \tag{6.3}$$

with the respective terms being the kinetic energy, non-local component of electron-nucleus interaction, and the local KS potential. The latter is a functional of the LDA density, $n_0(r)$, and contains the local electron-nucleus interaction, Hartree potential, and local exchange-correlation (XC) potential, taken here to be PW-LDA [PW92]):

$$v^0[n_0](r) = v_{eN}^{local}(r) + \int \frac{n_0(r')}{|r - r'|} dr' + v_{XC}^0[n_0](r). \tag{6.4}$$

The electron-nucleus interaction is handled with Troullier-Martins norm-conserving pseudopotentials.[T
Additionally, the Martyna-Tuckerman approach is used to avoid the effect of periodic images in our simulations.[MT99a]

We now turn to the GKS Hamiltonian. Here we employ a long-range hybrid, though the same formulation applies also to any other form, such as short-range or Becke-type fractional exchange. Note that to avoid a cluttering of indices we write here only the closed-shell GKS formalism, but the GKS Hamiltonian would generally be spin selective (unlike the LDA-DFT). In fact, the tuning procedure we use to yield the correct γ requires a spin-selective Hamiltonian, as discussed later.

The starting point is the long-range part of the Coulomb interaction, defined as $u^\gamma(|r - r'|) = \mathrm{erf}(\gamma|r - r'|)/|r - r'|$, so for the exchange the Coulomb kernel in position space is split as [LSW97]

$$\frac{1}{|r - r'|} = \frac{\mathrm{erfc}(\gamma|r - r'|)}{|r - r'|} + u^\gamma(|r - r'|). \tag{6.5}$$

The first term dominates at short-distances and is treated locally, while the second, long-range term, is accounted for explicitly.

Range-separated hybrid functionals excel in charge transfer and excitonic effects due to the correct $-1/|r-r'|$ asymptotic behavior of the exchange term. The use of exact exchange helps alleviate the non-physical long-range self-repulsion in the LDA potential. The range-separation parameter γ is best obtained by enforcing piece-wise linearity of the energy with electron number.[BLS10]

The GKS Hamiltonian is then

$$h = -\frac{1}{2}\nabla^2 + v_{eN}^{NL} + v^\gamma(r) + X_{val}^\gamma + X_{core}^\gamma, \tag{6.6}$$

where γ refers to one or more parameters of the hybrid exchange. The γ-dependent Kohn-Sham potential is:

$$v^\gamma(r) = v_{eN}^{local}(r) + \int \frac{n(r')}{|r - r'|} dr' + v_{XC}^{\mathrm{SR},\gamma}[n], \tag{6.7}$$

where SR denotes short-range and $n(r)$ is the overall density, made from a sum of core and valence densities:

$$n(r) = n^{core}(r) + n^{val}(r), \tag{6.8}$$

where $n^{core}(r) = 2\sum_{f\in core} |\phi_f(r)|^2$. The valence density is

$$n^{val}(r) = 2\sum_i f_i|\psi_i(r)|^2 = 2\sum_{pq} \phi_p(r)P_{pq}\phi_q(r), \tag{6.9}$$

where the density matrix is $P_{pq} = \sum_i C_{pi}f_iC_{qi}$. Here, the sum runs over all occupied (or partially occupied) valence GKS MOs, and f_i is the occupation, which can be fractional:

$$f_i(\varepsilon_i;\mu) = \frac{1}{1+e^{(\varepsilon_i-\mu)/k_BT}}. \tag{6.10}$$

The action of the valence (short-hand *val*) component of the γ-dependent exact exchange operator on a general function η is

$$(X^\gamma_{val}\eta)(r) = -\sum_i f_i\psi_i^*(r)\int u^\gamma(|r-r'|)\eta(r')\psi_i(r')dr'. \tag{6.11}$$

The contribution of the core states to the exchange part of the Hamiltonian will be done perturbatively as discussed later. The LDA$\rightarrow$ GKS rotation matrix, Eq. (6.2), is initially $C_{ps} = \delta_{ps}$ and is then iterated in the SCF procedure.

The Hamiltonian matrix elements in the valence-conduction basis are

$$h_{pq} = \langle\phi_p|h_0 + \delta v + X^\gamma_{val}|\phi_q\rangle, \tag{6.12}$$

where $\delta v \equiv v^\gamma(r) - v^0(r)$ is the difference between the current GKS and initial estimate KS potentials.

Formally, the matrix elements of the valence exact-exchange are written as a 4-index integral tensor by starting with:

$$\langle\phi_q|X^\gamma_{val}|\phi_p\rangle = -\sum_i f_i\langle\phi_q\psi_i|u^\gamma(|r-r'|)|\psi_i\phi_p\rangle, \tag{6.13}$$

and inserting the expanded wavefunction gives

$$\langle\phi_q|X^{\gamma}_{val}|\phi_p\rangle = -\sum_{st}\langle\phi_q\phi_s|u^{\gamma}|\phi_t\phi_p\rangle P_{st}, \tag{6.14}$$

where real-valued orbitals are used with the chemists' convention of $\langle rr|r'r'\rangle$.

6.2.2 Deterministic/Fragmented-Stochastic Representation of the Coulomb Kernel

Our starting point is the exchange kernel in Eq. (6.14) which requires a generic convolution form, written schematically as $w(r) = \int u^{\gamma}(r-r')y(r')dr'$. This form is diagonal in reciprocal space and for finite grids it reads:

$$w(k) = \frac{1}{V}\sum_{k} u^{\gamma}(k)y(k). \tag{6.15}$$

In the Martyna-Tuckerman approach V is the overall volume including full padding in each direction (i.e., V is $2^3 = 8$ times the wavefunctions volume). Further, $u^{\gamma}(k)$ is not necessarily positive due to the Martyna-Tuckerman construct.

Since $u^{\gamma}(k)$ is large at low k, its action is evaluated deterministically below an assigned cutoff, k_{cut}. (The results are correct upon convergence for any k_{cut}, as this parameter only affects the speed of convergence). Specifically, for a given k_{cut} we divide k-space into 3 subspaces; "low" – values of k below k_{cut}.; "high^{+}" – values above k_{cut} where $u^{\gamma}(k)$ is positive; and "high^{-}" – values above k_{cut} where $u^{\gamma}(k)$ is negative. The number of points in each space is denoted, respectively, as $N_{k_{\mathrm{low}}}$, $N_{k_{\mathrm{high}^+}}$, and $N_{k_{\mathrm{high}^-}}$. Formally we write then the identity operator in the reciprocal space as

$$\begin{aligned} I = &\sum_{k_{\mathrm{low}}} |k_{\mathrm{low}}\rangle \langle k_{\mathrm{low}}| \, | \\ &+ \sum_{k_{\mathrm{high}^+}} |k_{\mathrm{high}^+}\rangle \left\langle k_{\mathrm{high}^+}\right| \, | + \sum_{k_{\mathrm{high}^-}} |k_{\mathrm{high}^-}\rangle \left\langle k_{\mathrm{high}^-}\right| \, |. \end{aligned} \tag{6.16}$$

The Coulomb long-range operator is then

$$\begin{aligned} u^\gamma = &\sum_{k_{low}} |k_{low}\rangle u^\gamma(k_{low}) \langle k_{low}| \, | \\ &+ \sum_{k_{high^+}} \sqrt{u^\gamma(k_{high^+})} |k_{high^+}\rangle \langle k_{high^+}| \, | \sqrt{u^\gamma(k_{high^+})} \\ &- \sum_{k_{high^-}} \sqrt{|u^\gamma(k_{high^-})|} |k_{high^-}\rangle \langle k_{high^-}| \, | \sqrt{|u^\gamma(k_{high^-})|}. \end{aligned} \tag{6.17}$$

Next we introduce stochastic fragmented bases [VLB18b] for the positive and negative high-k components. We detail the discussion for the high$^+$ space, and it follows analogously for the high$^-$ space.

A set of N_{α^+} short vectors is chosen, where each is randomly positive and negative in a "strip", also labeled as "fragment":

$$\alpha^+(k_{high^+}) = \pm \sqrt{\frac{N_{k^+}}{L}} A_{\alpha^+}(k_{high^+}). \tag{6.18}$$

Here $A_{\alpha^+}(k)$ is a projection to a randomly placed fragment α^+ of length L, i.e., is 1 within the fragment and 0 outside, so $\alpha^+(k_{high^+})$ is randomly positive or negative in the fragment and vanishes outside. The strip length, L, is the same for each fragment. The fragments thus randomly and uniformly sample the entire $\{|k_{high^+}\rangle\}$ space.

The constant factor in Eq. (6.18) ensures that with sufficient sampling the α^+ vectors form an orthonormal set, as explained below. A technical point is that fragments that start near the edge of the k_{high^+} space, i.e., that their starting point is larger than $N_{k_{high^+}} - L$, need to wrap around; alternately one can zero pad the space of $N_{k_{high^+}}$ points by L points on both sides, and then the constant square root factor in Eq. (6.18) needs to be slightly modified.

The strip length L and the number of stochastic vectors N_{α^+} are chosen such that each k point in the high$^+$ space is sufficiently "covered", i.e., will be adequately visited by the stochastic basis α^+. Specifically, we choose a coverage parameter, *cov*, that samples how

Table 6.1: Fundamental gaps for naphthalene, fullerene, and a 476 atom hexamer dye complex. Also shown are the total number of occupied states, the maximum numbers valence and conduction states, and the range-separation parameter for each system. All energies are in eV. The atomic basis-set calculation uses the NWChem package. Both ngH-DFT and the atomic basis-set RSH-DFT use the BNL XC functional.

System	N_o	N_v^{max}	N_c^{max}	Optimal γ (Bohr^{-1})	Plane-wave LDA-DFT	Atomic Basis-Set LDA-DFT	ngH-DFT	Atomic Basis-Set RSH-DFT
Naphthalene	24	24	104	0.285	3.34	3.34	8.63	8.54
Fullerene	120	120	480	0.189	1.63	1.64	5.42	5.40
Hexamer	660	200	400	0.120	1.23		3.81	

often, on average, each point is sampled. The number of chosen stochastic vectors is then

$$N_{\alpha^+} = \frac{cov \cdot N_{k_{high^+}}}{L}. \tag{6.19}$$

In the limit that this coverage parameter is large the stochastic fragments form an orthonormal basis, i.e.,

$$\left\{\alpha^+(k_{high^+})\alpha^+(k'_{high^+})\right\} = \delta_{k_{high^+}\,k'_{high^+}} \tag{6.20}$$

where the large curly brackets denote a stochastic sampling with formally $cov \to \infty$. In practice it is enough to use $cov \simeq 5$.

We then define N_{α^+} states, $|\xi^+\rangle$, with components

$$\langle k_{high^+}|\xi^+\rangle = \sqrt{u^\gamma\left(k_{high^+}\right)}\ \alpha^+(k_{high^+}), \tag{6.21}$$

We repeat the whole procedure for the $high^-$ space, and end up with N_{α^-} states for the negative high-k portion of the exchange kernel

$$\langle k_{high^-}|\xi^-\rangle = \sqrt{\left|u^\gamma\left(k_{high^-}\right)\right|}\ \alpha^-(k_{high^-}). \tag{6.22}$$

We now define a combined set of states, of size $N_\xi = N_{k_{low}} + N_{\alpha^+} + N_{\alpha^-}$, that is glued together via direct summation

$$|\xi\rangle = \{\sqrt{|u^\gamma\,(k_{low})|}|k_{low}\rangle\} \oplus \{|\xi^+\rangle\} \oplus \{|\xi^-\rangle\}. \tag{6.23}$$

We similarly define a sign vector of length N_ξ

$$g_\xi = \{sign\,(u^\gamma(k_{low}))\} \oplus \{1\} \oplus \{-1\}, \tag{6.24}$$

i.e., in addition to the sign of the interaction for the low-k components, g is composed of N_{α^+} values of 1 and N_{α^-} values of -1.

With these definitions, we now reach the stochastic fragmented basis representation of the exchange operator

$$u^\gamma = \sum_\xi |\xi\rangle g_\xi \langle\xi|. \tag{6.25}$$

This is the central equation of the deterministic/stochastic-fragment representation of the Coulomb interaction. As mentioned, it is used here only for the exchange component and not for the direct Coulomb interaction.

Inserting this form of u^γ in the matrix element of Eq. (6.14)

$$\langle\phi_q|X^\gamma_{val}|\phi_p\rangle = -\sum_{st\xi i}\langle\phi_q\phi_s|\xi\rangle g_\xi \langle\xi|\phi_t\phi_p\rangle C_{si} f_i C_{ti}, \tag{6.26}$$

and defining

$$u_{\xi pi} \equiv \sum_t C_{ti}\langle\xi|\phi_t\phi_p\rangle, \tag{6.27}$$

yields the final expression for the exact exchange matrix elements:

$$\langle\phi_q|X^\gamma_{val}|\phi_p\rangle = -\sum_{i\xi} u^*_{\xi qi} f_i g_\xi u_{\xi pi}. \tag{6.28}$$

Note that for a spin-resolved calculation, the only difference is that, in addition to the amplitudes C_{ti} and the exchange correlation potential δv, the transformed exchange vectors $u_{\xi p}$ and the X^γ_{val} matrix would also gain a spin index.

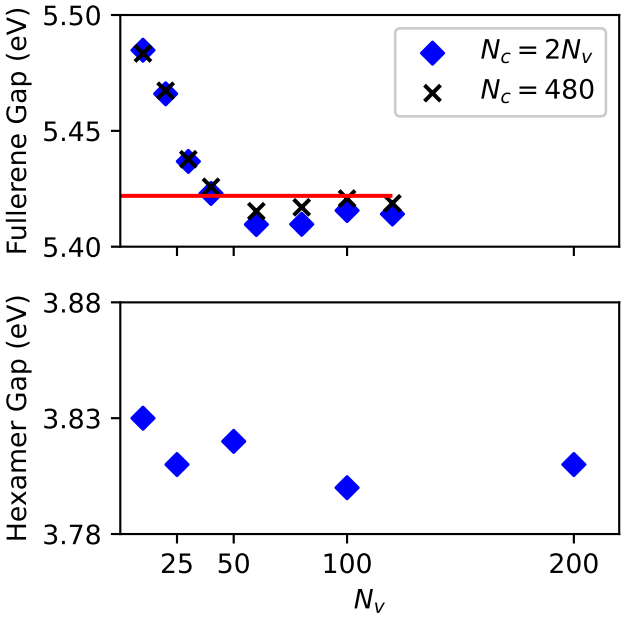

Figure 6.1: (Top) Convergence of the fundamental gaps of fullerene and (Bottom) hexamer with the number of valence states, N_v, and the number of conduction states, N_c, chosen either N_c=$2N_v$ (blue diamonds) or fixed at $N_c = 480$ (black x). The red-line is the reference value of the fullerene gap including all occupied states, $N_v = N_o = 120$ and $N_c = 480$.

6.2.3 Algorithm cost

In addition to the underlying local-DFT, the algorithm cost is mostly due to preparing the $\langle\phi|_q\,\phi_s|\xi\rangle$ and then calculating in each SCF iteration the exact exchange matrix elements. The steps are:

- First one Fourier transforms, i.e., prepares $\langle\phi|_q\,\phi_s|k\rangle$ from $\phi_q(r)\phi_s(r)$, which costs $\mathcal{O}(M^2 N\log N)$ operations, where N is the number of total number of grid and k points.

- Next one dot-products $\langle\phi|_q\,\phi_s|k\rangle$ with the $N_\alpha(\equiv N_{\alpha^+}+N_{\alpha^-})$ fragmented stochastic orbitals of length L each, to yield $\langle\phi|_q\,\phi_s|\xi^\pm\rangle$, at a cost of $\mathcal{O}(M^2 N_\alpha L)$ operations. For simplicity we choose here $N_\alpha = N_{k_{low}} = N_\xi/2$. Therefore, the dot product cost is $\mathcal{O}(M^2\cdot cov\cdot\, N_\xi)$.

- Finally, in each of the N_{scf} iterations one prepares the matrix elements via Eqs. (6.27) and (6.28), at a cost of $M^2 N_v N_\xi$ operations each.

The overall cost is therefore:

$$\mathcal{O}\Big(M^2\big(N(cov+\log N)+N_{scf}N_vN_\xi\big)\Big). \tag{6.29}$$

Since N_ξ does not grow with system size, as demonstrated below, the scaling is formally cubic with system size. However, in practice the scaling is gentler, since a very low number of near-gap (i.e., valence+conduction) states, M, is sufficient for large systems.

6.2.4 Core States Correction to the Exchange

In the previous sections, the core state contributions to the exact exchange were neglected. We will account for it by a perturbative correction to the KS eigenvalues $\varepsilon_s \to \varepsilon_s+\Delta_s$, where

$$\Delta_s = \langle\psi_s|X^\gamma_{core}|\psi_s\rangle, \tag{6.30}$$

is evaluated as

$$\Delta_s = -\sum_{f\in core} \langle\psi|_s\, \phi_f|u^\gamma|\phi_c\psi_f\rangle. \tag{6.31}$$

Since in this work we are only interested in the HOMO and LUMO energies, we calculate the correction for these two states only, labelled as Δ_{occ}, Δ_{unocc}. The core-corrections stabilize the frontier orbital eigenvalues and bandgap even when the number of active valence and conduction orbitals included in the GKS-Hamiltonian is dramatically reduced. Computationally these core corrections are very cheap as they are only added in the last iteration, and they are calculated as explicit convolution integrals.

6.3 Results

We test the ngH-DFT method with three molecular systems of increasing size: naphthalene (N_o=24), fullerene (N_o=120), and a hexamer dye complex (N_o=660). An initial PW-LDA DFT calculation is performed for all systems. The large dye system's nuclear coordinates, optimized at the PBE/def2-TZVP-MM level, were taken from [FV22b, SP22]. All simulations use a generous box size that extends 6 Bohr beyond the extent of the molecule in each direction, with real-space grids (before the Martyna-Tuckerman expansion) of N_g=50, 688, 216, 000, and 2, 273, 280 points respectively, and uniform grid spacings dx=dy=dz=0.5 Bohr. The RSH-DFT studies use the Baer-Neuhauser-Livshits (BNL) XC functional.

To balance the cost between the deterministic low-k and sparse stochastic high-k components of the exchange, we set, as mentioned, the size of the sparse basis, N_α, equal to the number of deterministic k-vectors, $N_{k_{low}}$. The k_{cut} parameter, separating the deterministic and fragmented-stochastic term, is adjusted so that for most of our simulations (except for a few reported in Table IV) a constant $N_{k_{low}} \simeq N_\alpha = 5000$ is used, so the auxiliary basis size is $N_\xi \simeq 10,000$. The associated k_{cut} values (in atomic units) are, respectively, 1.8, 1.1 and 0.5.

Note that at these values, and for the tuned values of γ listed below (0.285, 0.189 and

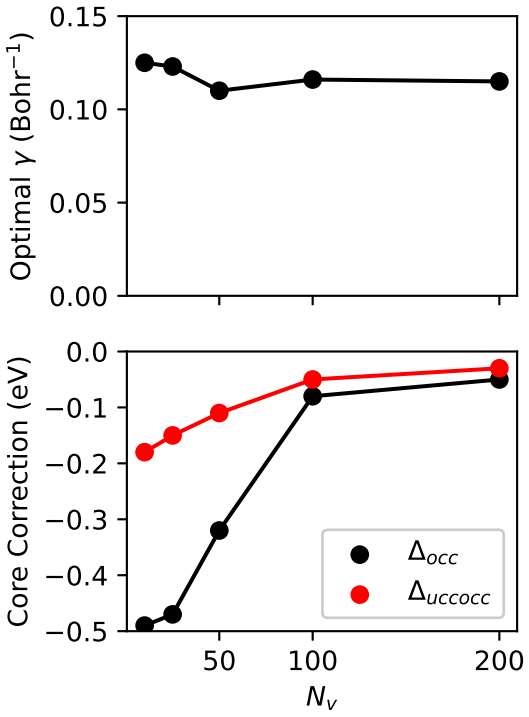

Figure 6.2: (Top) Convergence of γ, and (Bottom) the core corrections as a function of N_v for the hexamer system.

0.12 Bohr^{-1}, respectively), the high-k interaction is very small, as $v_\gamma(k) \propto \exp(-k^2/4\gamma^2)/k^2$ (although it is numerically somewhat larger in the Martyna Tuckerman approach). For a preliminary study of the potential usefulness of the approach for other types of Hybrid functionals, where $v_\gamma(k)$ is not so tiny at high k, we also include later results at a lower k_{cut}.

Before showing the promise of using only a fraction of near-gap states, we report in Table I the fundamental gaps obtained for naphthalene, fullerene and the hexamer, using a large number of valence and conduction states (including all N_o occupied states for the two smaller systems). For naphthalene and fullerene we benchmark vs. an all-electron calculation that uses the NWChem package,[ABJ20] with a Gaussian aug-cc-pvdz basis containing 302 atomic basis functions for naphthalene and 1380 for fullerene. The fundamental gaps agree well between ngH-DFT and NWCHEM, and we demonstrate below that this agreement is

Table 6.2: Naphthalene frontier orbital eigenvalues, fundamental gap, and core corrections for different numbers of valence to conduction states. All energies are in eV. The first row includes all occupied states so it has no core correction.

N_v:N_c	ε_H	ε_L	gap	Δ_{occ}	Δ_{unocc}
24:104	-8.77	-0.14	8.63		
20:40	-8.78	-0.15	8.63	-0.07	-0.04
10:20	-8.72	-0.08	8.64	-0.23	-0.03

maintained even when we reduce significantly the size of the valence-conduction near-gap space.

Both the ngH-DFT and RSH-DFT calculations use the same optimal range-separation parameter γ obtained by systematic tuning of the HOMO energies, i.e., ensuring that the HOMO energy does not change when the system is slightly ionized, and we use here $\varepsilon_{\mathrm{HOMO}}^{neutral} = \varepsilon_{\mathrm{HOMO}}^{+0.1}$. The ngH-DFT for the charged system is done via an open-shell calculation.

A side note is that to ensure rapid convergence with the valence basis size N_v, we find it important to do the initial LDA calculation with the right charge, as this ensures that the core eigenstates are correctly polarized. Thus, the charged system ngH-DFT requires a initial basis-set ϕ_s from an LDA SCF with fractional occupation $f_{HOMO} = 1 - 0.1$ (though done in a non-spin-selective calculation) rather than relying on the ϕ_s from the neutral LDA.

In Table II, we provide the HOMO and LUMO eigenvalues and gap for naphthalene for a chosen number of valence and conduction states. The first row in the table includes all occupied and a large number of unoccupied states, while the following two use a reduced valence-conduction space. Reduction of this active space necessitates the core corrections of the HOMO and LUMO eigenvalues. The gap is not changed much when the valence-conduction basis-set size is made smaller.

As Table III shows, the convergence is even better for the next bigger system, fullerene. The number of included valence and conduction states can now be much smaller than N_o.

Table 6.3: Fullerene frontier orbital eigenvalues, fundamental gap, and core corrections for different N_v:N_c. All energies are in eV.

N_v:N_c	ε_H	ε_L	gap	Δ_{occ}	Δ_{unocc}
120:480	-8.26	-2.84	5.42		
40:80	-8.20	-2.78	5.42	-0.15	-0.12
20:40	-8.23	-2.76	5.47	-0.42	-0.29
20:20	-8.23	-2.77	5.46	-0.42	-0.29
10:10	-8.25	-2.83	5.42	-1.12	-0.63

This rapid convergence with N_v is also shown in Fig.1a. The figure further shows that the results converge rapidly with the conduction basis size, so that $N_c = 2N_v$ gives essentially the same result as using a very large value of N_c.

The convergence with N_v further improves for the biggest system, the hexamer, as shown in Fig. 1b. The gaps shown all agree within ± 0.02 eV even for very small N_v and N_c. This implies that very large systems could be used with a small valence-conduction space.

Fig. 2 shows, for the hexamer, the convergence of the range-separation parameter as well as the core corrections. The extracted γ values are consistent, even with a valence-conduction space of only ten valence and ten conduction orbitals. This implies that optimal tuning of long-range separated hybrids of giant systems could be done rather cheaply.

The single-run stochastic error, i.e., the standard deviation of the energy, is shown in Table IV. It is estimated from the results of ten independent runs. As mentioned, for $N_{k_{low}} \simeq 5000$, k_{cut} is large for each of the three studied systems so that that the values of $v_\gamma(k)$ are very small for the stochastically-sampled high-k spaces. We therefore also include results with a smaller k_{cut} so $N_{k_{low}} \simeq 500$, for $N_\alpha = 500$ and $N_\alpha = 5000$ (i.e., $N_\xi \simeq 1000, 5500$). As shown, the statistical error is still quite small, about 0.01-0.03eV, and is lower than or similar to the low stochastic error associated with using a small value of N_v.

To conclude the results section, we show in Fig. 3, for the hexamer, the number of

Table 6.4: Fundamental gap and its standard deviation, σ, for three test systems (in eV), for different numbers of deterministic low-k terms, $N_{k_{low}}$, and sizes of the sparse stochastic basis, N_α.

System	N_v	N_c	$N_{k_{low}}$	N_α	gap	σ
Naphthalene	20	40	501	500	8.6329	0.0122
			501	5000	8.6373	0.0077
			4987	5000	8.6344	0.0004
Fullerene	40	80	515	500	5.4209	0.0066
			515	5000	5.4226	0.0051
			4945	5000	5.4228	0.0001
Hexamer	40	80	503	500	3.7914	0.0286
			503	5000	3.8018	0.0152
			4785	5000	3.8032	0.0002

CPU-core hours needed in ngH-DFT vs. N_v, using standard AMD Rome processors. The ngH-DFT cost is very small, and even for the largest sample studied $N_v = 200, N_c = 400$ the required effort is less than for the underlying LDA-DFT stage.

6.4 Discussion

We developed and demonstrated here a new method, ngH-DFT, for incorporating exact exchange within a GKS-DFT framework. Long wavelength (low k) components of the exchange are evaluated deterministically, and high momenta are represented by a sparse stochastic basis. Using an underlying MO basis from a preliminary LDA calculation the frontier eigenvalues converge with a small number of included valence and conduction orbitals.

We reiterate that this method only has stochasticity in its handling the high momenta components of the exchange, which are not as physically important as the low components.

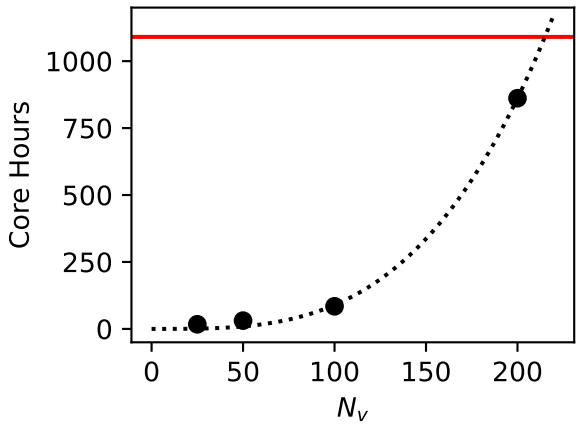

Figure 6.3: CPU-core hours required for the ngH-DFT method for the large hexamer complex. Parabolic scaling with the number of valence states (for a given grid) is shown. The red line indicates the core hours required for the initial LDA DFT calculation.

Treating less relevant degrees of freedom stochastically works very well here when combined with the sparse compression technique.

Future work will expand the method in several directions:

First, the stochastic compression gave equal weight to all high-k components, and could be replaced by preferred sampling of points with relatively higher $u^\gamma(k)$ within the h$igh^\pm$ spaces, either explicitly or division to several sub-spaces.

Next, a relatively simple extension would be to construct random combinations of the core states that would be used to calculate the core-exchange. This would reduce the memory requirements since the full set of core states would not need to be stored.[NRC16] Further, for the corrections of other states we could use a rigid scissor approximation [VBR18a], where the all occupied and unoccupied subspaces are shifted by the respective HOMO and LUMO orbital expectation values of X^γ_{core}; or, better yet, sample a few more states to determine an energy-dependent core-state contribution, analogous to our GW matrix elements.[NGA14b, VRB19] Since it will be applied only to the core states the contribution would be small and

therefore so will its underlying stochastic error.

The present near-gap approach method will be useful for many-body perturbation theory (MBPT). In MBPT methods, having access to exact exchange corrected eigenstates gives an improved starting point for methods such as one-shot G_0W_0 where the quality of the beginning canonical states is very important.[BM12, MHB22]

Our formalism will also apply to time-dependent Hybrid-DFT, where, like in GKS-DFT SCF, the $\langle\phi|_q\,\phi_s|\xi\rangle$ vectors would be evaluated once while the exchange matrix, Eqs. (6.27), (6.26) will be updated repeatedly, here once per time step. It will be useful both for real-time TDDFT and for frequency resolved TDDFT and BSE.[BNC22b, BAN23] We also expect applications within basis set based DFT codes, where the wavefunction is eventually represented on a complete grid. Additionally, we anticipate that this method will have applications in auxiliary field quantum Monte-Carlo methods (AFQMC), where the bulk of the computational effort also lies in evaluating exchange energy on many Slater determinants.[RCN97, CGO99, Zha18] Finally, the underlying LDA-DFT approach could be efficiently done with stochastic DFT, [BNR13b, NBR14b] so very large systems could be used, with tens of thousands of electrons or more. Eigenstates are not produced automatically in stochastic DFT, so the set of $N_v + N_c$ near-gap eigenstates, required for ngH-DFT, would be then extracted by filter-diagonalization.[WN95]

REFERENCES

[ABJ20] E. Aprà, E. J. Bylaska, W. A. de Jong, N. Govind, K. Kowalski, T. P. Straatsma, M. Valiev, H. J. J. van Dam, Y. Alexeev, J. Anchell, V. Anisimov, F. W. Aquino, R. Atta-Fynn, J. Autschbach, N. P. Bauman, J. C. Becca, D. E. Bernholdt, K. Bhaskaran-Nair, S. Bogatko, P. Borowski, J. Boschen, J. Brabec, A. Bruner, E. Cauët, Y. Chen, G. N. Chuev, C. J. Cramer, J. Daily, M. J. O. Deegan, Jr. Dunning, T. H., M. Dupuis, K. G. Dyall, G. I. Fann, S. A. Fischer, A. Fonari, H. Früchtl, L. Gagliardi, J. Garza, N. Gawande, S. Ghosh, K. Glaesemann, A. W. Götz, J. Hammond, V. Helms, E. D. Hermes, K. Hirao, S. Hirata, M. Jacquelin, L. Jensen, B. G. Johnson, H. Jónsson, R. A. Kendall, M. Klemm, R. Kobayashi, V. Konkov, S. Krishnamoorthy, M. Krishnan, Z. Lin, R. D. Lins, R. J. Littlefield, A. J. Logsdail, K. Lopata, W. Ma, A. V. Marenich, J. Martin del Campo, D. Mejia-Rodriguez, J. E. Moore, J. M. Mullin, T. Nakajima, D. R. Nascimento, J. A. Nichols, P. J. Nichols, J. Nieplocha, A. Otero-de-la Roza, B. Palmer, A. Panyala, T. Pirojsirikul, B. Peng, R. Peverati, J. Pittner, L. Pollack, R. M. Richard, P. Sadayappan, G. C. Schatz, W. A. Shelton, D. W. Silverstein, D. M. A. Smith, T. A. Soares, D. Song, M. Swart, H. L. Taylor, G. S. Thomas, V. Tipparaju, D. G. Truhlar, K. Tsemekhman, T. Van Voorhis, Á. Vázquez-Mayagoitia, P. Verma, O. Villa, A. Vishnu, K. D. Vogiatzis, D. Wang, J. H. Weare, M. J. Williamson, T. L. Windus, K. Woliński, A. T. Wong, Q. Wu, C. Yang, Q. Yu, M. Zacharias, Z. Zhang, Y. Zhao, and R. J. Harrison. "NWChem: Past, present, and future." *The Journal of Chemical Physics*, **152**(18):184102, 05 2020.

[ABW97] V. Agranovich, H. Benisty, and C. Weisbuch. "Organic and inorganic quantum wells in a microcavity: Frenkel-Wannier-Mott excitons hybridization and energy transformation." *Solid State Communications*, **102**(8):631–636, May 1997.

[AG07] V. M. Agranovich and Yu. N. Gartstein. "Nature and dynamics of low-energy exciton polaritons in semiconductor microcavities." *Physical Review B*, **75**(7):075302, February 2007.

[AKR23] Gustavo J. R. Aroeira, Kyle T. Kairys, and Raphael F. Ribeiro. "Theoretical Analysis of Exciton Wave Packet Dynamics in Polaritonic Wires." *The Journal of Physical Chemistry Letters*, **14**(24):5681–5691, June 2023.

[al21] Epifanovsky Evgeny et al. "Software for the frontiers of quantum chemistry: An overview of developments in the Q-Chem 5 package." *The Journal of Chemical Physics*, **155**(8):084801, 2021.

[ALL03] V. M. Agranovich, M. Litinskaia, and D. G. Lidzey. "Cavity polaritons in microcavities containing disordered organic semiconductors." *Physical Review B*, **67**(8):085311, February 2003.

[AM11] Darius Abramavicius and Shaul Mukamel. "Exciton dynamics in chromophore aggregates with correlated environment fluctuations." *The Journal of Chemical Physics*, **134**(17):174504, May 2011.

[ANC14] Lyudmyla Adamska, Iffat Nayyar, Hang Chen, Anna K. Swan, Nicolas Oldani, Sebastian Fernandez-Alberti, Matthew R. Golder, Ramesh Jasti, Stephen K. Doorn, and Sergei Tretiak. "Self-Trapping of Excitons, Violation of Condon Approximation, and Efficient Fluorescence in Conjugated Cycloparaphenylenes." *Nano Letters*, **14**(11):6539–6546, October 2014.

[AW53] P. W. Anderson and P. R. Weiss. "Exchange Narrowing in Paramagnetic Resonance." *Reviews of Modern Physics*, **25**(1):269–276, January 1953.

[AW22] Thomas F. Allard and Guillaume Weick. "Disorder-enhanced transport in a chain of lossy dipoles strongly coupled to cavity photons." *Physical Review B*, **106**(24):245424, December 2022.

[BAM12] Björn Baumeier, Denis Andrienko, Yuchen Ma, and Michael Rohlfing. "Excited States of Dicyanovinyl-Substituted Oligothiophenes from Many-Body Green's Functions Theory." *Journal of Chemical Theory and Computation*, **8**(3):997–1002, March 2012.

[BAN23] Nadine C. Bradbury, Tucker Allen, Minh Nguyen, Khaled Z. Ibrahim, and Daniel Neuhauser. "Optimized attenuated interaction: Enabling stochastic Bethe–Salpeter spectra for large systems." *The Journal of Chemical Physics*, **158**(15):154104, 04 2023.

[BBM20] Khadiza Begam, Srijana Bhandari, Buddhadev Maiti, and Barry D. Dunietz. "Screened Range-Separated Hybrid Functional with Polarizable Continuum Model Overcomes Challenges in Describing Triplet Excitations in the Condensed Phase Using TDDFT." *Journal of Chemical Theory and Computation*, **16**(5):3287–3293, April 2020.

[BCD20] Nadine C. Bradbury, Chern Chuang, Arundhati P. Deshmukh, Eran Rabani, Roi Baer, Justin R. Caram, and Daniel Neuhauser. "Stochastically Realized Observables for Excitonic Molecular Aggregates." *The Journal of Physical Chemistry A*, **124**(49):10111–10120, November 2020.

[BDB23] Austin D. Bailey, Arundhati P. Deshmukh, Nadine C. Bradbury, Monica Pengshung, Timothy L. Atallah, Jillian A. Williams, Ulugbek Barotov, Daniel Neuhauser, Ellen M. Sletten, and Justin R. Caram. "Exploring the design of superradiant J-aggregates from amphiphilic monomer units." *Nanoscale*, **15**(8):3841–3849, 2023.

[BDJ20] Xavier Blase, Ivan Duchemin, Denis Jacquemin, and Pierre-François Loos. "The Bethe–Salpeter Equation Formalism: From Physics to Chemistry." *The Journal of Physical Chemistry Letters*, **11**(17):7371–7382, August 2020.

[Bec93a] Axel D. Becke. "Density-functional thermochemistry. III. The role of exact exchange." *The Journal of Chemical Physics*, **98**(7):5648–5652, April 1993.

[Bec93b] Axel D. Becke. "A new mixing of Hartree-Fock and local density-functional theories." *The Journal of Chemical Physics*, **98**(2):1372–1377, January 1993.

[BGC01] Stefano Baroni, Stefano de Gironcoli, Andrea Dal Corso, and Paolo Giannozzi. "Phonons and related crystal properties from density-functional perturbation theory." *Reviews of Modern Physics*, **73**(2):515–562, July 2001.

[BHK17] Tobias Brixner, Richard Hildner, Jürgen Köhler, Christoph Lambert, and Frank Würthner. "Exciton Transport in Molecular Aggregates - From Natural Antennas to Synthetic Chromophore Systems." *Advanced Energy Materials*, **7**(16):1700236, July 2017.

[BHS20] T. Botzung, D. Hagenmüller, S. Schütz, J. Dubail, G. Pupillo, and J. Schachenmayer. "Dark state semilocalization of quantum emitters in a cavity." *Physical Review B*, **102**(14):144202, October 2020.

[BJK20] Anna S. Bondarenko, Thomas L. C. Jansen, and Jasper Knoester. "Exciton localization in tubular molecular aggregates: Size effects and optical response." *The Journal of Chemical Physics*, **152**(19):194302, May 2020.

[BKS15] Julia L. Bricks, Alexei D. Kachkovskii, Yurii L. Slominskii, Andrii O. Gerasov, and Sergei V. Popov. "Molecular design of near infrared polymethine dyes: A review." *Dyes and Pigments*, **121**:238–255, October 2015.

[BLH16] Amartya S. Banerjee, Lin Lin, Wei Hu, Chao Yang, and John E. Pask. "Chebyshev polynomial filtered subspace iteration in the discontinuous Galerkin method for large-scale electronic structure calculations." *The Journal of Chemical Physics*, **145**(15):154101, October 2016.

[BLS10] Roi Baer, Ester Livshits, and Ulrike Salzner. "Tuned Range-Separated Hybrids in Density Functional Theory." *Annual Review of Physical Chemistry*, **61**(1):85–109, 2010.

[BM12] Fabien Bruneval and Miguel A. L. Marques. "Benchmarking the Starting Points of the GW Approximation for Molecules." *Journal of Chemical Theory and Computation*, **9**(1):324–329, dec 2012.

[BN04] Roi Baer and Daniel Neuhauser. "Real-time linear response for time-dependent density-functional theory." *The Journal of Chemical Physics*, **121**(20):9803–9807, November 2004.

[BN05] Roi Baer and Daniel Neuhauser. "Density Functional Theory with Correct Long-Range Asymptotic Behavior." *Phys. Rev. Lett.*, **94**:043002, Feb 2005.

[BN12] Roi Baer and Daniel Neuhauser. "Communication: Monte Carlo calculation of the exchange energy." *The Journal of Chemical Physics*, **137**(5):051103, August 2012.

[BNC22a] Nadine C. Bradbury, Minh Nguyen, Justin R. Caram, and Daniel Neuhauser. "Bethe–Salpeter equation spectra for very large systems." *The Journal of Chemical Physics*, **157**(3):031104, July 2022.

[BNC22b] Nadine C. Bradbury, Minh Nguyen, Justin R. Caram, and Daniel Neuhauser. "Bethe–Salpeter equation spectra for very large systems." *The Journal of Chemical Physics*, **157**(3):031104, 07 2022.

[BNR13a] Roi Baer, Daniel Neuhauser, and Eran Rabani. "Self-Averaging Stochastic Kohn-Sham Density-Functional Theory." *Physical Review Letters*, **111**(10):106402, September 2013.

[BNR13b] Roi Baer, Daniel Neuhauser, and Eran Rabani. "Self-Averaging Stochastic Kohn-Sham Density-Functional Theory." *Phys. Rev. Lett.*, **111**:106402, Sep 2013.

[BNR22] Roi Baer, Daniel Neuhauser, and Eran Rabani. "Stochastic Vector Techniques in Ground-State Electronic Structure." *Annual Review of Physical Chemistry*, **73**(1):255–272, April 2022.

[BR12] Roi Baer and Eran Rabani. "Expeditious Stochastic Calculation of Multiexciton Generation Rates in Semiconductor Nanocrystals." *Nano Letters*, **12**(4):2123–2128, March 2012.

[BSV04] Silvana Botti, Francesco Sottile, Nathalie Vast, Valerio Olevano, Lucia Reining, Hans-Christian Weissker, Angel Rubio, Giovanni Onida, Rodolfo Del Sole, and R. W. Godby. "Long-range contribution to the exchange-correlation kernel of time-dependent density functional theory." *Physical Review B*, **69**(15):155112, April 2004.

[BW73] Carl Blumstein and John C. Wheeler. "Modified-Moments Method: Applications to Harmonic Solids." *Physical Review B*, **8**(4):1764–1776, August 1973.

[BWB07] Pierre-Antoine Bouit, Guillaume Wetzel, Gérard Berginc, Brigitte Loiseaux, Loïc Toupet, Patrick Feneyrou, Yann Bretonnière, Kenji Kamada, Olivier Maury, and Chantal Andraud. "Near IR Nonlinear Absorbing Chromophores with Optical

Limiting Properties at Telecommunication Wavelengths." *Chemistry of Materials*, **19**(22):5325–5335, October 2007.

[CBC19] Chern Chuang, Doran I.G. Bennett, Justin R. Caram, Alán Aspuru-Guzik, Moungi G. Bawendi, and Jianshu Cao. "Generalized Kasha's Model: T-Dependent Spectroscopy Reveals Short-Range Structures of 2D Excitonic Systems." *Chem*, **5**(12):3135–3150, December 2019.

[CBM12] Giuseppe L. Celardo, Fausto Borgonovi, Marco Merkli, Vladimir I. Tsifrinovich, and Gennady P. Berman. "Superradiance Transition in Photosynthetic Light-Harvesting Complexes." *The Journal of Physical Chemistry C*, **116**(42):22105–22111, October 2012.

[CCC19] Wei Chen, Chi-An Cheng, Emily D. Cosco, Shyam Ramakrishnan, Jakob G. P. Lingg, Oliver T. Bruns, Jeffrey I. Zink, and Ellen M. Sletten. "Shortwave Infrared Imaging with J-Aggregates Stabilized in Hollow Mesoporous Silica Nanoparticles." *Journal of the American Chemical Society*, **141**(32):12475–12480, July 2019.

[CDE16] Justin R. Caram, Sandra Doria, Dörthe M. Eisele, Francesca S. Freyria, Timothy S. Sinclair, Patrick Rebentrost, Seth Lloyd, and Moungi G. Bawendi. "Room-Temperature Micron-Scale Exciton Migration in a Stabilized Emissive Molecular Aggregate." *Nano Letters*, **16**(11):6808–6815, October 2016.

[CGO99] J. Carlson, J. E. Gubernatis, G. Ortiz, and Shiwei Zhang. "Issues and observations on applications of the constrained-path Monte Carlo method to many-fermion systems." *Physical Review B*, **59**(20):12788–12798, May 1999.

[CLH22] Yi-Ting Chuang, Ming-Wei Lee, and Liang-Yan Hsu. "Tavis-Cummings model revisited: A perspective from macroscopic quantum electrodynamics." *Frontiers in Physics*, **10**, October 2022.

[CLM16] Chern Chuang, Chee Kong Lee, Jeremy M. Moix, Jasper Knoester, and Jianshu Cao. "Quantum Diffusion on Molecular Tubes: Universal Scaling of the 1D to 2D Transition." *Physical Review Letters*, **116**(19):196803, May 2016.

[CPM15] Elsa Cassette, Ryan D. Pensack, Benoît Mahler, and Gregory D. Scholes. "Room-temperature exciton coherence and dephasing in two-dimensional nanostructures." *Nature Communications*, **6**(1):6086, January 2015.

[CSM14] David M. Coles, Niccolo Somaschi, Paolo Michetti, Caspar Clark, Pavlos G. Lagoudakis, Pavlos G. Savvidis, and David G. Lidzey. "Polariton-mediated energy transfer between organic dyes in a strongly coupled optical microcavity." *Nature Materials*, **13**(7):712–719, May 2014.

[CTL16] José C.S. Costa, Ricardo J.S. Taveira, Carlos F.R.A.C. Lima, Adélio Mendes, and Luís M.N.B.F. Santos. "Optical band gaps of organic semiconductor materials." *Optical Materials*, **58**:51–60, August 2016.

[CWB02] Seth Coe, Wing-Keung Woo, Moungi Bawendi, and Vladimir Bulović. "Electroluminescence from single monolayers of nanocrystals in molecular organic devices." *Nature*, **420**(6917):800–803, December 2002.

[CY22] Jorge A. Campos-Gonzalez-Angulo and Joel Yuen-Zhou. "Generalization of the Tavis–Cummings model for multi-level anharmonic systems: Insights on the second excitation manifold." *The Journal of Chemical Physics*, **156**(19), May 2022.

[CZD13] Justin R. Caram, Haibin Zheng, Peter D. Dahlberg, Brian S. Rolczynski, Graham B. Griffin, Andrew F. Fidler, Dmitriy S. Dolzhnikov, Dmitri V. Talapin, and Gregory S. Engel. "Persistent Interexcitonic Quantum Coherence in CdSe Quantum Dots." *The Journal of Physical Chemistry Letters*, **5**(1):196–204, December 2013.

[Dav64] A S Davydov. "The Theory of Molecular Aggregates." *Soviet Physics Uspekhi*, **7**(2):145–178, February 1964.

[Dav71] Aleksandr Sergeevich Davydov. *Theory of Molecular Excitons*. Springer US, 1971.

[DB19] Ivan Duchemin and Xavier Blase. "Separable resolution-of-the-identity with all-electron Gaussian bases: Application to cubic-scaling RPA." *The Journal of Chemical Physics*, **150**(17):174120, May 2019.

[DCT20] Wenjie Dou, Ming Chen, Tyler Y. Takeshita, Roi Baer, Daniel Neuhauser, and Eran Rabani. "Range-separated stochastic resolution of identity: Formulation and application to second-order Green's function theory." *The Journal of Chemical Physics*, **153**(7):074113, 08 2020.

[DGB22] Arundhati P. Deshmukh, Niklas Geue, Nadine C. Bradbury, Timothy L. Atallah, Chern Chuang, Monica Pengshung, Jianshu Cao, Ellen M. Sletten, Daniel Neuhauser, and Justin R. Caram. "Bridging the gap between H- and J-aggregates: Classification and supramolecular tunability for excitonic band structures in two-dimensional molecular aggregates." *Chemical Physics Reviews*, **3**(2):021401, June 2022.

[DH04] Andreas Dreuw and Martin Head-Gordon. "Failure of Time-Dependent Density Functional Theory for Long-Range Charge-Transfer Excited States: The Zincbacteriochlorin-Bacteriochlorin and Bacteriochlorophyll-Spheroidene Complexes." *Journal of the American Chemical Society*, **126**(12):4007–4016, March 2004.

[Dic54] R. H. Dicke. "Coherence in Spontaneous Radiation Processes." *Physical Review*, **93**(1):99–110, January 1954.

[DKC19] Arundhati P. Deshmukh, Danielle Koppel, Chern Chuang, Danielle M. Cadena, Jianshu Cao, and Justin R. Caram. "Design Principles for Two-Dimensional Molecular Aggregates Using Kasha's Model: Tunable Photophysics in Near and Short-Wave Infrared." *The Journal of Physical Chemistry C*, **123**(30):18702–18710, July 2019.

[DKK02] Catalin Didraga, Joost A. Klugkist, and Jasper Knoester. "Optical Properties of Helical Cylindrical Molecular Aggregates: The Homogeneous Limit." *The Journal of Physical Chemistry B*, **106**(44):11474–11486, November 2002.

[DKP89] D. H. Dunlap, Kalyan Kundu, and Philip Phillips. "Absence of localization in certain statically disordered lattices in any spatial dimension." *Physical Review B*, **40**(16):10999–11006, December 1989.

[DKP21] Courtney A. DelPo, Saeed-Uz-Zaman Khan, Kyu Hyung Park, Bryan Kudisch, Barry P. Rand, and Gregory D. Scholes. "Polariton Decay in Donor–Acceptor Cavity Systems." *The Journal of Physical Chemistry Letters*, **12**(40):9774–9782, October 2021.

[DLY15] Anil Damle, Lin Lin, and Lexing Ying. "Compressed Representation of Kohn–Sham Orbitals via Selected Columns of the Density Matrix." *Journal of Chemical Theory and Computation*, **11**(4):1463–1469, 2015.

[DPH04] Catalin Didraga, Audrius Pugžlys, P. Ralph Hania, Hans von Berlepsch, Koos Duppen, and Jasper Knoester. "Structure, Spectroscopy, and Microscopic Model of Tubular Carbocyanine Dye Aggregates." *The Journal of Physical Chemistry B*, **108**(39):14976–14985, September 2004.

[DS93] David A. Drabold and Otto F. Sankey. "Maximum entropy approach for linear scaling in the electronic structure problem." *Physical Review Letters*, **70**(23):3631–3634, June 1993.

[DSK18] Sandra Doria, Timothy S. Sinclair, Nathan D. Klein, Doran I. G. Bennett, Chern Chuang, Francesca S. Freyria, Colby P. Steiner, Paolo Foggi, Keith A. Nelson, and et al. "Photochemical Control of Exciton Superradiance in Light-Harvesting Nanotubes." *ACS Nano*, **12**(5):4556–4564, April 2018.

[DSS12] Jack Deslippe, Georgy Samsonidze, David A. Strubbe, Manish Jain, Marvin L. Cohen, and Steven G. Louie. "BerkeleyGW: A massively parallel computer package for the calculation of the quasiparticle and optical properties of materials and nanostructures." *Computer Physics Communications*, **183**(6):1269–1289, June 2012.

[DTC19] Wenjie Dou, Tyler Y. Takeshita, Ming Chen, Roi Baer, Daniel Neuhauser, and Eran Rabani. "Stochastic Resolution of Identity for Real-Time Second-Order Green's Function: Ionization Potential and Quasi-particle Spectrum." *arXiv:1909.06525 [physics]*, September 2019. arXiv: 1909.06525.

[EC22] Georg Engelhardt and Jianshu Cao. "Unusual dynamical properties of disordered polaritons in microcavities." *Physical Review B*, **105**(6):064205, February 2022.

[EC23] Georg Engelhardt and Jianshu Cao. "Polariton Localization and Dispersion Properties of Disordered Quantum Emitters in Multimode Microcavities." *Physical Review Letters*, **130**(21):213602, May 2023.

[ECB12] D. M. Eisele, C. W. Cone, E. A. Bloemsma, S. M. Vlaming, C. G. F. van der Kwaak, R. J. Silbey, M. G. Bawendi, J. Knoester, J. P. Rabe, and D. A. Vanden Bout. "Utilizing redox-chemistry to elucidate the nature of exciton transitions in supramolecular dye nanotubes." *Nature Chemistry*, **4**(8):655–662, July 2012.

[FCH12] Andrew F Fidler, Justin R Caram, Dugan Hayes, and Gregory S Engel. "Towards a coherent picture of excitonic coherence in the Fenna–Matthews–Olson complex." *Journal of Physics B: Atomic, Molecular and Optical Physics*, **45**(15):154013, July 2012.

[FCI12] Mamoru Fujitsuka, Dae Won Cho, Takahiro Iwamoto, Shigeru Yamago, and Tetsuro Majima. "Size-dependent fluorescence properties of [n]cycloparaphenylenes (n = 8-13), hoop-shaped π-conjugated molecules." *Physical Chemistry Chemical Physics*, **14**(42):14585, 2012.

[FJ05] M. Frigo and S.G. Johnson. "The Design and Implementation of FFTW3." *Proceedings of the IEEE*, **93**(2):216–231, February 2005.

[FKW91] Henk Fidder, Jasper Knoester, and Douwe A. Wiersma. "Optical properties of disordered molecular aggregates: A numerical study." *The Journal of Chemical Physics*, **95**(11):7880–7890, December 1991.

[FKW93] Henk Fidder, Jasper Knoester, and Douwe A. Wiersma. "Observation of the one-exciton to two-exciton transition in a J aggregate." *The Journal of Chemical Physics*, **98**(8):6564–6566, April 1993.

[Fox10] Mark Fox. *Optical properties of solids*. Oxford Master Series in Physics. Oxford University Press, London, England, 2 edition, March 2010.

[FRS08] F. Fuchs, C. Rödl, A. Schleife, and F. Bechstedt. "Efficient $\mathcal{O}(N^2)$ approach to solve the Bethe-Salpeter equation for excitonic bound states." *Physical Review B*, **78**(8), August 2008.

[FV21] Arno Förster and Lucas Visscher. "Low-Order Scaling Quasiparticle Self-Consistent GW for Molecules." *Frontiers in Chemistry*, **9**, September 2021.

[FV22a] Arno Förster and Lucas Visscher. "Quasiparticle Self-Consistent GW - Bethe–Salpeter Equation Calculations for Large Chromophoric Systems." *Journal of Chemical Theory and Computation*, October 2022.

[FV22b] Arno Förster and Lucas Visscher. "Quasiparticle Self-Consistent GW-Bethe-Salpeter Equation Calculations for Large Chromophoric Systems." *Journal of Chemical Theory and Computation*, **18**(11):6779–6793, October 2022.

[Gau68] Walter Gautschi. "Construction of Gauss-Christoffel quadrature formulas." *Mathematics of Computation*, **22**(102):251–251, May 1968.

[Gau70] Walter Gautschi. "On the construction of Gaussian quadrature rules from modified moments." *Mathematics of Computation*, **24**(110):245–245, May 1970.

[GBR14] Xiaochuan Ge, Simon J. Binnie, Dario Rocca, Ralph Gebauer, and Stefano Baroni. "turboTDDFT 2.0—Hybrid functionals and new algorithms within time-dependent density-functional perturbation theory." *Computer Physics Communications*, **185**(7):2080–2089, July 2014.

[GBS18] Daniel Graf, Matthias Beuerle, Henry F. Schurkus, Arne Luenser, Gökcen Savasci, and Christian Ochsenfeld. "Accurate and Efficient Parallel Implementation of an Effective Linear-Scaling Direct Random Phase Approximation Method." *Journal of Chemical Theory and Computation*, **14**(5):2505–2515, apr 2018.

[GGB13] Qinghui Ge, Yi Gao, Roi Baer, Eran Rabani, and Daniel Neuhauser. "A Guided Stochastic Energy-Domain Formulation of the Second Order Møller–Plesset Perturbation Theory." *The Journal of Physical Chemistry Letters*, **5**(1):185–189, December 2013.

[GHK18] Xin Gui, Christof Holzer, and Wim Klopper. "Accuracy Assessment of *GW* Starting Points for Calculating Molecular Excitation Energies Using the Bethe–Salpeter Formalism." *Journal of Chemical Theory and Computation*, **14**(4):2127–2136, March 2018.

[GK22] Tommaso Giovannini and Henrik Koch. "Fragment Localized Molecular Orbitals." *Journal of Chemical Theory and Computation*, **18**(8):4806–4813, 2022.

[GNB15] Yi Gao, Daniel Neuhauser, Roi Baer, and Eran Rabani. "Sublinear scaling for time-dependent stochastic density functional theory." *The Journal of Chemical Physics*, **142**(3):034106, January 2015.

[GPA20] Alberto García, Nick Papior, Arsalan Akhtar, Emilio Artacho, Volker Blum, Emanuele Bosoni, Pedro Brandimarte, Mads Brandbyge, J. I. Cerdá, Fabiano Corsetti, Ramón Cuadrado, Vladimir Dikan, Jaime Ferrer, Julian Gale, Pablo García-Fernández, V. M. García-Suárez, Sandra García, Georg Huhs, Sergio Illera, Richard Korytár, Peter Koval, Irina Lebedeva, Lin Lin, Pablo López-Tarifa, Sara G. Mayo, Stephan Mohr, Pablo Ordejón, Andrei Postnikov, Yann Pouillon, Miguel Pruneda, Roberto Robles, Daniel Sánchez-Portal, Jose M. Soler, Rafi Ullah, Victor Wen zhe Yu, and Javier Junquera. "Siesta: Recent developments and applications." *The Journal of Chemical Physics*, **152**(20):204108, May 2020.

[HC12] Pengfei Huo and David F. Coker. "Influence of environment induced correlated fluctuations in electronic coupling on coherent excitation energy transfer dynamics in model photosynthetic systems." *The Journal of Chemical Physics*, **136**(11):115102, March 2012.

[HIR11] Miquel Huix-Rotllant, Andrei Ipatov, Angel Rubio, and Mark E. Casida. "Assessment of dressed time-dependent density-functional theory for the low-lying valence states of 28 organic chromophores." *Chemical Physics*, **391**(1):120–129, November 2011.

[HKW16] Nicholas J. Hestand, Roman V. Kazantsev, Adam S. Weingarten, Liam C. Palmer, Samuel I. Stupp, and Frank C. Spano. "Extended-Charge-Transfer Excitons in Crystalline Supramolecular Photocatalytic Scaffolds." *Journal of the American Chemical Society*, **138**(36):11762–11774, September 2016.

[HL85] Mark S. Hybertsen and Steven G. Louie. "First-Principles Theory of Quasiparticles: Calculation of Band Gaps in Semiconductors and Insulators." *Physical Review Letters*, **55**(13):1418–1421, September 1985.

[HM08] Marc P. Hansen and Douglas S. Malchow. "Overview of SWIR detectors, cameras, and applications." In Vladimir P. Vavilov and Douglas D. Burleigh, editors, *Proc. SPIE 6939, Thermosense XXX, 69390I*. SPIE, March 17 2008. doi:10.1117/12.777776.

[HS17] Nicholas J. Hestand and Frank C. Spano. "Molecular Aggregate Photophysics beyond the Kasha Model: Novel Design Principles for Organic Materials." *Accounts of Chemical Research*, **50**(2):341–350, February 2017.

[HS18] Nicholas J. Hestand and Frank C. Spano. "Expanded Theory of H- and J-Molecular Aggregates: The Effects of Vibronic Coupling and Intermolecular Charge Transfer." *Chemical Reviews*, **118**(15):7069–7163, April 2018.

[HSE03] Jochen Heyd, Gustavo E. Scuseria, and Matthias Ernzerhof. "Hybrid functionals based on a screened Coulomb potential." *The Journal of Chemical Physics*, **118**(18):8207–8215, May 2003.

[Hut90] M.F. Hutchinson. "A stochastic estimator of the trace of the influence matrix for laplacian smoothing splines." *Communications in Statistics - Simulation and Computation*, **19**(2):433–450, January 1990.

[IKM12] F.M. Izrailev, A.A. Krokhin, and N.M. Makarov. "Anomalous localization in low-dimensional systems with correlated disorder." *Physics Reports*, **512**(3):125–254, March 2012.

[IR60] AF Ioffe and AR Regel. "Non-crystalline, amorphous, and liquid electronic semiconductors." In *Progress in semiconductors*, pp. 237–291. Heywood & Co, 1960.

[ISB16] Roberto Improta, Fabrizio Santoro, and Lluís Blancafort. "Quantum Mechanical Studies on the Photophysics and the Photochemistry of Nucleic Acids and Nucleobases." *Chemical Reviews*, **116**(6):3540–3593, March 2016.

[IWS11] Takahiro Iwamoto, Yoshiki Watanabe, Tatsuya Sadahiro, Takeharu Haino, and Shigeru Yamago. "Size-Selective Encapsulation of C60 by [10]Cycloparaphenylene: Formation of the Shortest Fullerene-Peapod." *Angewandte Chemie International Edition*, **50**(36):8342–8344, July 2011.

[JC63] E.T. Jaynes and F.W. Cummings. "Comparison of quantum and semiclassical radiation theories with application to the beam maser." *Proceedings of the IEEE*, **51**(1):89–109, 1963.

[Jel36] Edwin E. Jelley. "Spectral Absorption and Fluorescence of Dyes in the Molecular State." *Nature*, **138**(3502):1009–1010, December 1936.

[JSG05] Yousung Jung, Alex Sodt, Peter M. W. Gill, and Martin Head-Gordon. "Auxiliary basis expansions for large-scale electronic structure calculations." *Proceedings of the National Academy of Sciences*, **102**(19):6692–6697, apr 2005.

[Kas63] Michael Kasha. "Energy Transfer Mechanisms and the Molecular Exciton Model for Molecular Aggregates." *Radiation Research*, **20**(1):55, September 1963.

[KB09] Bernard Kippelen and Jean-Luc Brédas. "Organic photovoltaics." *Energy & Environmental Science*, **2**(3):251, 2009.

[KEA17] Justus Krüger, Frank Eisenhut, José M. Alonso, Thomas Lehmann, Enrique Guitián, Dolores Pérez, Dmitry Skidin, Florian Gamaleja, Dmitry A. Ryndyk, Christian Joachim, Diego Peña, Francesca Moresco, and Gianaurelio Cuniberti. "Imaging the electronic structure of on-surface generated hexacene." *Chemical Communications*, **53**(10):1583–1586, 2017.

[KF10] S. Kéna-Cohen and S. R. Forrest. "Room-temperature polariton lasing in an organic single-crystal microcavity." *Nature Photonics*, **4**(6):371–375, April 2010.

[KLO21] Jörg Kussmann, Henryk Laqua, and Christian Ochsenfeld. "Highly Efficient Resolution-of-Identity Density Functional Theory Calculations on Central and Graphics Processing Units." *Journal of Chemical Theory and Computation*, **17**(3):1512–1521, feb 2021.

[Kna84] E.W. Knapp. "Lineshapes of molecular aggregates, exchange narrowing and intersite correlation." *Chemical Physics*, **85**(1):73–82, March 1984.

[Kno93] Jasper Knoester. "Nonlinear optical line shapes of disordered molecular aggregates: Motional narrowing and the effect of intersite correlations." *The Journal of Chemical Physics*, **99**(11):8466–8479, December 1993.

[Kos88] Ronnie Kosloff. "Time-dependent quantum-mechanical methods for molecular dynamics." *The Journal of Physical Chemistry*, **92**(8):2087–2100, April 1988.

[KRE65] M. Kasha, H. R. Rawls, and M. Ashraf El-Bayoumi. "The exciton model in molecular spectroscopy." *Pure and Applied Chemistry*, **11**(3-4):371–392, January 1965.

[KSP08] Aliaksandr V. Krukau, Gustavo E. Scuseria, John P. Perdew, and Andreas Savin. "Hybrid functionals with local range separation." *The Journal of Chemical Physics*, **129**(12):124103, September 2008.

[Kub57] Ryogo Kubo. "Statistical-Mechanical Theory of Irreversible Processes. I. General Theory and Simple Applications to Magnetic and Conduction Problems." *Journal of the Physical Society of Japan*, **12**(6):570–586, June 1957.

[Lan50] C. Lanczos. "An iteration method for the solution of the eigenvalue problem of linear differential and integral operators." *Journal of Research of the National Bureau of Standards*, **45**(4):255, October 1950.

[Lan88] Cornelius Lanczos. *Applied analysis*. Dover Publications, New York, 1988.

[LB20] Pierre-François Loos and Xavier Blase. "Dynamical correction to the Bethe–Salpeter equation beyond the plasmon-pole approximation." *The Journal of Chemical Physics*, **153**(11):114120, September 2020.

[LBS98] D. G. Lidzey, D. D. C. Bradley, M. S. Skolnick, T. Virgili, S. Walker, and D. M. Whittaker. "Strong exciton–photon coupling in an organic semiconductor microcavity." *Nature*, **395**(6697):53–55, September 1998.

[LCF07] H. Lee, Y.-C. Cheng, and G. R. Fleming. "Coherence Dynamics in Photosynthesis: Protein Protection of Excitonic Coherence." *Science*, **316**(5830):1462–1465, June 2007.

[LJ19] Erik J. Leonhardt and Ramesh Jasti. "Emerging applications of carbon nanohoops." *Nature Reviews Chemistry*, **3**(12):672–686, October 2019.

[LKF15] M. P. Ljungberg, P. Koval, F. Ferrari, D. Foerster, and D. Sánchez-Portal. "Cubic-scaling iterative solution of the Bethe-Salpeter equation for finite systems." *Physical Review B*, **92**(7), August 2015.

[LN20] Wenfei Li and Daniel Neuhauser. "Real-space orthogonal projector-augmented-wave method." *Physical Review B*, **102**(19):195118, November 2020.

[LR06] Marina Litinskaya and Peter Reineker. "Loss of coherence of exciton polaritons in inhomogeneous organic microcavities." *Physical Review B*, **74**(16):165320, October 2006.

[LSW97] Thierry Leininger, Hermann Stoll, Hans-Joachim Werner, and Andreas Savin. "Combining long-range configuration interaction with short-range density functionals." *Chemical Physics Letters*, **275**(3):151–160, 1997.

[LTZ22] Thomas Liu, Claire Tonnelé, Shen Zhao, Loïc Rondin, Christine Elias, Daniel Medina-Lopez, Hanako Okuno, Akimitsu Narita, Yannick Chassagneux, Christophe Voisin, Stéphane Campidelli, David Beljonne, and Jean-Sébastien Lauret. "Vibronic effect and influence of aggregation on the photophysics of graphene quantum dots." *Nanoscale*, **14**(10):3826–3833, 2022.

[LVJ95] R.W. Lof, M.A. van Veenendaal, H.T. Jonkman, and G.A. Sawatzky. "Band gap, excitons and Coulomb interactions of solid C60." *Journal of Electron Spectroscopy and Related Phenomena*, **72**:83–87, March 1995.

[May11] Volkhard May. *Charge and Energy Transfer Dynamics in Molecular Systems*. Wiley-VCH, mar 2011.

[MD82] J. W. Mintmire and B. I. Dunlap. "Fitting the Coulomb potential variationally in linear-combination-of-atomic-orbitals density-functional calculations." *Physical Review A*, **25**(1):88–95, jan 1982.

[MD99] V.A. Malyshev and F. Domínguez-Adame. "Motional narrowing effect in one-dimensional Frenkel chains with configurational disorder." *Chemical Physics Letters*, **313**(1-2):255–260, November 1999.

[MDM19] Angiras Menon, Jochen A. H. Dreyer, Jacob W. Martin, Jethro Akroyd, John Robertson, and Markus Kraft. "Optical band gap of cross-linked, curved, and radical polyaromatic hydrocarbons." *Physical Chemistry Chemical Physics*, **21**(29):16240–16251, 2019.

[MDM23] Riley Murray, James Demmel, Michael W. Mahoney, N. Benjamin Erichson, Maksim Melnichenko, Osman Asif Malik, Laura Grigori, Piotr Luszczek, Michał Dereziński, Miles E. Lopes, Tianyu Liang, Hengrui Luo, and Jack Dongarra. "Randomized Numerical Linear Algebra : A Perspective on the Field With an Eye to Software.", 2023.

[MDR18] Luis A. Martínez-Martínez, Matthew Du, Raphael F. Ribeiro, Stéphane Kéna-Cohen, and Joel Yuen-Zhou. "Polariton-Assisted Singlet Fission in Acene Aggregates." *The Journal of Physical Chemistry Letters*, **9**(8):1951–1957, March 2018.

[Mer61] R. E. Merrifield. "Ionized States in a One-Dimensional Molecular Crystal." *The Journal of Chemical Physics*, **34**(5):1835–1839, May 1961.

[MHB22] Caroline A. McKeon, Samia M. Hamed, Fabien Bruneval, and Jeffrey B. Neaton. "An optimally tuned range-separated hybrid starting point for GW plus Bethe–Salpeter equation calculations of molecules." *The Journal of Chemical Physics*, **157**(7), August 2022.

[MM01] A.V. Malyshev and V.A. Malyshev. "Level and wave function statistics of a localized 1D Frenkel exciton at the bottom of the band." *Journal of Luminescence*, **94-95**:369–372, December 2001.

[Mou10] F.A.B.F. de Moura. "Absence of localization on the 2d model with long-range correlated off-diagonal disorder." *The European Physical Journal B*, **78**(3):335–339, November 2010.

[MPP98] R. W. Munn, Barbara Pac, and Piotr Petelenz. "Charge-transfer-induced Frenkel exciton splitting in crystalline fullerene." *Physical Review B*, **57**(3):1328–1331, January 1998.

[MR05] P. Michetti and G. C. La Rocca. "Polariton states in disordered organic microcavities." *Physical Review B*, **71**(11):115320, March 2005.

[MRM09] Yuchen Ma, Michael Rohlfing, and Carla Molteni. "Excited states of biological chromophores studied using many-body perturbation theory: Effects of resonant-antiresonant coupling and dynamical screening." *Physical Review B*, **80**(24), December 2009.

[MRT93] V. A. Mandelshtam, T. R. Ravuri, and H. S. Taylor. "Calculation of the density of resonance states using the stabilization method." *Physical Review Letters*, **70**(13):1932–1935, March 1993.

[MT99a] Glenn J. Martyna and Mark E. Tuckerman. "A reciprocal space based method for treating long range interactions in ab initio and force-field-based calculations in clusters." *The Journal of Chemical Physics*, **110**(6):2810–2821, 02 1999.

[MT99b] Glenn J. Martyna and Mark E. Tuckerman. "A reciprocal space based method for treating long range interactions in ab initio and force-field-based calculations in clusters." *The Journal of Chemical Physics*, **110**(6):2810–2821, February 1999.

[MTK09] Rajib Mondal, Christina Tönshoff, Dmitriy Khon, Douglas C. Neckers, and Holger F. Bettinger. "Synthesis, Stability, and Photochemistry of Pentacene, Hexacene, and Heptacene: A Matrix Isolation Study." *Journal of the American Chemical Society*, **131**(40):14281–14289, September 2009.

[MXF20] Martin B. Minameyer, Youzhi Xu, Stefan Frühwald, Andreas Görling, Max Delius, and Thomas Drewello. "Investigation of Cycloparaphenylenes (CPPs) and their Noncovalent Ring-in-Ring and Fullerene-in-Ring Complexes by (Matrix-Assisted) Laser Desorption/Ionization and Density Functional Theory." *Chemistry – A European Journal*, **26**(40):8729–8741, July 2020.

[MXM23] Arkajit Mandal, Ding Xu, Ankit Mahajan, Joonho Lee, Milan Delor, and David R. Reichman. "Microscopic Theory of Multimode Polariton Dispersion in Multilayered Materials." *Nano Letters*, **23**(9):4082–4089, April 2023.

[NB05] Daniel Neuhauser and Roi Baer. "Efficient linear-response method circumventing the exchange-correlation kernel: Theory for molecular conductance under finite bias." *The Journal of Chemical Physics*, **123**(20):204105, November 2005.

[NBR14a] Daniel Neuhauser, Roi Baer, and Eran Rabani. "Communication: Embedded fragment stochastic density functional theory." *The Journal of Chemical Physics*, **141**(4):041102, July 2014.

[NBR14b] Daniel Neuhauser, Roi Baer, and Eran Rabani. "Communication: Embedded fragment stochastic density functional theory." *J. Chem. Phys.*, **141**(4):041102, 2014.

[NDQ14] Dorota Niedzialek, Ivan Duchemin, Thiago Branquinho de Queiroz, Silvio Osella, Akshay Rao, Richard Friend, Xavier Blase, Stephan Kümmel, and David Beljonne. "First Principles Calculations of Charge Transfer Excitations in Polymer-Fullerene Complexes: Influence of Excess Energy." *Advanced Functional Materials*, **25**(13):1972–1984, October 2014.

[Neg82] J. W. Negele. "The mean-field theory of nuclear structure and dynamics." *Reviews of Modern Physics*, **54**(4):913–1015, October 1982.

[Neu90a] Daniel Neuhauser. "Bound state eigenfunctions from wave packets: Time to energy resolution." *J. Chem. Phys.*, **93**(4):2611–2616, August 1990.

[Neu90b] Daniel Neuhauser. "Bound state eigenfunctions from wave packets: Time→energy resolution." *The Journal of Chemical Physics*, **93**(4):2611–2616, August 1990.

[NGA14a] Daniel Neuhauser, Yi Gao, Christopher Arntsen, Cyrus Karshenas, Eran Rabani, and Roi Baer. "Breaking the Theoretical Scaling Limit for Predicting Quasiparticle Energies: The Stochastic GW Approach." *Physical Review Letters*, **113**(7):076402, August 2014.

[NGA14b] Daniel Neuhauser, Yi Gao, Christopher Arntsen, Cyrus Karshenas, Eran Rabani, and Roi Baer. "Breaking the Theoretical Scaling Limit for Predicting Quasiparticle Energies: The Stochastic GW Approach." *Phys. Rev. Lett.*, **113**(7):076402, 2014.

[NRB12] Daniel Neuhauser, Eran Rabani, and Roi Baer. "Expeditious Stochastic Approach for MP2 Energies in Large Electronic Systems." *Journal of Chemical Theory and Computation*, **9**(1):24–27, December 2012.

[NRB13] Daniel Neuhauser, Eran Rabani, and Roi Baer. "Expeditious Stochastic Calculation of Random-Phase Approximation Energies for Thousands of Electrons in Three Dimensions." *The Journal of Physical Chemistry Letters*, **4**(7):1172–1176, March 2013.

[NRC15a] Daniel Neuhauser, Eran Rabani, Yael Cytter, and Roi Baer. "Stochastic Optimally Tuned Range-Separated Hybrid Density Functional Theory." *The Journal of Physical Chemistry A*, **120**(19):3071–3078, December 2015.

[NRC15b] Daniel Neuhauser, Eran Rabani, Yael Cytter, and Roi Baer. "Stochastic Optimally Tuned Range-Separated Hybrid Density Functional Theory." *The Journal of Physical Chemistry A*, **120**(19):3071–3078, December 2015.

[NRC16] Daniel Neuhauser, Eran Rabani, Yael Cytter, and Roi Baer. "Stochastic Optimally Tuned Range-Separated Hybrid Density Functional Theory." *The Journal of Physical Chemistry A*, **120**(19):3071–3078, 2016.

[ORG95] Giovanni Onida, Lucia Reining, R. W. Godby, R. Del Sole, and Wanda Andreoni. "Ab Initio Calculations of the Quasiparticle and Absorption Spectra of Clusters: The Sodium Tetramer." *Physical Review Letters*, **75**(5):818–821, July 1995.

[OSS11] Carsten Olbrich, Johan Strümpfer, Klaus Schulten, and Ulrich Kleinekathöfer. "Quest for Spatially Correlated Fluctuations in the FMO Light-Harvesting Complex." *The Journal of Physical Chemistry B*, **115**(4):758–764, February 2011.

[PAW20] Joseph C. A. Prentice, Jolyon Aarons, James C. Womack, Alice E. A. Allen, Lampros Andrinopoulos, Lucian Anton, Robert A. Bell, Arihant Bhandari, Gabriel A. Bramley, Robert J. Charlton, Rebecca J. Clements, Daniel J. Cole, Gabriel Constantinescu, Fabiano Corsetti, Simon M.-M. Dubois, Kevin K. B. Duff, José María Escartín, Andrea Greco, Quintin Hill, Louis P. Lee, Edward Linscott, David D.

O'Regan, Maximillian J. S. Phipps, Laura E. Ratcliff, Álvaro Ruiz Serrano, Edward W. Tait, Gilberto Teobaldi, Valerio Vitale, Nelson Yeung, Tim J. Zuehlsdorff, Jacek Dziedzic, Peter D. Haynes, Nicholas D. M. Hine, Arash A. Mostofi, Mike C. Payne, and Chris-Kriton Skylaris. "The ONETEP linear-scaling density functional theory program." *The Journal of Chemical Physics*, **152**(17), may 2020.

[PCC18] Raj Pandya, Richard Y. S. Chen, Alexandre Cheminal, Tudor Thomas, Arya Thampi, Arelo Tanoh, Johannes Richter, Ravichandran Shivanna, Felix Deschler, Christoph Schnedermann, and et al. "Observation of Vibronic-Coupling-Mediated Energy Transfer in Light-Harvesting Nanotubes Stabilized in a Solid-State Matrix." *The Journal of Physical Chemistry Letters*, **9**(18):5604–5611, August 2018.

[PCG19] Raj Pandya, Richard Y. S. Chen, Qifei Gu, Jooyoung Sung, Christoph Schnedermann, Oluwafemi S. Ojambati, Rohit Chikkaraddy, Jeffrey Gorman, Gianni Jacucci, Olimpia D. Onelli, and et al. "Ultrafast long-range energy transport via light-matter coupling in organic semiconductor films.", 2019.

[Pei94] Rudolf Peierls. "Yakov Il'ich Frenkel." *Physics Today*, **47**(6):44–49, June 1994.

[PHF10] G. Panitchayangkoon, D. Hayes, K. A. Fransted, J. R. Caram, E. Harel, J. Wen, R. E. Blankenship, and G. S. Engel. "Long-lived quantum coherence in photosynthetic complexes at physiological temperature." *Proceedings of the National Academy of Sciences*, **107**(29):12766–12770, July 2010.

[PNF17] Sougata Pal, Parmeet Nijjar, Thomas Frauenheim, and Oleg V. Prezhdo. "Atomistic Analysis of Room Temperature Quantum Coherence in Two-Dimensional CdSe Nanostructures." *Nano Letters*, **17**(4):2389–2396, March 2017.

[PPG22] Liang Peng, Daoling Peng, Feng Long Gu, and Weitao Yang. "Regularized Localized Molecular Orbitals in a Divide-and-Conquer Approach for Linear Scaling Calculations." *Journal of Chemical Theory and Computation*, **18**(5):2975–2982, April 2022.

[PW92] John P. Perdew and Yue Wang. "Accurate and simple analytic representation of the electron-gas correlation energy." *Phys. Rev. B*, **45**:13244–13249, Jun 1992.

[RBN15] Eran Rabani, Roi Baer, and Daniel Neuhauser. "Time-dependent stochastic Bethe-Salpeter approach." *Physical Review B*, **91**(23):235302, June 2015.

[RCN97] Naomi Rom, D.M. Charutz, and Daniel Neuhauser. "Shifted-contour auxiliary-field Monte Carlo: circumventing the sign difficulty for electronic-structure calculations." *Chemical Physics Letters*, **270**(3-4):382–386, May 1997.

[Rib22] Raphael F. Ribeiro. "Multimode polariton effects on molecular energy transport and spectral fluctuations." *Communications Chemistry*, **5**(1), April 2022.

[RJS08] Gaël Rouillé, Cornelia Jäger, Mathias Steglich, Friedrich Huisken, Thomas Henning, Gabriele Theumer, Ingmar Bauer, and Hans-Joachim Knölker. "IR, Raman, and UV/Vis Spectra of Corannulene for Use in Possible Interstellar Identification." *ChemPhysChem*, **9**(14):2085–2091, October 2008.

[RMA09] Patrick Rebentrost, Masoud Mohseni, and Alan Aspuru-Guzik. "Role of Quantum Coherence and Environmental Fluctuations in Chromophoric Energy Transport." *The Journal of Physical Chemistry B*, **113**(29):9942–9947, July 2009.

[RMG18] Michael Reitz, Francesca Mineo, and Claudiu Genes. "Energy transfer and correlations in cavity-embedded donor-acceptor configurations." *Scientific Reports*, **8**(1), June 2018.

[RPG12] Dario Rocca, Yuan Ping, Ralph Gebauer, and Giulia Galli. "Solution of the Bethe-Salpeter equation without empty electronic states: Application to the absorption spectra of bulk systems." *Physical Review B*, **85**(4):045116, January 2012.

[RPM03] Carlos L. Reis, J. M. Pacheco, and José Luís Martins. "First-principles norm-conserving pseudopotential with explicit incorporation of semicore states." *Physical Review B*, **68**(15):155111, October 2003.

[RRB12] Xinguo Ren, Patrick Rinke, Volker Blum, Jürgen Wieferink, Alexandre Tkatchenko, Andrea Sanfilippo, Karsten Reuter, and Matthias Scheffler. "Resolution-of-identity approach to Hartree–Fock, hybrid density functionals, RPA, MP2 and GW with numeric atom-centered orbital basis functions." *New Journal of Physics*, **14**(5):053020, may 2012.

[RSB09] P. Romaniello, D. Sangalli, J. A. Berger, F. Sottile, L. G. Molinari, L. Reining, and G. Onida. "Double excitations in finite systems." *The Journal of Chemical Physics*, **130**(4):044108, January 2009.

[RSK93] T. Rabenau, A. Simon, R. K. Kremer, and E. Sohmen. "The energy gaps of fullerene C60 and C70 determined from the temperature dependent microwave conductivity." *Zeitschrift for Physik B Condensed Matter*, **90**(1):69–72, March 1993.

[RT16] Elisa Rebolini and Julien Toulouse. "Range-separated time-dependent density-functional theory with a frequency-dependent second-order Bethe-Salpeter correlation kernel." *The Journal of Chemical Physics*, **144**(9):094107, March 2016.

[RV22] Mariya Romanova and Vojtěch Vlček. "Stochastic many-body calculations of moiré states in twisted bilayer graphene at high pressures." *npj Computational Materials*, **8**:11, January 2022.

[RVM06] Carlo A. Rozzi, Daniele Varsano, Andrea Marini, Eberhard K. U. Gross, and Angel Rubio. "Exact Coulomb cutoff technique for supercell calculations." *Physical Review B*, **73**(20):205119, May 2006.

[SAB24] Mykola Sereda, Tucker Allen, Nadine C. Bradbury, Khaled Z. Ibrahim, and Daniel Neuhauser. "Sparse-Stochastic Fragmented Exchange for Large-Scale Hybrid Time-Dependent Density Functional Theory Calculations." *Journal of Chemical Theory and Computation*, May 2024.

[Sch20] Gregory D. Scholes. "Polaritons and excitons: Hamiltonian design for enhanced coherence." *Proceedings of the Royal Society A: Mathematical, Physical and Engineering Sciences*, **476**(2242), October 2020.

[SCS09] Frank C. Spano, Jenny Clark, Carlos Silva, and Richard H. Friend. "Determining exciton coherence from the photoluminescence spectral line shape in poly(3-hexylthiophene) thin films." *The Journal of Chemical Physics*, **130**(7):074904, February 2009.

[SD71] R. A. Sack and A. F. Donovan. "An algorithm for Gaussian quadrature given modified moments." *Numerische Mathematik*, **18**(5):465–478, October 1971.

[SDC94] P. J. Stephens, F. J. Devlin, C. F. Chabalowski, and M. J. Frisch. "Ab Initio Calculation of Vibrational Absorption and Circular Dichroism Spectra Using Density Functional Force Fields." *The Journal of Physical Chemistry*, **98**(45):11623–11627, November 1994.

[SFM19] D Sangalli, A Ferretti, H Miranda, C Attaccalite, I Marri, E Cannuccia, P Melo, M Marsili, F Paleari, A Marrazzo, G Prandini, P Bonfà, M O Atambo, F Affinito, M Palummo, A Molina-Sánchez, C Hogan, M Grüning, D Varsano, and A Marini. "Many-body perturbation theory calculations using the yambo code." *Journal of Physics: Condensed Matter*, **31**(32):325902, May 2019.

[SHG11] T. Schwartz, J. A. Hutchison, C. Genet, and T. W. Ebbesen. "Reversible Switching of Ultrastrong Light-Molecule Coupling." *Physical Review Letters*, **106**(19), May 2011.

[SKO02] Christian Spitz, Jasper Knoester, André Ouart, and Siegfried Daehne. "Polarized absorption and anomalous temperature dependence of fluorescence depolarization in cylindrical J-aggregates." *Chemical Physics*, **275**(1-3):271–284, January 2002.

[SM89] Francis C. Spano and Shaul Mukamel. "Nonlinear susceptibilities of molecular aggregates: Enhancement of χ^3 by size." *Physical Review A*, **40**(10):5783–5801, November 1989.

[SP22] Abhishek Sirohiwal and Dimitrios A. Pantazis. "The Electronic Origin of Far-Red-Light-Driven Oxygenic Photosynthesis." *Angewandte Chemie International Edition*, **61**(16):e202200356, 2022.

[Spa05] Frank C. Spano. "Modeling disorder in polymer aggregates: The optical spectroscopy of regioregular poly(3-hexylthiophene) thin films." *The Journal of Chemical Physics*, **122**(23):234701, June 2005.

[SR94] R N Silver and H Röder. "Densities of States of Mega-Dimensional Hamiltonian Matrices." *International Journal of Modern Physics C*, **05**(04):735–753, August 1994.

[SR23] Enes Suyabatmaz and Raphael F. Ribeiro. "Vibrational polariton transport in disordered media." *The Journal of Chemical Physics*, **159**(3), July 2023.

[SSS21] Olga A. Stasyuk, Anton J. Stasyuk, Miquel Solà, and Alexander A. Voityuk. "[10]CPP-Based Inclusion Complexes of Charged Fulleropyrrolidines. Effect of the Charge Location on the Photoinduced Electron Transfer." *Chemistry – A European Journal*, **27**(34):8737–8744, June 2021.

[Str88] G. Strinati. "Application of the Green's functions method to the study of the optical properties of semiconductors." *La Rivista del Nuovo Cimento*, **11**(12):1–86, December 1988.

[Sum77] H. Sumi. "Exciton–lattice interaction and the line shape of exciton absorption in molecular crystals." *The Journal of Chemical Physics*, **67**(7):2943–2954, October 1977.

[TB10] Christina Tönshoff and Holger F. Bettinger. "Photogeneration of Octacene and Nonacene." *Angewandte Chemie International Edition*, **49**(24):4125–4128, April 2010.

[TB20] Christina Tönshoff and Holger F. Bettinger. "Pushing the Limits of Acene Chemistry: The Recent Surge of Large Acenes." *Chemistry – A European Journal*, **27**(10):3193–3212, December 2020.

[TC68] Michael Tavis and Frederick W. Cummings. "Exact Solution for an N-Molecule—Radiation-Field Hamiltonian." *Physical Review*, **170**(2):379–384, June 1968.

[TC06] Murilo L. Tiago and James R. Chelikowsky. "Optical excitations in organic molecules, clusters, and defects studied by first-principles Green's function methods." *Physical Review B*, **73**(20):205334, May 2006.

[TFG21] Ruth H. Tichauer, Johannes Feist, and Gerrit Groenhof. "Multi-scale dynamics simulations of molecular polaritons: The effect of multiple cavity modes on polariton relaxation." *The Journal of Chemical Physics*, **154**(10):104112, March 2021.

[Tho74] D.J. Thouless. "Electrons in disordered systems and the theory of localization." *Physics Reports*, **13**(3):93–142, October 1974.

[TJK17] Roel Tempelaar, Thomas L. C. Jansen, and Jasper Knoester. "Exciton–Exciton Annihilation Is Coherently Suppressed in H-Aggregates, but Not in J-Aggregates." *The Journal of Physical Chemistry Letters*, **8**(24):6113–6117, December 2017.

[TM91] N. Troullier and José Luís Martins. "Efficient pseudopotentials for plane-wave calculations." *Phys. Rev. B*, **43**:1993–2006, Jan 1991.

[TMK02] Nir Tessler, Vlad Medvedev, Miri Kazes, ShiHai Kan, and Uri Banin. "Efficient Near-Infrared Polymer Nanocrystal Light-Emitting Diodes." *Science*, **295**(5559):1506–1508, February 2002.

[TMS22] Ruth H. Tichauer, Dmitry Morozov, Ilia Sokolovskii, J. Jussi Toppari, and Gerrit Groenhof. "Identifying Vibrations that Control Non-adiabatic Relaxation of Polaritons in Strongly Coupled Molecule–Cavity Systems." *The Journal of Physical Chemistry Letters*, **13**(27):6259–6267, June 2022.

[TRK92] R. J. Thompson, G. Rempe, and H. J. Kimble. "Observation of normal-mode splitting for an atom in an optical cavity." *Physical Review Letters*, **68**(8):1132–1135, February 1992.

[TSB17] Elijah Thimsen, Bryce Sadtler, and Mikhail Y. Berezin. "Shortwave-infrared (SWIR) emitters for biological imaging: a review of challenges and opportunities." *Nanophotonics*, **6**(5):1043–1054, June 2017.

[UM08] Ivan S. Ufimtsev and Todd J. Martínez. "Quantum Chemistry on Graphical Processing Units. 1. Strategies for Two-Electron Integral Evaluation." *Journal of Chemical Theory and Computation*, **4**(2):222–231, January 2008.

[VAF93] O. Vahtras, J. Almlöf, and M.W. Feyereisen. "Integral approximations for LCAO-SCF calculations." *Chemical Physics Letters*, **213**(5-6):514–518, oct 1993.

[VBR18a] Vojtech Vlcek, Roi Baer, Eran Rabani, and Daniel Neuhauser. "Simple eigenvalue-self-consistent ΔGW_0." *J. Chem. Phys.*, **149**(17):174107, November 2018.

[VBR18b] Vojtěch Vlček, Roi Baer, Eran Rabani, and Daniel Neuhauser. "Simple eigenvalue-self-consistent ΔGW0." *The Journal of Chemical Physics*, **149**(17):174107, November 2018.

[VLB18a] Vojtěch Vlček, Wenfei Li, Roi Baer, Eran Rabani, and Daniel Neuhauser. "Swift GW beyond 10, 000 electrons using sparse stochastic compression." *Physical Review B*, **98**(7):075107, August 2018.

[VLB18b] Vojtěch Vlček, Wenfei Li, Roi Baer, Eran Rabani, and Daniel Neuhauser. "Swift *GW* beyond 10,000 electrons using sparse stochastic compression." *Phys. Rev. B*, **98**:075107, Aug 2018.

[VLR18] Vojtech Vlcek, Wenfei Li, Eran Rabani, Roi Baer, and Daniel Neuhauser. ""StochasticGW" (2018-2019), http://www.stochasticgw.com/.", 2018.

[VRB19] Vojtech Vlcek, Eran Rabani, Roi Baer, and Daniel Neuhauser. "Nonmonotonic band gap evolution in bent phosphorene nanosheets." *Phys. Rev. Mater.*, **3**(6):064601, June 2019.

[VRN18] Vojtěch Vlček, Eran Rabani, and Daniel Neuhauser. "Quasiparticle spectra from molecules to bulk." *Physical Review Materials*, **2**(3):030801(R), March 2018.

[Wan37] Gregory H. Wannier. "The Structure of Electronic Excitation Levels in Insulating Crystals." *Physical Review*, **52**(3):191–197, August 1937.

[Wan94] Lin-Wang Wang. "Calculating the density of states and optical-absorption spectra of large quantum systems by the plane-wave moments method." *Phys. Rev. B*, **49**:10154–10158, Apr 1994.

[WB72] John C. Wheeler and Carl Blumstein. "Modified Moments for Harmonic Solids." *Physical Review B*, **6**(12):4380–4382, December 1972.

[WCT19] Xin-Ping Wu, Indrani Choudhuri, and Donald G. Truhlar. "Computational Studies of Photocatalysis with Metal–Organic Frameworks." *Energy & Environmental Materials*, **2**(4):251–263, October 2019.

[WGG08] Hugh F. Wilson, François Gygi, and Giulia Galli. "Efficient iterative method for calculations of dielectric matrices." *Physical Review B*, **78**(11):113303, September 2008.

[WKG13] Alex Willand, Yaroslav O. Kvashnin, Luigi Genovese, Álvaro Vázquez-Mayagoitia, Arpan Krishna Deb, Ali Sadeghi, Thierry Deutsch, and Stefan Goedecker. "Norm-conserving pseudopotentials with chemical accuracy compared to all-electron calculations." *The Journal of Chemical Physics*, **138**(10):104109, March 2013.

[WN95] Michael R. Wall and Daniel Neuhauser. "Extraction, through filter-diagonalization, of general quantum eigenvalues or classical normal mode frequencies from a small number of residues or a short-time segment of a signal. I. Theory and application to a quantum-dynamics model." *J. Chem. Phys.*, **102**(20):8011–8022, May 1995.

[Won09] Bryan M. Wong. "Optoelectronic Properties of Carbon Nanorings: Excitonic Effects from Time-Dependent Density Functional Theory." *The Journal of Physical Chemistry C*, **113**(52):21921–21927, December 2009.

[WSG06] Brent Walker, A. Marco Saitta, Ralph Gebauer, and Stefano Baroni. "Efficient Approach to Time-Dependent Density-Functional Perturbation Theory for Optical Spectroscopy." *Physical Review Letters*, **96**(11):113001, March 2006.

[WWA06] Alexander Weiße, Gerhard Wellein, Andreas Alvermann, and Holger Fehske. "The kernel polynomial method." *Rev. Mod. Phys.*, **78**:275–306, Mar 2006.

[WWH20] Yu-Chen Wei, Sheng Fu Wang, Yun Hu, Liang-Sheng Liao, Deng-Gao Chen, Kai-Hsin Chang, Chi-Wei Wang, Shih-Hung Liu, Wei-Hsiang Chan, Jia-Ling Liao, and et al. "Overcoming the energy gap law in near-infrared OLEDs by exciton–vibration decoupling." *Nature Photonics*, **14**:570–577, June 2020.

[WZ94] Lin-Wang Wang and Alex Zunger. "Solving Schrödinger's equation around a desired energy: Application to silicon quantum dots." *The Journal of Chemical Physics*, **100**(3):2394–2397, February 1994.

[XBJ12] Jianlong Xia, Jeffrey W. Bacon, and Ramesh Jasti. "Gram-scale synthesis and crystal structures of [8]- and [10]CPP, and the solid-state structure of C60@[10]CPP." *Chemical Science*, **3**(10):3018, 2012.

[XKW18] Youzhi Xu, Ramandeep Kaur, Bingzhe Wang, Martin B. Minameyer, Sebastian Gsänger, Bernd Meyer, Thomas Drewello, Dirk M. Guldi, and Max von Delius. "Concave-Convex $\pi - \pi$ Template Approach Enables the Synthesis of [10]Cycloparaphenylene-Fullerene [2]Rotaxanes." *Journal of the American Chemical Society*, **140**(41):13413–13420, September 2018.

[YDY16] Yang Yang, Ernest R. Davidson, and Weitao Yang. "Nature of ground and electronic excited states of higher acenes." *Proceedings of the National Academy of Sciences*, **113**(35), August 2016.

[YZZ15] Kun Yuan, Cai-Hua Zhou, Yuan-Cheng Zhu, and Xiang Zhao. "Theoretical exploration of the nanoscale host–guest interactions between [n]cycloparaphenylenes (n = 10, 8 and 9) and fullerene C_{60}: from single- to three-potential well." *Physical Chemistry Chemical Physics*, **17**(28):18802–18812, 2015.

[ZCS22] Zeyu Zhou, Hsing-Ta Chen, Joseph E. Subotnik, and Abraham Nitzan. "The Interplay between Disorder, Local Relaxation and Collective Behaviors for an ensemble of emitters outside vs inside cavity.", 2022.

[ZCW16] Xiaolan Zhong, Thibault Chervy, Shaojun Wang, Jino George, Anoop Thomas, James A. Hutchison, Eloise Devaux, Cyriaque Genet, and Thomas W. Ebbesen. "Non-Radiative Energy Transfer Mediated by Hybrid Light-Matter States." *Angewandte Chemie International Edition*, **55**(21):6202–6206, April 2016.

[ZCZ17] Xiaolan Zhong, Thibault Chervy, Lei Zhang, Anoop Thomas, Jino George, Cyriaque Genet, James A. Hutchison, and Thomas W. Ebbesen. "Energy Transfer between Spatially Separated Entangled Molecules." *Angewandte Chemie International Edition*, **56**(31):9034–9038, June 2017.

[Zha18] Shiwei Zhang. "Ab Initio Electronic Structure Calculations by Auxiliary-Field Quantum Monte Carlo." In *Handbook of Materials Modeling*, pp. 1–27. Springer International Publishing, 2018.

[ZL15] Xu Zhang and Gang Lu. "Subspace formulation of time-dependent density functional theory for large-scale calculations." *The Journal of Chemical Physics*, **143**(6):064110, August 2015.